DISSERTATION

CHLORIDE BINDING AND DESORPTION MECHANISM IN BLENDED CEMENT CONTAINING SUPPLEMENTARY CEMENTITIOUS MATERIALS EXPOSED TO DE-ICING BRINE SOLUTIONS

Submitted by

Mohammad Teymouri Moogooee

Department of Civil and Environmental Engineering

In partial fulfillment of the requirements

For the Degree of Doctor of Philosophy

Colorado State University

Fort Collins, Colorado

Spring 2024

Doctoral Committee:

Advisor: Rebecca Atadero
Co-Advisor: Todd Fantz

Gaofeng Jia
Travis Bailey

ABSTRACT

CHLORIDE BINDING AND DESORPTION MECHANISM IN BLENDED CEMENT CONTAINING SUPPLEMENTARY CEMENTIOTUS MATERIALS EXPOSED TO DE-ICING BRINE SOLUTIONS

Concrete, the most widely used construction material globally, faces significant challenges due to its porous nature, particularly from chloride-induced corrosion. This corrosion, primarily caused by chloride ions penetrating concrete, affects over 7.5% of U.S. concrete bridges, incurring annual costs ranging from $5.9 to $9.7 billion. Chlorides enter concrete from various sources, including de-icing salts. Maritime infrastructures also suffer from severe chloride-induced corrosion because seawater contains a high concentration of chloride ions. Irrespective of how chlorides enter the concrete, chlorides can exist in concrete in two forms: free and bound chlorides. While bound chlorides are beneficial, they can be released due to environmental factors like carbonation and chemical attacks, exacerbating corrosion rates. These attacks cause pH reduction in concrete and subsequently can result in the release of bound chlorides (chloride desorption).

This dissertation aims to address three main objectives: (1) investigate factors influencing chloride binding measurements due to lack of a standardized method for chloride binding measurements, (2) study chloride desorption mechanisms in different cementitious systems exposed to de-icing brines, and (3) analyze pH and compositional changes in blended pastes under chloride contamination and carbonation.

First, factors impacting chloride binding measurements were identified, such as sample form and saturation level, solution composition, and solution volume. Vacuum-saturated samples exhibited higher chloride binding than partially saturated or dried samples, with powdered samples showing the highest binding. Secondly, chloride desorption mechanisms were investigated in both Ordinary Portland Cement (OPC) pastes and pastes containing supplementary cementitious materials (SCMs) like fly ash, slag, and silica fume. Results indicated that the type of cation in the brine solution influenced bound chloride levels, with SCMs improving chloride binding capacity. Slag inclusion was effective in promoting chloride binding, while silica fume showed the least effect. The degree of chloride desorption under acid attack depended on the acid-to-paste mass ratio. The results reveal that inclusion of fly ash and slag is favorable in terms of chloride desorption, and silica fume is not recommended for use when chloride-induced corrosion is a concern. $MgCl_2$ and $CaCl_2$ de-icers demonstrated a lower chloride desorption compared to NaCl.

Finally, the synergistic effects of chloride contamination and carbonation were examined in OPC and fly ash-containing pastes. Carbonation led to over 95% chloride desorption after two weeks, with fly ash-containing pastes exhibiting lower pH levels due to reduced portlandite content. Incorporation of fly ash is not recommended when carbonation is a concern. Therefore, caution should be exercised when considering fly ash inclusion in mixtures where both chloride contamination and carbonation are simultaneous concerns.

This dissertation shed lights on primary factors influencing chloride binding measurements, enhancing the accuracy of chloride binding results. This dissertation contributes to understanding chloride desorption in cementitious systems, essential for enhancing the durability and service life of concrete structures.

ACKNOWLEDGEMENTS

My promising journey at Colorado State University has been incredibly rewarding, not only shaping me into an independent researcher but also fostering significant personal growth. I owe heartfelt thanks to my wonderful parents, who instilled in me the values of kindness and resilience in the face of life's challenges.

I am deeply grateful for the unwavering support, guidance, and encouragement provided by my beloved wife, Elham, from day one of my graduate studies. Her support has been instrumental in my success, and I acknowledge that none of my achievements would have been possible without her sacrifices.

I extend my sincere appreciation to my advisor, Professor Rebecca Atadero, for her invaluable mentorship, especially during challenging times. I am also grateful to my esteemed committee members, Professor Todd Fantz, Professor Travis Baily, and Professor Gaofeng Jia, for their guidance, insights, and unwavering support throughout this remarkable journey.

I was in a unique joint program between the Civil and Environmental Engineering and Construction Management Departments. I am thankful for the access to various facilities and laboratories provided by both departments, as well as the Center for Materials and Molecular Analysis (ARC-MMA) at Colorado State University. I would like to express my gratitude for the assistance and support I received as a graduate teaching assistant and graduate research assistant from Professor Charles Shackelford, Head of the Civil Engineering Department, and Professor Paul Goodrum, Head of the Construction Management Department.

I am immensely appreciative of the financial support provided for this thesis by the American Concrete Institute Foundation (Grant number P0042), the College of Health and Human Sciences (Dean's Fellowship) at Colorado State University, and the Portland Cement Association Foundation (J. P. Gleason Research Fellowship).

DEDICATION

To my darling wife, Elham, and my parents, Hayat Soltan and Heshmat Khan, and our beautiful Iran.

TABLE OF CONTENTS

LIST OF TABLES

LIST OF FIGURES

Chapter 1 : Introduction

1.1. Overview

Concrete is the second most consumed material in the world after water, the most consumed human-made material, and the most-used construction material [1]. It has been used to construct buildings, roads, and bridges due to its strength, durability, and versatility. Even floating bridges like the Evergreen Point Floating Bridge in Washington, and a colossal neoclassical sculpture, the Statue of Liberty in New York, are made of tons of concrete [2].

However, concrete is a porous and permeable material, and different chemical agents applied to concrete surface can penetrate the concrete, making the concrete vulnerable to various types of deterioration and causing corrosion of the reinforcing steel [3]. While building codes provide comprehensive guidelines for the design of concrete structures, they offer limited specifications concerning the corrosion resistance and service life of concrete infrastructures.

Chloride ions enter concrete from a variety of sources. Chlorides can be internally introduced into concrete through various constituent materials such as aggregates, cement, admixtures, and even water during the mixing process [4, 5]. The external chloride ions are primarily introduced to the concrete from marine environments and de-icing salts. Maritime infrastructure are suffering from severe chloride-induced corrosion because seawater contains a high concentration of chloride ions and they have significant economic and social values [6].

In winter seasons, the surfaces of concrete pavements and reinforced concrete bridge decks are treated with chloride-bearing de-icing salts to minimize the risk of icy roads and sidewalks, reducing the number of car accidents and injuries from falls on frozen sidewalks [7].

The application of de-icing salts is a low-cost solution and the most common method to quickly melt snow and ice when cold weather arrives. The most common de-icing salts are sodium chloride (NaCl), calcium chloride ($CaCl_2$), and magnesium chloride ($MgCl_2$) [8]. For example, in Fort Collins, Colorado, a magnesium chloride brine, Meltdown Apex, is the primary liquid deicer, which the producer claims delivers a 12°F improvement in freeze point over other deicers [9].

The are contradictory reports regarding the sufficient concentration of chlorides, expressed as a chloride threshold value or a critical concentration, that potentially initiates chloride-induced corrosion [10-13]. However, if a concrete infrastructure is near an external or internal source of chloride, reaching a critical concentration and initiating chloride-induced corrosion is only a matter of time and will eventually happen.

When the amount of chlorides at the surface of the embedded reinforcing steel reaches a high enough concentration and sufficient oxygen and moisture are present, chloride-induced corrosion initiates. Chloride-induced corrosion is one of the leading deterioration on concrete infrastructures, causing spalling and cracking, loss of bond between reinforcements and concrete, and reduction in the cross-section of reinforcements [14, 15].

Figure 1.1 presents a basic depiction of the process of chloride-induced corrosion. Reinforcements in concrete are protected from corrosion by a protective layer, called passive film. The passive film is formed due to a high pH level in sound concrete, which is typically around 12.5 to 13.5 [16]. The film is a thin and dense layer of iron oxide on the steel surface that acts as an effective protective film on the surface of embedded reinforcing steel in concrete [17]. Before corrosion takes place, first this passive film should be broken. Chloride and carbon dioxide in the presence of moisture and oxygen can break the passive layer.

Upon the introduction of chloride ions to the concrete surface, chloride ions eventually

make their way to the surfaces of the reinforcing rebars, due to the porosity of concrete and interconnected pores in concrete. The presence of chloride ions results in partial or complete loss of the passive layer on steel reinforcement in concrete, which is usually called reinforcement depassivation. Reinforcement depassivation leads to a significant risk of active corrosion on reinforcements [15,16]. Continuing chemical reactions between chloride ions and reinforcements result in the formation of rusts and pits and corrosion on the surfaces of reinforcing rebars. More details are provided in Chapter 2.

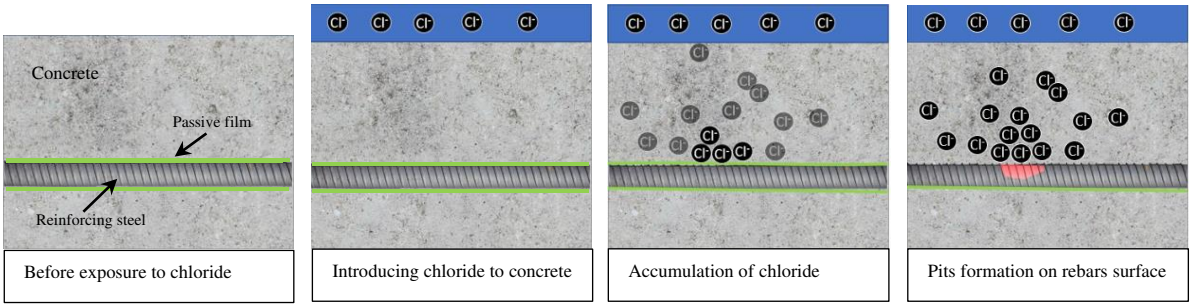

Figure 1.1. Simplified chloride-induced corrosion mechanism

1.2. Problem Statement

As mentioned earlier chloride ions can enter concrete either from external or internal sources. Irrespective of how chlorides enter the concrete, chlorides can exist in concrete in two forms: free and bound chlorides [18]. Free chlorides are the primary cause of chloride-induced corrosion in concrete structures because they can move freely in concrete pores, reaching the rebar surface to initiate corrosion. Figure 1.2.a displays a schematic representation of free and bound chlorides in concrete.

The free chloride ions in the pore solution are able to actively participate in the corrosion of reinforcement rebars [19]. The pore solution of cement pastes is an essential yet often overlooked component of hydrated cements [20]. The pore solution refers to the liquid phase

within the microstructure of hydrated cement paste. It is a highly alkaline solution, primarily composed of hydroxide ions, sodium, potassium, calcium, sulfate, silicon, and aluminium [20]. Several studies reported that reinforcement depassivation is more related to the pore solution composition such as Cl^-/ OH^- ratio rather than chloride concentration [21-23] which shows the importance of concrete pore solution in chloride-induced corrosion process.

Some of these free chlorides in concrete pore solutions can either form a physical or chemical bond with the cement hydration products, becoming bound chlorides [24, 25]. Bound chlorides are those chloride ions that are adsorbed by the concrete matrix and cannot actively participate in reinforcement corrosion. Therefore, chloride binding is a favorable phenomenon.

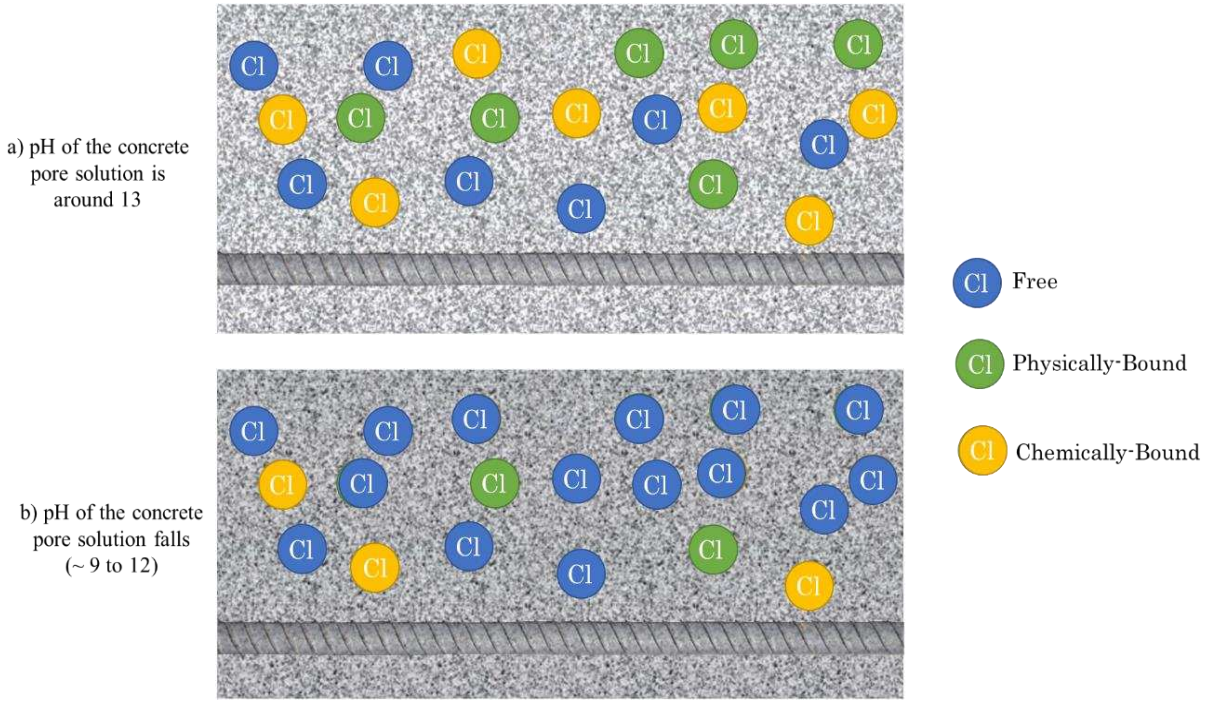

Figure 1.2. Schematic representation of a) free and bound chlorides in concrete and b) released bound chloride in concrete due to pH reduction

Although chloride binding is a beneficial process, chloride binding cannot be assumed to be permanent and lasting forever. In real case scenarios, most concrete infrastructures, such as

concrete pavements and bridges, are subject to environmental attacks such as carbonation and chemical attacks. These chemical attacks cause pH reduction in the concrete pore solution and subsequently can result in reduced chloride binding capacity [26] and the release of bound chlorides. In other words, chloride binding is a reversible process.

In previous studies, there is a lack of understanding of the degree to which chloride binding is reversible. Changes in concrete composition over time, often due to chemical attacks, such as carbonation, acid attack, and sulfate attack, and the decrease in pH can lead to the reversibility of chloride binding, as shown in Figure 1.2b. It should be noted that carbonation in concrete is when atmospheric carbon dioxide (CO_2) penetrates into concrete and reacts with cement hydration products such as $Ca(OH)_2$, forming carbonic acid (H_2CO_3) within the concrete pore solution, resulting in a pH drop in the pore solution. In such scenarios, chlorides previously bound to the cement hydration products can dissociate and re-enter the pore solution, raising the concentration of free chloride as shown in Figure 1.2b. In this thesis, we refer to this phenomenon as "chloride desorption". In terms of concrete durability, chloride desorption is an unfavorable mechanism because it releases some previously bound chlorides into the concrete pore solution, increasing the concentration of free chlorides and the corrosion risk of reinforcements in concrete structures.

To the best of the author's knowledge, current service life models do not take into account the chloride binding reversibility. However, in reality, when the pH of the concrete pore solution changes, whether due to carbonation, acid attack, or sulfate attack, the chloride binding capacity and the concentration of free chloride ions in the concrete pore solution also change. This leads to an increased risk of corrosion. In other words, existing service life models tend to overestimate the lifespan of concrete infrastructure by simply neglecting the chloride desorption phenomenon. Therefore, investigating the chloride desorption mechanism and providing reliable information

and data for incorporating the desorption mechanism in service life modeling would significantly enhance the reliability of current service life predictions.

This thesis aims to address the chloride desorption phenomena, as defined earlier, in various cementitious systems in low pH environments. This study investigates how much bound chloride would disassociate from cement hydration products and return to cement pore solution when there is a reduction in pH. This thesis also aims to provide an understanding of how incorporation of diverse types and replacement levels of supplementary cementitious materials (SCMs) can potentially impact chloride binding, and more importantly, chloride desorption when the pH drops within different ranges.

1.3. Significance

Chloride-induced corrosion impacts the strength and serviceability of more than 7.5% of the concrete bridges in the U.S. [27], resulting in significant social and economic losses. Official reports on the annual direct and indirect costs of chloride-induced corrosion in concrete infrastructure are rarely easy to find whether from federal or non-federal agencies. The primary challenge may be related to the difficulty in distinguishing between various forms of concrete deterioration. Based on a Federal Highway Administration (FHWA) report in July 2007, the annual direct cost of rebar corrosion in concrete bridges is $5.9 to $9.7 billion in the U.S. If indirect costs, such as traffic delays, detours, and road closures are also considered , the total cost of chloride induced corrosion can be much higher [28]. Another quite dated report by Building Research Establishment (BRE) in UK estimated the annual cost incurred in UK due to the corrosion damage to concrete is around £ 750 million [29].

While chloride-induced corrosion is a widespread concern across the globe, there are still many aspects of it that have not been fully understood, highlighting the need for more in-depth

research. Gaining a better understanding of chloride binding and desorption mechanisms contributes to the mitigation and delay of chloride-induced corrosion in concrete infrastructures, ultimately leading to cost savings in repair, maintenance, and rehabilitation projects.

Contrary to the chloride binding capacity of cementitious materials, which has gained lot of attention and also been incorporated in service life modelling, the chloride desorption mechanism is barely investigated. The chloride desorption mechanism is an underrated phenomenon which contributes to the reduction of the lifespan of concrete and significantly impacts chloride-induced corrosion rate and magnitude by increasing the concentration of free chlorides in concrete pore solution. Therefore, there is an undeniable need to thoroughly investigate the process to understand how much bound chloride in different cementitious materials and under diverse low pH environments potentially disassociate and return to the concrete pore solution. This novel research can significantly contribute to the body of the current knowledge by methodically investigating the chloride binding mechanism.

1.4. Outline of the Dissertation

This dissertation contains five chapters providing background, materials and methods, results, and discussion for four separate yet connected objectives.

Chapter 2: Comprehensive Background and Literature Review: This chapter provides a comprehensive literature review of previous findings and knowledge gaps on chloride binding capacity in cementitious systems and explores current understanding of the chloride desorption mechanism in various cementitious systems. At the end of this chapter, the research questions and objectives are presented.

Chapter 3: Methodology: The third chapter presents a detailed description of the materials,

equipment, methods, calculations, and testing procedures employed in this research project. To maintain clarity and coherence in the presentation of research methodology, each defined objective is accompanied by its own dedicated methodology section.

Chapter 4: Results and Discussion: This chapter summarizes the results of this project based on experimental tests. For clear and cohesive presentation of outcomes, the results and discussion for each specific objective are distinctly outlined in separate sections.

Chapter 5: Conclusion and Recommendation for Future Works: Chapter five emphasizes the key findings from the four investigations, outlines the contributions of this research, and offers guidance for future scholars in the domain.

Chapter 2 : Background and Literature Review on Chloride Binding and Desorption in Blended Cement Exposed to Brine Solutions

2.1. Introduction

Concrete infrastructures are of great importance to societies, providing the means to connect cities, transport people and goods, and protect the land against flooding and erosion. Reinforced concrete is used in the majority of civil and construction projects. Concrete performs well under compression and steel is strong in tension. The unique combination of reinforcing steel and concrete helps bear high loads in diverse civil projects including roads, bridges, building, pipes, parking garages, etc.

While concrete is one of the most economical construction materials, even well-designed and constructed concrete structures are prone to deterioration due to poor durability performance. Reinforced concrete structures are frequently exposed to a variety of environmental conditions such as chemical attack, carbonation, freeze-thaw cycles, acid rain, etc. One of the leading durability problems for reinforced concrete structures is corrosion of reinforcements with related cracking on the concrete surface and spalling of concrete cover [30].

Corrosion of the reinforcing steel in reinforced concrete leads to unserviceability of the structures and aesthetics problems. More importantly, rebar corrosion in reinforced concrete poses economic liability to private or public owners [31], forcing them to repair and rehabilitate the corroded reinforced concrete structures. The corroded reinforced concrete structures are unsustainable, as maintaining them in operation necessitates the consumption of additional precious natural resources. One of the most fundamental causes of reinforcement corrosion and degradation of concrete structures, is chloride-induced corrosion [32].

Rebar corrosion can be initiated by the penetration of chloride in concrete, such as from exposure to seawater or road deicing salts. Chloride-induced corrosion is a widespread concern across the globe, impacting diverse infrastructures including but not limited to bridges, pavements, and marine structures. While chloride-induced corrosion has been studied for decades, there are still many unanswered questions regarding corrosion onset and rate, the critical chloride concentration that initiates the corrosion, impacts of cracking and spalling on corrosion rate, impacts of concrete composition on corrosion rate and corrosion initiation, effects of chloride binding on corrosion rate, etc. [31].

Chloride-induced corrosion causes colossal economic losses worldwide [33]. The chloride-induced corrosion leads to strength reduction, cracks, and serviceability in reinforced concrete structures. Transportation agencies annually spend billions of dollars of taxpayer's money on the maintenance, repair, and construction of reinforced concrete structures [31]. A considerable portion of these infrastructures are in cold-climate regions and in marine environments where they frequently are in contact with deicers and seawater, increasing the risk of chloride-induced corrosion [34]. Seawater and de-icers are two main sources of external chlorides. Seawater contains roughly 3.5% salts by weight, primarily including ions such as Na^+, Mg^{2+}, Cl^-, and SO_4^{2-} [32]. Chloride bearing de-icing salt solutions are being used in winters to melt snow. The snow removal practices in different states recommend different application rates of brine salt solutions on pavements, depending on temperature, weather conditions, and type of maintenance activity [35]. In addition, after the snow melts, there is no washing-out process to remove excessive salts sprayed on concrete surfaces. The washing-out process can be highly effective in mitigating the risk of chloride-induced corrosion. This process helps remove chlorides-bearing salts from the

concrete surface before chloride ions have a chance to penetrate the concrete.

Understanding the chloride-induced corrosion mechanism and parameters that impact this phenomenon is a key step in improving longevity of reinforced concrete infrastructure. In this chapter, first a detailed description of chloride-induced corrosion in reinforced concrete is provided. Following on this, the impacts of chloride binding on chloride-induced corrosion is explained. Then, a review of prior studies on chloride binding in cementitious systems and key factors impacting chloride binding capacity is presented. Then a review of testing methods for chloride binding measurements is presented. Following on this, previous findings and current knowledge of chloride desorption is provided. At the end, a summary of knowledge gaps in the existing body of knowledge, proposed research questions, and primary objectives is presented.

2.2. Chloride-Induced Corrosion Mechanism

The onset of chloride-induced corrosion requires the presence of chloride ions, originating either from seawater or deicers, in combination with oxygen and humidity. When the chloride concentration exceeds a specific threshold, chloride-induced corrosion in reinforcement concrete can occur. This threshold value is typically called chloride threshold value or critical chloride content [31]. After more than 60 years of intense research, still there is a significant discrepancy on reported values of critical chloride content in the literature review [31] due to differences in measuring methods and experimental conditions [12, 31]. Reported critical chloride concentrations that initiated chloride-induced corrosion for Portland cement, range from as low as 0.05% to as high as 3% (percentage of cement weight) [12]. As per the Federal Highway Administration (FHWA) criteria, a chloride ion concentration of 0.15%, by weight of the cement, is acceptable but that 0.3% is considered dangerous and unacceptable [36]. ACI Committee 222 has been developing a standard method for testing and measuring the critical chloride value. However, the document

has not yet been released while this thesis is under investigation.

For reinforcing rebars in concrete, the concrete acts as a barrier that restricts the penetration of water and oxygen to the reinforcements' surface. Additionally, the alkaline environment within the concrete's pore solution contributes positively by forming a thin protective layer, known as a passive film, approximately a few nanometers thick, on the steel. However, this protective film becomes unstable in the presence of chloride ions or when the pH drops below around 9 [36]. Unfortunately, concrete is porous which permits chloride ions from de-icing salts or seawater to seep in. Atmospheric CO_2 can react with concrete to reduce the alkalinity of the concrete pore solution. The breakdown of the passive film by either chlorides or the CO_2 reaction, known as carbonation, leads to localized corrosion, resulting in significant metal loss. The rate of this localized corrosion can reach up to as high as one millimeter per year at high chloride ions concentration [37].

Corrosion of embedded steel reinforcements in concrete is an electrochemical process. Corrosion in reinforcing steel rebars in reinforced concrete structures involves the establishment of an anode and a cathode. The steel reinforcement plays as electrode and the concrete pore solution plays as electrolyte, i.e. an aqueous medium [38], forming a corrosion microcell at the microscopic level on the reinforcements. This microcell consists of adjacent anodes and cathodes. It should be noted that both an anode and a cathode can exist on the same metal piece, often due to a potential difference, or voltage, between two points on the metal [39]. This potential difference, which is the driving force for the microcell formation, is the measure of energy transfer between two circuit points, prompting electron flow from one point to another to achieve balance [40]. Factors contributing to these potential differences include the metal's non-uniformity, variations in the physical and surface conditions of steel, and the electrolyte's non-uniformity [37,

40]. For instance, areas of steel exposed to salts or solutions with lower pH levels can experience these differential conditions. An engineering example is reinforced concrete columns and piers in seawater environments supporting a bridge deck.

In the formed microcell on the surface of embedded steel in concrete, four primary reactions take place, ultimately leading to the formation of rust on the reinforcements. Equations (2.1) to (2.4) shows these four reactions [38, 41]. Within the corrosion microcell, the anodic area is where the corrosion process occurs. The anodic reaction, also known as oxidation, is shown in Eq. (2.1). This process involves consumption of steel reinforcements and release of electrons. The anodic reaction is the oxidation of iron (Fe) to iron II ions (Fe^{2+}), releasing electrons in the process. The anodic reaction is balanced by the cathodic reaction. The electrons released by the anodic reaction travel through the steel reinforcement to the cathodic area. Eq. (2.2) shows the cathodic reaction, known as reduction reaction. The cathodic reaction involves the reduction of oxygen in the presence of water, forming hydroxide ions (OH^-).

Additionally, chloride ions react with steel reinforcements to create ferrous chloride, as illustrated in Eq. (2.3). Subsequently, in the presence of moisture, ferrous chloride reacts with water, leading to the formation of ferrous hydroxide [40], commonly known as rust, on the reinforcement's surface, as shown in Eq. (2.4).

$$Fe \longrightarrow Fe^{2+} + 2e^{-} \quad \text{(Oxidation reaction)} \quad (2.1)$$

$$0.5O_2 + H_2O + 2e^{-} \longrightarrow 2(OH)^{-} \quad \text{(Reduction reaction)} \quad (2.2)$$

$$Fe^{2+} + 2\,Cl^{-} \longrightarrow FeCl_2 \quad \text{(Ferrous chloride formation)} \quad (2.3)$$

$$FeCl_2 + 2\,H_2O \longrightarrow 2\,HCl + Fe(OH)_2 \quad \text{(Rust formation: Ferrous Hydroxide)} \quad (2.4)$$

When corrosion happens, the volume of the rust is roughly two to six times greater than that of iron steel [42]. The growth of rust generates tensile stress on the adjacent concrete, resulting cracking, delamination, and spalling of concrete cover. Figure 2.1 displays a cross section of corroded reinforced concrete. In addition, HCl forms as a result of the ferrous chloride and water reaction, creating an acidic environment lowering the pH of the concrete [43]. Formed HCl will precipitate again into two H^+ and Cl^- ions, which can again react with Fe^{2+} and form more rust.

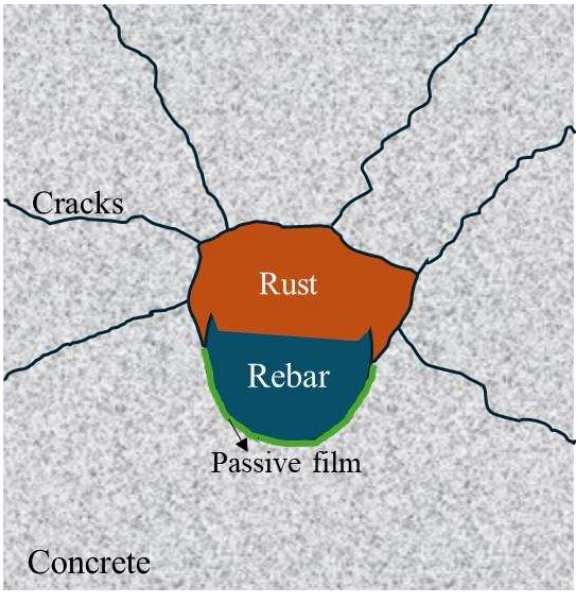

Figure 2.1. Schematic drawing of rebars corrosion on a cross section of reinforced concrete

2.3. Impacts of Chloride Binding on Service Life Prediction of Concrete Structures and the Chloride-Induced Corrosion Risk

There is not a single definition of the service life of a concrete structure, and it should be defined based on the project requirements, importance, etc. The service life of a structure can be defined as the time to corrosion initiation or the time the first repair is needed. In other words, the end of service life should be clearly defined whether by the owner or specific standard in the contract. One definition for end of service life if when the foreseen and expected function

(including but not limited to safety, appearance, structural or architectural requirements, etc.) is no longer fulfilled [44].

The service life predictions for existing concrete structures provide valuable insights on remaining service lifetime and use to plan repair and maintenance, if necessary [45]. In the service life-based design for new structures, the industry practice is that take into account the exposure condition of a concrete structure and design concrete mixture based on weathering and environmental factors. In addition, primary parameters in concrete mix design like w/cm ratio, min strength, min concrete cover, and maximum acceptable crack widths are selected in such a way to fulfill exposure condition such as frequent exposure to chloride ions. Service life models can be utilized for both new and existing concrete structures.

Several models are proposed to estimate the service life of reinforced concrete in a corrosive environment. Figure 2.2 shows an overview of service life prediction for concrete structures including primary inputs, common modeling software, and main outputs. As shown in Figure 2.2, exposure conditions such as the presence of chloride in the environment (in seawater or during winter season by using brine solution) and chloride transfer properties (such as chloride ion diffusivity) are two main inputs in the service life prediction models for concrete structures. Previous investigations showed that chloride ingress and transfer properties are influenced by chloride binding capacity of cementitious materials. The greater the chloride binding capacity of the concrete, the lower chloride ionic transport will be [46], meaning the longer the service life of concrete structures. This phenomenon has been addressed in Fickian service life models by incorporating the chloride binding capacity of a cementitious system in the chloride diffusion coefficient or as a sink term in service life models using the Nernst–Plank equation [47-49]. This

suggests that a key factor in extending the durability of concrete structures is enhancing their ability to bind chloride ions.

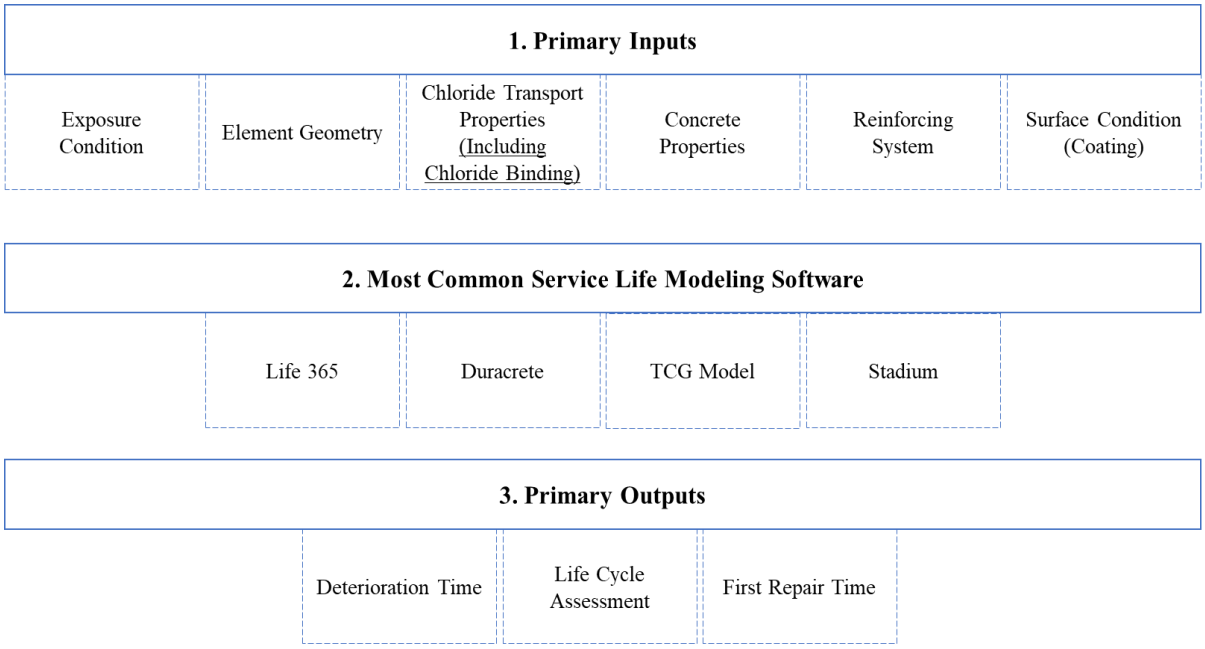

Figure 2.2. Overview of service life prediction for concrete structures: inputs, modeling software, and outputs

Chloride binding reduces the quantity of mobile chloride within concrete at almost all areas exposed to a chloride solution [50]. In addition, the chemical and physical bonds that form between the cement hydrates and chlorides can immobilize some fraction of the ingressed chlorides and slow the transport of the free chlorides in the concrete pore solution [51-53]. Thus, the chloride binding limits the free movement of chlorides inside concrete pores and is considered a favorable mechanism for reducing the risk of corrosion from a durability standpoint.

Chloride diffusion models are being used in service life prediction to estimate how fast chloride ions can ingress in a concrete structure. Several formula and models have been developed to predict how chloride diffuses in concrete containing different types of binders [54]. Each of these chloride diffusion models uses a different formula for chloride binding, often referred to as

a chloride binding isotherm. Consequently, accurate prediction of chloride transport goes hand to hand with understanding the chloride binding capacity of the binder. This involves employing chloride binding equations based on empirical data to predict the chloride binding capacity, thereby improving the prediction of the actual amount of chlorides available for causing corrosion in models that estimate the service life of concrete structures [55].

Therefore, increasing the chloride binding capacity of a cementitious system is one of the best practices to mitigate the risk of chloride induced corrosion and delay the time by which the chlorides can reach the steel. Increasing the chloride binding capacity in concrete reduces the availability of free chlorides to interact with concrete components and attack the reinforcement, enhancing the durability of concrete structures [56]. However, it should be taken into account that chloride binding is a reversible process.

The mentioned software packages in Figure 2.2 are capable of advanced modeling to take into account cracks, multi-layer systems (like having a coating on top and bottom of the concrete surface), and repairs (like having a 2" cover on top of the concrete surface after 50 years). While these numerical service life prediction models consider multiple properties as inputs including but not limited to concrete aging (which can change the concrete microstructure), changes in concrete pore solution pH, and chloride binding, the chloride desorption have not been considered yet.

2.4. Literature Review on Chloride Binding in Cementitious Systems

Chloride binding refers to a process by which chlorides form a physical or chemical bond with cement hydration products and are removed from the pore solution. Bound chlorides in cementitious systems are generally classified as chemically bound chlorides, in which chlorides substitute anions such as OH^-, CO_3^{2-}, SO_4^{2-} in the interlayer of the AFm phase to produce Friedel's

salt ($Ca_4Al_2(OH)_{12}Cl_2.4H_2O$) [57], and physically bound chlorides, which are mainly adsorbed on the surface of calcium silicate hydrates (C-S-H) [58].

Numerous variables can influence the mechanism of chloride binding. The factors most frequently reported as affecting chloride binding capacity of cementitious materials include, but are not limited to, chemical composition of cementitious materials [22, 23, 59-61], amount of water in the mixture (usually represented as a water to cement ratio) [62-64], curing condition [61, 65], chloride solution type and molarity [66-68], exposure solution condition (duration, temperatures, etc.) [69-72], testing sample saturation, chemical admixture types and dosage [73-76], testing sample type (Paste, mortar, and concrete), testing sample form (Disk, powder, or synthesized pore solution).

2.4.1 Impact of Binder Composition on Chloride Binding Capacity

Many research works have investigated how the composition of the binder affects the mechanism of chloride binding [61, 77, 78]. The aluminum content, significantly affects chemically bound chloride due to formation of more AFm (hydrated calcium aluminate phases) phases that have the ability to chemically react with chloride ions and form a new phase [19]. Ipavec et al. [79] studied the impact of different SCMs and limestone on chloride binding. Their findings suggest that chloride-bearing AFm compounds, like calcium monochloroaluminate hydrate (Friedel's salt), are the main forms of chemically bound chlorides. Rasheeduzzafar et al. [21, 59] noted that an increase in tricalcium aluminate (C3A) enhances chemical chloride binding and Friedel's salt formation. They found that chlorides mixed into the concrete bind more effectively than those entering from external sources.

The binding capacity of AFm phases, such as monosulfate, is stronger compared to C-S-H. However, given the higher prevalence of C-S-H in hydrated cementitious systems, the

proportion of chemically bound chlorides in Friedel's salt versus adsorbed chlorides on C-S-H depends on free chloride concentration. At concentrations below 1 M, chemical binding dominates, but at higher levels, physical binding becomes more significant [68].

The CaO-to-Al_2O_3 ratio (C/A) in the binder also influences chloride binding capacity. Both CaO and Al_2O_3 contribute to forming C-S-H and AFm phases, enhancing chloride binding. Wang et al. [80] studied varied binder chemical compositions and reported that when the C/A ratio is between 3 to 7 chloride binding capacity is maximum. At a C/A ratio above 7, chloride binding relies more on aluminum content and calcium is excessive. Conversely, a C/A ratio below 3 results in excess alumina, the chloride binding is highly linked to the calcium content.

For many decades, blended cements composed of ordinary Portland cement (OPC) with supplementary cementitious materials (SCMs) have been the first line of defense against durability issues and to extend the service life of concrete structures. The incorporation of supplementary cementitious materials (SCMs), which change the chemical composition of binders, influences chloride binding capacity in concrete [56, 61, 63]. The impact of various SCMs on chloride binding capacity has yielded mixed results. Using fly ash and slag generally enhances chloride binding, while silica fume tends to reduce it. The chloride binding capacity in cementitious systems with SCMs largely depends on the SCMs aluminum content [79]. Additionally, incorporating an SCM alters the pore solution chemistry, typically lowering its pH [81], due to the pozzolanic reaction where portlandite is consumed to form C-S-H [82, 83]. The three most commonly used SCMs in the concrete industry are fly ash, slag, and silica fume. In the following section the impacts of these SCMs on chloride binding are reviewed in detail.

2.4.1.1. Impact of Fly Ash Incorporation on Chloride Binding Capacity

Among various products available commercially, fly ash has been the cheapest and perhaps the most widely used SCM in the world [84]. Fly ash, a coal-fired power plant byproduct, is the most prevalent SCM in the United States, mainly due to its abundance. Geng et al. [56] reported that replacing 30% of OPC with class F fly ash and slag improves chloride binding capacity, with fly ash showing higher efficacy. Xu et al. [52] found similar results, noting that silica fume inclusion reduces chloride binding, but partial replacement of cement with fly ash and slag increases it. Ramirez-Ortiz et al. [85] examined the chloride binding performance of different cement pastes in NaCl solutions using ultrasonic detectors. Their results showed that incorporating 40% fly ash (40% fly ash + 60 % OPC) resulted in the highest chloride binding, followed by 10% silica fume (10% silica fume + 90% OPC), 20% fly ash (20% fly ash + 80% OPC), and OPC (100% OPC, no SCMs).

2.4.1.2. Impact of Slag Incorporation on Chloride Binding Capacity

The availability of fly ash has been considerably reduced due to recent environmental restrictions placed on coal-fired power plants [86]. Therefore, many state highway agencies and departments of transportation in the United States are exploring alternatives to fly ash. In recent years, the US concrete industry has used increasing amounts of ground granulated blast-furnace slag (GGBFS) cement, a by-product of steel production.

According to the Slag Cement Association, most states in the US witnessed an average increase of 11% to 14% in the annual consumption of GGBFS between 2015 and 2019 [87]. The increased usage of GGBFS is mainly due to the growing concerns about reducing the carbon footprint of concrete and the positive effects of GGBFS in this matter. The cradle-to-gate impact of producing GGBFS on global warming potential is almost seven times lower than that of OPC [88, 89].

Moreover, research shows that GGBFS concrete has a lower permeability [90-92], is more resistant to sulfate attack [93, 94] and the alkali–silica reaction [95, 96], and compared to Type I/II OPC, GGBFS-blended concrete generates less hydration heat, making it more suitable for mass concreting [97, 98].

The chloride-induced corrosion resistance of GGBFS concrete, among various durability issues, has received significant attention in the past 20 years [57, 99-104]. Research has shown that incorporating GGBFS in concrete can refine the concrete microstructure and immobilize the free movement of chloride ions in the concrete pore solution, slowing the ingress of chlorides in concrete [105, 106]. Compared to OPC, slag containing concrete contains less CaO but more Al_2O_3, leading to the formation of more AFm and C–S–H phases with a lower C/S ratio [107]. AFm phases are capable of chemically reacting with chloride ions [108], forming Friedel's salt which is a form of chemically bound chloride. Chlorides adsorbed on C-S-H gel is the main form of physically-bound chloride [109], enhancing chloride binding capacity.

2.4.1.3. Impact of Silica Fume Ash Incorporation on Chloride Binding Capacity

Silica fume has long been used to enhance the performance of high-strength concrete, improving both concrete mechanical strength and durability. In the concrete industry, the preferred type is densified silica fume, which is highly pozzolanic and rich in amorphous silica (over 85%). This amorphous silica reacts with portlandite ($Ca(OH)_2$) to form more C-S-H, enhancing the concrete's strength, density, and microstructure. Compared to other SCMs like fly ash and slag, densified silica fume features much smaller particles (0.1-0.5 μm) and a larger BET-specific surface area (greater than 13 m^2/g), leading to its typical usage being restricted to 5-10% of the weight of cementitious materials [110].

Incorporating silica fume in cement paste affects the chloride binding capacity in several ways. Silica fume incorporation in a mixture decreases chemical binding due to a reduction in aluminum-bearing hydrates (AFm phases) because there is almost no alumina content in silica fume that can participate in formation of AFm phases [111, 112]. The inclusion of silica fume can improve physical chloride binding by creating more C-S-H. However, the Ca/Si molar ratio of C-S-H is lowered, which results in a lower chloride binding capacity. Additionally, incorporating silica fume into concrete mixtures lowers the pH of the pore solution, which negatively impacts the stability of Friedel's salt [113], lowering the chloride binding capacity. Thomas et al. [114] reported that adding 8% silica fume (92% OPC + 8% silica fume) to ternary concrete reduced its chloride binding capacity. Similarly, Xu et al. [115] observed that partially replacing cement with silica fume could diminish the chloride binding capacity, attributing this effect to several factors: a decrease in pore solution pH, a lower Ca/Si ratio, and the dilution of C3A.

While these changes can negatively impact chloride binding, silica fume positively influences the physical characteristics of paste and concrete such as permeability and porosity. Silica fume inclusion enhances particle packing [116, 117] and serves as a nucleation site for cement hydration [118-121], significantly decreasing permeability and porosity, thereby boosting the material's overall durability [122, 123].

2.4.2. Impact of Brine Solution Type on Chloride Binding Capacity

Another key factor influencing the chloride-binding characteristics of cementitious systems is the type of cation present in the chloride salt. Sodium chloride includes sodium ions (Na^+) that carry a single positive charge. Calcium chloride and magnesium chloride contain calcium ions (Ca^{2+}) and magnesium ions (Mg^{2+}), respectively, with a double positive charge. The distinct cations of sodium chloride, calcium chloride, and magnesium chloride potentially

influence their solubility, conductivity, and reaction in various solutions and chloride binding in cementitious systems [124, 125].

It is well-known that bound chloride quantities for binders exposed to $CaCl_2$ and $MgCl_2$ solutions are higher than NaCl solution. However, there are discrepancies in the reported results for $CaCl_2$ and $MgCl_2$. Some investigations reported higher chloride binding capacity for $MgCl_2$ than $CaCl_2$ and others reported the opposite.

Zhu et al. [124] reported that the chloride binding capability and the pore solution pH are considerably affected by chloride cation type with binding capacity of Ca^{2+}> Mg^{2+} > Na^{+}. They concluded that Na^{+} resulted in a rise of the pore solution pH, increasing the solubility of Friedel's salt and releasing the bound chlorides. Conversely, Mg^{2+} leads to a decrease of the pore solution pH through consuming hydrated C–S–H, consequently producing a lower pH and less free chloride ions than Na^{+}. Having Ca^{2+} can form more C–S–H compared to Na^{+} and Mg^{2+}. C–S–H binds more chloride ions than M–S–H, therefore, a higher bound chloride capability resulted in Ca^{2+} than Mg^{2+} and Na^{+}.

De Weerdt et al [126] found a higher or equal chloride binding capacity when the cation is Mg^{2+} compared to Ca^{2+}. They reported that, in general, bivalent cations, such as calcium and magnesium, resulted in higher chloride binding compared to monovalent sodium. They reported that the main reason for their observation is that adsorption of calcium onto the calcium silicate (aluminate) hydrate C(-A)-S-H) surface increases when a binder is exposed to Mg^{2+} and Ca^{2+}. Calcium uptake increases the positive charge of C(-A)-S-H surface, facilitating the retention of chloride ions within the diffuse layer.

Babaahmadi et al. [127] found that exposure of cement binders to $CaCl_2$ resulted in a higher chloride binding compared to NaCl. The underlying reason is twofold, first the formation of more

Cl-AFm (chemically chloride binding) in binders exposed to $CaCl_2$. Second, exposure to $CaCl_2$ results in a greater extent of physical chloride binding compared to NaCl exposure. The former is attributed to a higher reduction in aluminum uptake in the C-S-H (or C(-A)-S-H) when binders are exposed to $CaCl_2$ and the latter is explained by the higher calcium concentration in the exposure solution, coupled with the lower Al/Si ratio in the C-S-H (or C(-A)-S-H).

Past studies have indicated that the pore solution's pH rises when NaCl is present, while it decreases with the presence of $CaCl_2$ and $MgCl_2$ [73, 74, 124]. When NaCl reacts with cement hydration products the following reaction happens as described in Eq. (2.5). The sodium and hydroxide ions combine to form sodium hydroxide, as shown in Eq. (2.6). Sodium hydroxide is a strong base, leading to an increase in the pH of the pore solution.

$$C_3A + Ca(OH)_2 + 2NaCl + 10H2O \rightarrow 2Na^+ + 2OH^- + C_3A.CaCl_2 + 10H_2O \quad (2.5)$$

$$Na^+ + OH^- \rightarrow NaOH \quad (2.6)$$

In general, an increase in the pH of the pore solution leads to a decrease in the amount of bound chlorides [111, 128, 129]. This is because chlorides first form a chemical bond with tricalcium aluminate or its hydrates to form Friedel's salt [130]. The pH of the pore solution increases in the presence of NaCl, and the solubility of Friedel's salt is also pH dependent. An increase in the pH of the pore solution leads to a decrease in the number of bound chlorides and an increases the solubility of Friedel's salt [62, 129].

Ca^{2+} from calcium-bearing salts, however, can contribute to the development of more C–S–H, which can take up more chlorides from the solution and release H^+ back to the solution in return, leading to a significant reduction in the pH of the solution [131]. The presence of Mg^{2+} can lead to the formation of brucite and an increased Ca/Si ratio in the C–S–H gel, which in turn can increase the chloride uptake capability of the C–S–H [82].

2.4.3. The Relationship between Free and Bound Chloride in Cementitious Materials

The interaction and relations between free and bound chloride concentrations in different cementitious systems has been extensively studied [19, 132, 133]. The relationship between free and bound chloride ions in various free chloride concentrations at a specific temperature is described as chloride binding isotherms.

Extensive research [134-136] has proposed various models and equations to estimate chloride binding, calculating the proportion of chlorides that penetrate concrete and actively contribute to the corrosion of reinforcing steel bars. This knowledge is crucial for predicting when rebar corrosion in concrete structures will begin. Thus, accurate determination of the chloride binding isotherms of cement-based materials is vital for forecasting the service life of reinforced concrete structures. The Langmuir and Freundlich isotherms are two commonly used equations in this field of research. They help estimate chloride binding and describe the relationship between free and bound chlorides in cementitious systems.

These isotherms, shown in Equations (2.7) and (2.8), predict chloride binding levels based on known concentrations of free chloride. Free chloride levels can be easily determined using methods like titration, whether dealing with chloride-containing deicers or seawater chloride ions.

$$C_b\big|_{Langmuir} = \frac{\alpha_L C_f}{\left(1+\beta_L C_f\right)} \tag{2.7}$$

$$C_b\big|_{Freundlich} = \alpha_F C_f^{\beta_F} \tag{2.8}$$

C_f : Measured free chloride

C_b: Calculated bound chloride

$\alpha_{.}$ and $\beta_{.}$: Values calculated numerically by fitting Eq. (2.7) or Eq. (2.8) to the results obtained from titration results

When the β value in the Langmuir isotherm is zero, the model simplifies to a linear equation, commonly referred to as a linear chloride binding isotherm. A key distinction between the Langmuir and Freundlich isotherms is their behavior at high chloride concentrations. The Langmuir isotherm's slope gradually levels off at high concentrations of free chloride, while the Freundlich isotherm's slope can continue to increase indefinitely.

The concrete matrix has a limited amount of hydration products available for binding chlorides, both physically and chemically. Once these binding sites and hydration products are fully utilized, no additional binding can occur, meaning the rate of chloride binding eventually drops to zero. Consequently, the binding capacity of cementitious systems is finite. In research literature, this capacity is often quantified as the rate of change in bound chloride relative to free chloride. Equations (2.9) and (2.10) demonstrate how the binding capacities are calculated for the Langmuir and Freundlich isotherms, respectively.

$$\frac{\partial C_b}{\partial C_f}\Big|_{Langnuir} = \frac{\alpha_L}{\left(1+\beta_L C_f\right)^2} \tag{2.9}$$

$$\frac{\partial C_b}{\partial C_f}\Big|_{Freundlich} = \alpha_F \beta_F C_f^{\beta_f - 1} \tag{2.10}$$

2.4.4. Effects of pH of Concrete Pore Solution on Chloride Binding Capacity

Previous research has shown that the pH of the pore solution increases in the presence of NaCl and decreases in the presence of $CaCl_2$ and $MgCl_2$ [82, 124, 128]. In general, an increase in the pH of the pore solution leads to a decrease in the number of bound chlorides [111, 128, 129].

In the chloride binding process, chloride ions first form a chemical bond with tricalcium aluminate or its hydrates to form Friedel's salt $C_3A.CaCl_2.10H_2O$ [130]. The solubility of Friedel's

salt is pH-dependent, and, therefore, the rise in pH as a result of the exposure to NaCl solution can increase the solubility of Friedel's salt and reduce the concentration of bound chlorides [62, 129].

Ca^{2+} from calcium-bearing salts, however, can contribute to the development of more C–S–H, which can take up more chlorides from the solution and release H^+ back to the solution in return, leading to a significant reduction in the pH of the solution [131]. Similarly, the presence of Mg^{2+} can lead to the formation of brucite and an increased Ca/Si ratio in the C–S–H gel, which in turn can increase the chloride uptake capability of the C–S–H [82].

Alkali content affects chloride binding in two ways. Increased alkali levels inhibit chloride binding, as chlorides and alkalis compete for binding with hydration products like C-S-H. Additionally, higher alkali content raises pore solution pH [137], lowering the Cl^-/ OH^- [59]. Tritthart et al. [131] found an inverse relationship between OH^- concentration in the pore solution and bound chloride numbers, as Cl^- and OH^- ions compete for adsorption on hydrated cement.

2.4.5 Limitations of the Chloride Binding Test Method

In the early 1990s, Luping and Nilsson [138] introduced an equilibrium testing procedure to measure the bound chlorides in mortar samples using ordinary Portland cement. The original test proposed by Luping and Nilsson takes at least 59 days to complete. The test involves exposing pulverized pieces of vacuumed mortar samples to a saturated lime solution at different known chloride concentrations and measuring the concentration of the supernatant solution after the sample reaches equilibrium with the solution.

Although extensive research has been conducted to examine the various factors that impact chloride binding in cementitious materials [4, 18, 58, 62, 63, 77, 78, 82, 97, 101, 106, 124, 131, 136, 139-153], little attention has been paid to the effects of changes to the testing protocol. There

are several factors that can affect the results of chloride binding tests, such as the sample's saturation state, the exposure solution's composition, the form of the sample or its surface area-to-volume ratio, and the solid-to-exposure liquid mass ratio.

The state of saturation of a sample plays a crucial role in chloride binding, and it is important to take this into consideration when evaluating the performance of a sample in real-world conditions [154]. When a sample is in a dry state, capillary action is strong and liquid is drawn into the capillaries. This increases the concentration of chlorides and increases the chances of chloride binding in the pores [155]. However, in a saturated sample the pressure of the liquid in the pores partially counteracts the capillary forces, resulting in a weaker driving force for additional liquid to be drawn in. This means that the movement of chlorides is instead governed predominantly by diffusion [139, 156]. As such, ignoring the saturation state of a sample can lead to inaccurate estimates of its behavior and performance in real-world conditions [157].

In chloride binding tests, there is also a lack of standardization when it comes to different exposure solutions. Some tests use pure chloride solutions made with water, while others add other ions to create a solution that more closely resembles the pore solution found in concrete. This lack of standardization can lead to discrepancies between results when comparing different tests and exposes a need for further research and development in order to achieve a more uniform standard [111, 157]. The presence of ions such as calcium, magnesium, and sulfates in the exposure solution can impact the stability and solubility of chlorides and their ability to bond with cement hydration products [56, 144, 158-161]. The pH of the pore solution can also affect the bonding ability of chlorides, with higher pH promoting chloride bonding and lower pH inhibiting it [129, 150]. The choice of exposure solution, such as a saturated lime solution or synthetic pore solution, can result in different outcomes, due to differences in ionic composition and pH. This may lead to inaccurate

results, as the exposure solution may not reflect realistic conditions in the concrete's pore solution. Choosing the right exposure solution is crucial for achieving accurate results and ensuring their relevance to real-world scenarios.

The selection between solid, crushed, and ground concrete samples, can also have a major effect on the precision and consistency of the results in chloride binding tests [162]. Powder concrete samples, which are made by grinding or pulverizing a solid concrete sample, tend to have a larger exposed surface area, making them more likely to bind chlorides. By contrast, solid concrete samples are more representative of field conditions and have less surface area and lower chloride binding potential than pulverized samples. Furthermore, the shape of the sample can affect the distribution of chloride ions inside the sample, potentially impacting the accuracy of the results. For instance, pulverized concrete samples are exposed to uniform chloride concentrations, while the concentration of ingressed chlorides decreases with depth in solid samples. Although the chloride binding capacity in solid samples is averaged over depth and may lead to an underestimation of binding capacity, it may provide a more representative value for actual field conditions.

Another overlooked testing parameter in chloride binding tests is the mass ratio of solids to exposure liquid. The quantity of exposure fluid used normally depends on the area of the sample, but this may vary based on the test method and equipment. It is important for the chloride solution to be enough to fully submerge the concrete sample. Despite this, there is no available information or experimentation looking into the effects of solid-to-exposure liquid ratio on chloride binding results. This ratio can have an effect on the exposure's uniformity and the distribution of chloride ions in the sample, which may then lead to inaccuracies in the results.

In real case scenarios, the majority of concrete infrastructures, including concrete

pavements and bridges, are exposed to carbonation and chemical attacks that can lead to release of bound chloride, which in this dissertation, it is called “chloride desorption”. Chloride desorption, which means the release of bound chloride from cement hydration products, increases the concentration of free chloride in the concrete, increasing the risk of chloride induced corrosion. In the following section, a review of current knowledge and reports on change in chloride binding after a pH change and chloride desorption mechanism is provided.

Many researchers have adopted or modified the Luping and Nilsso method to estimate the chloride binding capacity of various cementitious systems, however, it has several drawbacks including:

i) The test has a tendency to oversimplify actual environmental conditions, such as the impact of the exposure environment and the presence of other impurities, which may affect the accuracy of the results.

ii) The test frequently concentrates on short-term performance and may not precisely reflect the long-term behavior of concrete in real-world situations.

iii) The methods used in the test are not standardized, making it challenging to compare findings across different laboratories and studies.

2.5. Literature Review on Chloride Desorption Mechanism

Various studies examining the effects of pH changes on chloride binding in cementitious materials have noted alterations in chloride binding capacity at different pH levels. Although these studies did not specifically focus on or discuss the mechanism of chloride desorption, their findings offer worthy insights.

As mentioned earlier, the release of bound chlorides, often triggered by a decrease in the alkalinity (lowering of pH) of the cement pore solution, can initiate due to processes such as

carbonation [163], sulfate attack [164], and acid attack [83]. Bound chlorides can be released to their free state in the pore solution if the pH of the concrete pore solution falls below 12 [66, 165].

Long et al. [166] have observed that up to 88% of bound chlorides in powdered cement samples exposed to a 3 M NaCl solution were released when the pH dropped below 9. Similarly, Hemstad et al. [83] have reported 100% chloride desorption in paste specimens subjected to a 4 mol/L HCl solution. Cheng [140] has also found that a fully carbonated OPC paste with a pH of 7 is incapable of any form of chloride binding.

Many gaps in understanding remain regarding the chloride desorption mechanism, and little is known about the roles of different types of SCMs in resisting the release of bound chlorides.

2.5.1. Impacts of Carbonation on Chloride Desorption Mechanism

When atmospheric carbon dioxide (CO_2) enters concrete, it reacts and forms carbonic acid. The pH levels in fully carbonated concrete varies according to different studies: Chang [140] found it to be around 7, Geng et al. [167] noted it closer to 9, and Sun et al. [168] observed 8.3.

It is important to note that since chloride ions move through concrete faster than carbonation, it is generally more representative of what actually happens in the field, to first expose concrete to chlorides before carbonating it [169].

Carbonation also affects how concrete binds with chloride. Carbonation breaks down certain hydration products, like C-S-H, which are essential for trapping chlorides [3]. Carbonation can dissolve Friedel's salt [169], as shown in Equations (2.11) and (2.14). This process can increase the concentration of free chlorides in the concrete.

$$CO_2 + H_2O \rightarrow H_2CO_3 \tag{2.11}$$

$$H_2CO_3 + Ca(OH)_2 \rightarrow CaCO_3 + 2H_2O \tag{2.12}$$

$$CO_2 + H_2O + \text{C-S-H} \rightarrow CaCO_3 + SiO_2.nH_2O \tag{2.13}$$

$$3CaO.Al_2O_3.CaCl_2.10H_2O + 3CO_2 \rightarrow 3CaCO_3 + Al_2O_3 + Ca^{+2} + 2Cl^{-} + 10H_2O \quad (2.14)$$

In binders that include supplementary cementitious materials (SCMs), the rate and extent of carbonation, especially in the C-S-H phase, are higher than in ordinary Portland cement (OPC) under similar conditions. This is largely due to the reduced presence of portlandite in SCM binders[163, 170]. Zheng et al. [163] conducted research on how carbonation affects chloride binding in binders with various compositions and water-to-binder ratios. They found that SCM-containing binders had a lower pH after carbonation and a corresponding decrease in chloride binding as the pH dropped.

Chang [140] reported on the chloride binding capacity in two sets of binders: one carbonated before chloride exposure and the other exposed to chlorides before carbonation. The results indicated that, in both scenarios, the amount of bound chloride dwindled to nearly zero after complete carbonation.

2.5.2. Impacts of Acid Attack on Chloride Desorption Mechanism

An acid attack on cementitious materials comprises several complicated processes and typically involves the dissolution of hydrated phases capable of binding chlorides [171]. The chemical reactions of an acid with a general formula of HA and cement hydration products can dissolve the main hydrated phases, producing calcium salts. The generic forms of the acid reaction with portlandite and calcium silicate hydrate are shown in Equations (2.15) and (2.16) [171].

$$2HA + Ca(OH)_2 \rightarrow CaA_2 + 2H_2O \quad (2.15)$$

$$2xHA + xCaO \times ySiO_2 \times nH_2O \rightarrow CaA_2 + ySi(OH)_4 + (x + n - 2y)H_2O \quad (2.16)$$

During an acid attack, a highly porous layer of silicate hydrates and ferric hydroxide is formed on the surface of the concrete (or paste). This layer acts as a buffering layer against the drop in pH and progression of acid damage [172, 173]. An acid attack on cementitious systems is

followed by shrinkage cracks leading to increased permeability of the concrete [171, 174]. Therefore, when chloride ions are present during an acid attack, they can enter the concrete through these cracks.

The current state-of-the-art in chloride binding indicates that the dissolution of hydrated phases can significantly reduce the chloride binding capacity of cementitious systems. In one study, Hemstad et al. [83] observed reduced chloride binding at pH below 12, and no chloride binding at pH below 9 in OPC samples exposed to hydrochloric acid. They attributed the reduction in chloride binding to the dissolution of the AFm phase, which is primarily responsible for the chemical binding of chloride. In addition, they observed a higher free chloride concentration when acid molarity and volume were increased.

Similarly, Long et al. [166] reported that at pH levels below 9, 88% of the previously bound chlorides in an OPC system disassociated and returned to the pore solution. They noted that the highest desorption of bound chlorides was detected at a pH of 9. Gutberlet et al. [175] also observed the conversion of monosulfate to Friedel's salt and ettringite when hydrated Portland cement disks were exposed to hydrochloric acid. In a recent study, Teymouri et al. showed that despite the common view that a continuous reduction in the pH of the exposure solution leads to a continuous release of bound chlorides, the desorption of bound chlorides is a very complex phenomenon involving releasing and rebinding of chlorides by the hydrogels that are produced during an acid attack.

Based on the findings reported in previous studies [83, 166, 176], a reduction in the pH of the pore solution, whether triggered by carbonation, sulfate, or acid, can significantly influence the chloride binding mechanism, leading to chloride desorption in cementitious systems. In terms of acid attack, there is a complex interplay between leaching of cement hydration products, formation

of new phases, alteration of microstructure, cracking, and increased concrete permeability. A few investigations have studied how acid attacks lead to chloride desorption in cementitious systems [66, 83, 176]. In addition, while chloride binding mechanism for various cementitious systems have been investigated, it is not yet clear what proportion of bound chlorides are released and returned to the concrete pore solution when samples made of blended cement are exposed to a low pH environment.

2.5.3. Impacts of Sulfate Attack on Chloride Desorption Mechanism

Sulfate ions, which can come from sources like seawater, soil, groundwater, and industrial waste, have a notable impact on concrete. When sulfate ions are present in the pore solution, they reduce the system's ability to bind with chlorides. This is because they lead to the creation of more ettringite, a substance incapable of binding with chloride ions. Furthermore, these sulfate ions can transform Fridel’s salt into ettringite, increasing the concentration of free chlorides in the pore solution and heightening the risk of corrosion caused by chlorides [177]. Additionally, these ions vie with chlorides for absorption onto C-S-H phases. The C-S-H phases tend to bond more readily with sulfate ions, integrating more sulfates and consequently diminishing the concrete's capacity to bind with chlorides [115, 159, 177].

When sulfates enter concrete, they first react with portlandite to create gypsum ($CaSO_4$). This gypsum then interacts with C3A, forming a substance called ettringite [115, 178]. Research by Geng et al. [56] has shown that chloride binding stability in pastes changes under attacks from sodium sulfate (Na_2SO_4) and magnesium sulfate ($MgSO_4$). They noticed that while most bound chlorides are released under a sulfate attack, the presence of $MgSO_4$ leads to less conversion of Fridel's salt to ettringite due to brucite formation, which hinders ionic movement. The same observation was reported in [159]. Sulfate ions don't just increase free chlorides; they also compete

with them for space on C-S-H phases. C-S-H tends to bond more with sulfates than chlorides, leading to a reduced ability to bind chlorides in the concrete. De Weerdt et al. [128] have proposed that sulfate ions encourage the conversion of AFm to ettringite while increasing sulfate binding in C-S-H.

In marine environments, where seawater's sulfate concentration is high, nearly 2700 ppm SO_4^{2-} [179], concrete samples often show significant chloride release. This is mainly due to the transformation of Fridel's salt into ettringite. Xu et al. [115] found that the extent of chloride release is influenced by factors like the water-to-binder ratio, the total chloride content, and the type of sulfate cations present. Their studies revealed that out of various sulfate salts, exposure to potassium sulfate (K_2SO_4) resulted in the highest chloride desorption.

2.6. What Has Been Accomplished and What Remains to be Addressed in Chloride Binding and Chloride-Induced Corrosion Research?

Chloride-induced corrosion is a complex process depending on multiple factors including but not limited to concrete properties, construction practices, reinforcement type and condition, chloride ion concentration, and concrete permeability. The complexity increases as the moisture content and humidity levels vary across different structures [180].

Numerous studies have been conducted on the diffusion of chloride and chloride binding capacity in concrete containing various cementitious materials, assessing the impact of different environmental conditions [71, 136, 181, 182]. These studies have adequately highlighted the prime role of chloride binding mechanism in delaying chloride ingress and the onset of reinforcement corrosion [183]. The formation of chemical and physical bonds between cement hydrates and chlorides can effectively immobilize some of the penetrating chlorides, reducing the movement of free chlorides within the concrete pore solution [51-53].

There are still many unanswered questions necessitating further research, including the roles of SCMs and the cation of the chloride salt in the desorption mechanism of bound chlorides. Although the positive impacts of SCMs on increased chloride binding capacity have been well documented [53, 77], the role of SCMs in suppressing the release of bound chlorides when the pH of the pore solution drops remains unclear, and the current state-of-the-art in chloride-induced corrosion and service life modeling is limited to quantifying the portion of released chlorides due to the decreased pH of the exposure environment.

2.7. Identified Knowledge Gaps

Based on the previous research findings described and analyzed in the current literature review on chloride binding mechanism and chloride desorption phenomenon the following knowledge gaps are recognized:

1- There is an undeniable need for standardizing the chloride binding testing procedure to minimize the risk of result variations under varying testing conditions. These testing conditions included but are not limited to saturation states, solution chemistry, sample form, and solid-to-liquid mass ratios. In addition, these testing conditions must be representative of the real-case scenario. For instance, exposing powdered (grinded) paste or concrete samples to salt solutions and measuring chloride binding capacity is not representative of the real condition. Another example is that using fully dried paste or concrete samples and then exposing them to salts for measuring the chloride binding capacity is not realistic, leading to misleading results.

2- There is limited knowledge of the chloride desorption mechanism in conventional concrete and concrete containing SCMs such as fly ash, slag, and silica fume. As an underrated phenomenon that can impact the chloride-induced corrosion rate in concrete structures more details and methodic investigations are needed to have a full grasp of chloride desorption

mechanism. The existing methods for estimating the service life of concrete structures effectively assess the rate of chloride binding and its impact on the initiation of corrosion. However, there has been no empirical or theoretical research so far to evaluate the kinetics of chloride desorption and its effects on the residual service life of concrete structures.

3- The chloride desorption mechanism and pH change in cement exposed to de-icing brine solutions under carbonation as one of the most critical durability issues. The combined and synergic impacts of these phenomenon have not been fully addressed.

2.8. Research Questions and Objectives

The overarching aim of this dissertation is to enhance the existing body of knowledge regarding chloride desorption mechanism and address current shortcomings in the reliable service life prediction of concrete infrastructure. Based on the recognized knowledge gaps in the literature review and preliminary data research questions are developed and listed in Table 2.1.

Table 2.1. Proposed research questions

	Proposed Research Questions
Question 1	How does the type of brine solution affect chloride binding measurements in specimens (varying in shape, saturation conditions, and solution-to-sample mass ratios)?
Question 2	What are the chloride binding and desorption capacities of Portland cement concrete when exposed to NaCl, $CaCl_2$, and $MgCl_2$ brine solutions?
Question 3	How does exposure to brine solutions impact the chloride binding capacity and desorption in cementitious systems containing slag, fly ash, and silica fume?
Question 4	What are the combined effects of brine solutions and carbonation on pH change over time and chloride desorption in Portland cement paste?

The approach of this thesis is to conduct a methodical and comprehensive study of the chloride desorption behavior in different cementitious systems, containing ordinary Portland

cement (OPC) Type I/II and the three most commonly used SCMs in construction projects including fly ash, slag, and silica fume. In addition, due to the absence of standardized testing protocols for chloride binding measurements, this dissertation investigates the impact of various testing protocols on chloride binding capacity in cement pastes.

These objectives are conducted in a sequential order, with the knowledge gained at each step informing the subsequent ones. The first objective recognizes the lack of uniformity in current practices for chloride binding measurements and provides recommendations for future chloride binding measurements, which were utilized in testing procedures for the other objectives.

Following this, the second and third objectives focus on exploring the chloride desorption mechanism in pastes containing OPC and various types and replacements of SCMs. Finally, the fourth objective bridges the gap between laboratory findings regarding chloride desorption and their practical application. This objective investigates how environmental factors, like carbonation and exposure to a brine solution, affect the pH of cementitious systems, thereby impacting chloride binding and desorption, facilitating the estimation of chloride desorption in real infrastructure over time by measuring pH levels.

Objective 1: Investigate the factors impacting chloride binding measurements: No standard method for chloride binding tests has yet been introduced. This objective aims to investigate the impact of various factors on chloride binding capacity to establish a standardized testing methodology. Four key factors will be evaluated, including the saturation state of the concrete sample, the composition of the exposure solution, the form of the sample, and the solid-to-exposure solution mass ratio. By controlling these factors, this study aims to ensure consistent and comparable results in future investigations.

Objective 2: Investigate the chloride binding and desorption capacity for ordinary Portland cement (OPC) cement paste: This objective represents one of the first systematic efforts to investigate the kinetics of chloride desorption in Type I/II cement. In this objective, the dissociation behavior of bound chloride in a low-pH environment is utilized as an indicator for comparing the chloride-binding strength of OPC paste when exposed to de-icing salt solutions.

Objective 3: Investigate the chloride binding capacity and desorption for pastes containing SCMs: This objective explores the chloride binding and desorption mechanisms in ordinary Portland cement and seven different blended binders including 15% and 30% fly ash, 25% and 50% Slag, 5% and 10% silica fume, when exposed to different de-icing salt solutions in a low pH environment.

Objective 4: Synergic effects of exposure of blended cement pastes containing fly ash to NaCl salt solution and carbonation on pH and composition of pastes: The primary goal of the last objective is to monitor change in pH and composition of pastes over time to measure the release of bound chloride (chloride desorption) under carbonation. This objective aims to bridge the gap between laboratory and field measurements. Chloride desorption in pH dependent. By using a straightforward pH measuring technique, this approach offers a practical method for estimating chloride desorption in cement over time.

Chapter 3 : Methodology

To ensure clarity and coherence in presenting the research methodology, a separate methods section for each objective is provided. It is important to note that all cementitious materials, salts, and equipment were sourced from a single, respective source, ensuring uniformity and accuracy throughout the study.

3.1. Objective 1: Evaluating the Effects of Sample Forms, Saturation Rates, and Solution Types on Chloride Binding Measurements

Figure 3.1 provides a summary of experimental variables for this objective. The primary aim is to assess the influence of sample forms, saturation rates, and solution types on chloride binding measurements. The investigated factors included three different saturation levels of pastes right before immersion in salt solutions (0%, 50%, and fully saturated), four exposure solutions with varying chemical compositions including pure NaCl, NaCl dissolved in $Ca(OH)_2$, NaCl dissolved in ($Ca(OH)_2$ + KOH), and NaCl dissolved in pore solution ($Ca(OH)_2$,+NaOH,+KOH), three sample forms (disk, crushed, and powder), and three solid-to-exposure solution mass ratio (1:3, 1:6, and 1:10).

Paste samples were made using ordinary Portland cement (OPC) meeting the requirements for Type I-II Portland cement as specified by ASTM C150 [184] and AASHTO M 85 [185] standards. Table 3.1 lists the oxide composition of OPC cement. All solutions including NaCl, $Ca(OH)_2$, ($Ca(OH)_2$ + KOH), and pore solution ($Ca(OH)_2$,+NaOH,+KOH were prepared using ACS-grade NaCl, $Ca(OH)_2$, KOH, and NaOH with distilled water. The details of solution preparations are provided in the following sections.

OPC Paste samples were prepared using a 5-liter mortar mixer (Humboldt Mfg.) with a water-to-cement ratio (w/c) of 0.4, following the mixing process outlined in ASTM C305 [186]. Once mixed, the samples were poured into disk-shaped molds that were 33 mm in diameter and 15 mm deep. A total of 64 disks were produced and then sealed in molds and placed in an environmental chamber at a temperature of 25°C and a relative humidity of 95%. After 24 hours, the samples were removed from the molds, stored in Ziplock bags, and sealed before being cured in the environmental chamber at a temperature of 25°C and relative humidity of 95% for 28 days.

Table 3.1. Chemical composition of ordinary Portland cement

	SiO_2	Al_2O_3	Fe_2O_3	CaO	MgO	SO_3	Na_2O	K_2O	LOI
Cement Type I/II	19.24	3.80	2.75	59.05	1.5	2.49	0.17	0.60	9.90

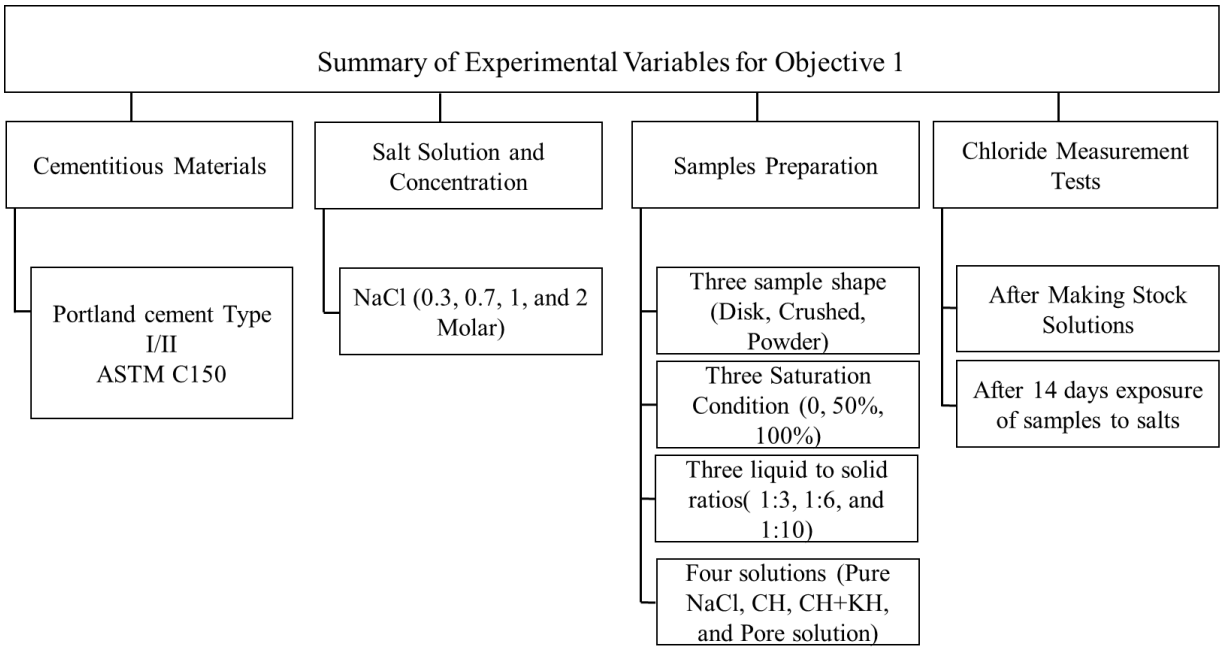

Figure 3.1. Summary of experimental variables for objective 1

Figure 3.2 displays a visual representation of the experimental design implemented in this study. The figure utilizes various colors and patterns to indicate the specific types of samples,

saturation state, and chloride solution chemistry that were utilized to test each variable. For instance, samples in the form of disks (represented with a net pattern) were used to examine the effect of saturation state and solution chemistry. All the samples that were utilized to test the impact of solution chemistry, sample form, and solid-to-exposure were in a dry state, which is indicated by a light grey color. Finally, crushed samples were used to assess the influence of the solid-to-exposure solution mass ratio. The asterisk accompanying each sub-experiment indicate that the exposure solution used in that particular experiment was prepared using plain distilled water and NaCl at a specific concentration.

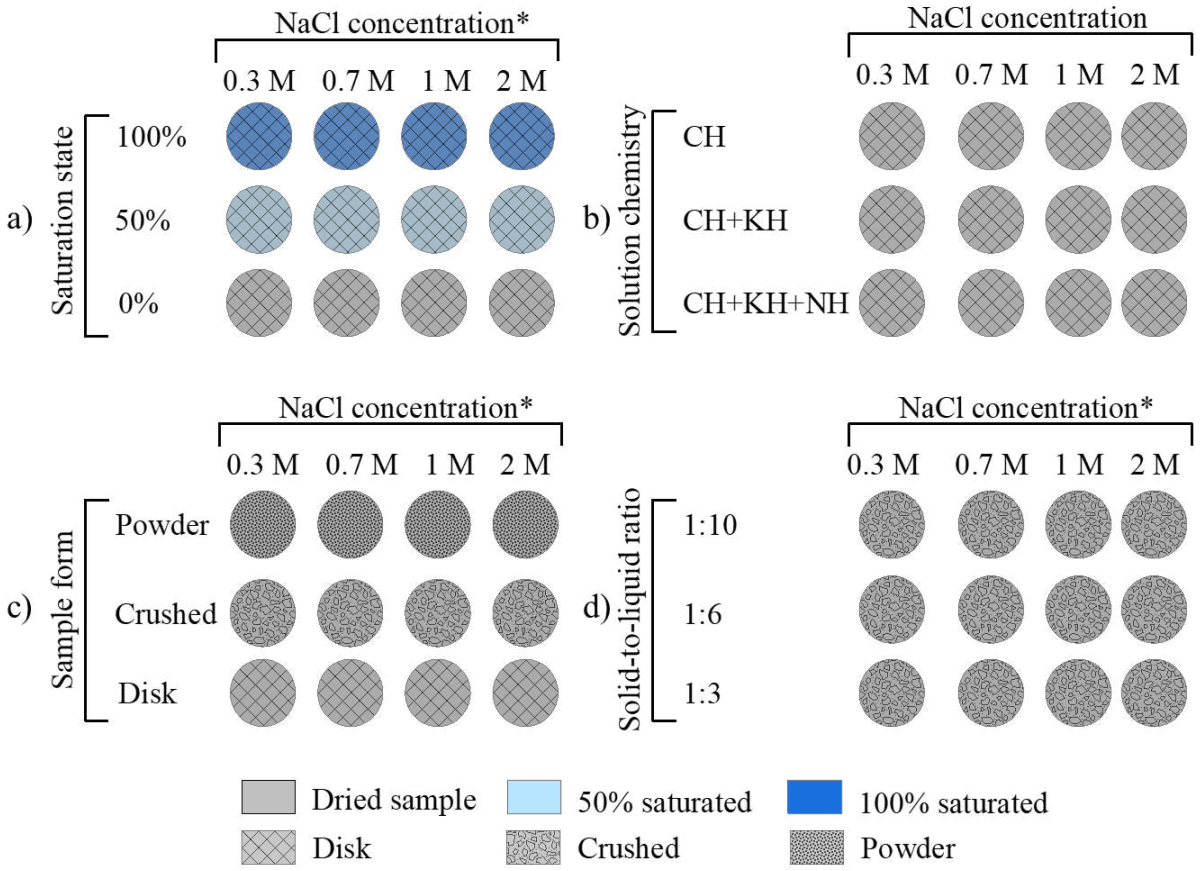

Figure 3.2. Schematic drawing of test setup (a) saturation state, (b) solution chemistry, (c) shape form, and (d) solid-to-liquid ratio. (CH: $Ca(OH)_2$; KH: KOH; NH: NaOH)
(The * indicates that the exposure solution was prepared by dissolving NaCl in distilled water)

3.1.1. Sample Saturation

The impact of saturation state on chloride binding was examined using disk samples. The disks were first subjected to a temperature of 57°C within a vacuum oven for a period of one week. To ensure complete drying and prevent carbonation, soda lime and silica gel pellets were placed inside the oven. Following the drying process, a total of 16 disks were weighed and submerged in distilled water. They were then left inside a BACOENG vacuum chamber, as shown in Figure 3.3, for 36 hours, during which a vacuum pump produced negative pressure of 82 kPa (0.82 bar) within the chamber. Following this, the weight of the samples in the fully saturated state was recorded. To achieve a saturation level of 50%, 8 fully saturated samples were placed in an oven and exposed to a temperature of 57°C. Their weight was monitored at 15-minute intervals to determine the point of 50% saturation based on the difference between their dry and fully saturated weights.

Figure 3.3. The experimental setup used for saturating disk samples

3.1.2. Exposure Solutions

To investigate chloride binding capacity of OPC samples, four different concentrations of chloride (0.3, 0.7, 1, and 2 M) were used in this study. NaCl solution is the most commonly used deicer and, as such, was tested in different concentrations ranging from 0.3 mol/L to 2 mol/L. The initial step was to make a 2 M NaCl solution (stock solution) by dissolving 116.88 g of NaCl powder in distilled water. The stock solution was then diluted to create 0.3, 0.7, and 1 M NaCl

solutions, which were then used to study the effects of saturation state, sample form, and the sample-to-the exposure solution mass ratio.

To investigate the impact of exposure solution chemical composition on chloride binding, three alternative solutions were used. The first solution was made by dissolving 2 grams of $Ca(OH)_2$ in 500 mL of distilled water and then adjusting the final volume to 1 L in a volumetric flask. The second solution was created by mixing 2 grams of $Ca(OH)_2$ and 10.64 grams of KOH in 500 mL of distilled water and adjusting the volume to 1 L. Lastly, a synthetic pore solution was prepared in compliance with ASTM C1876 [187] by dissolving 2 grams of $Ca(OH)_2$, 7.6 grams of NaOH, and 10.64 grams of KOH in distilled water and adjusting the final volume to 1 L. To create the chloride exposure solution, 116.88, 58.44, 40.91, and 17.53 g of NaCl powder were dissolved in 500 mL of each of these solutions and the volume was adjusted to 1 L.

3.1.3. Preparing Different Sample Forms

Three different sample forms were used. Disk-shaped, crushed, and powdered samples. Disk-shaped samples were cast using plastic molds. Then, these samples were used to make crushed and powdered samples. For crushed samples, a standard manual compaction hammer, commonly used to compact soils in accordance with ASTM D3282 [188], was employed to produce crushed samples and minimize any inconsistencies. Figure 3.4a shows the procedure to make crushed samples. The hammer had a weight of 2.54 kg (5.60 lbs.) and drops from a height of 305 mm (12 in). All crushed samples were generated by a single drop onto disks shaped pastes.

Figure 3.4b shows the procedure for grinding pastes. Paste samples were ground into a fine powder using a mortar and pestle. The grinding process is shown in Figure 3.4 and lasted approximately 5 minutes for each sample until they reached a uniform texture.

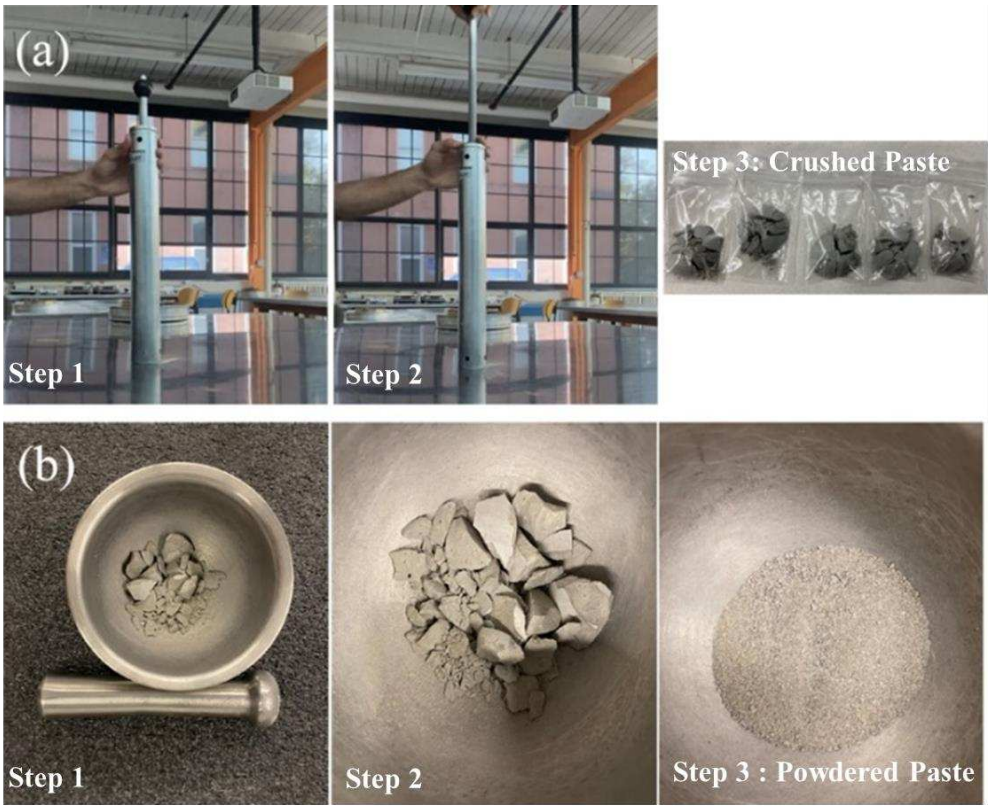

Figure 3.4. (a) crushed and (b) powdered paste samples

3.1.4. Sample-to-Exposure Solution Mass ratio

To simulate different sample-to-exposure solution mass ratios, first 10 g of crushed samples were weighted and then 30, 60, and 100 g of exposure solution (corresponding to 1:3, 1:6, and 1:10 solid-to-exposure solution mass ratios) were added to the testing containers. Throughout this procedure, care was taken to ensure that all pieces of the sample were covered by the solution and that none were protruding, as shown in Figure 3.5.

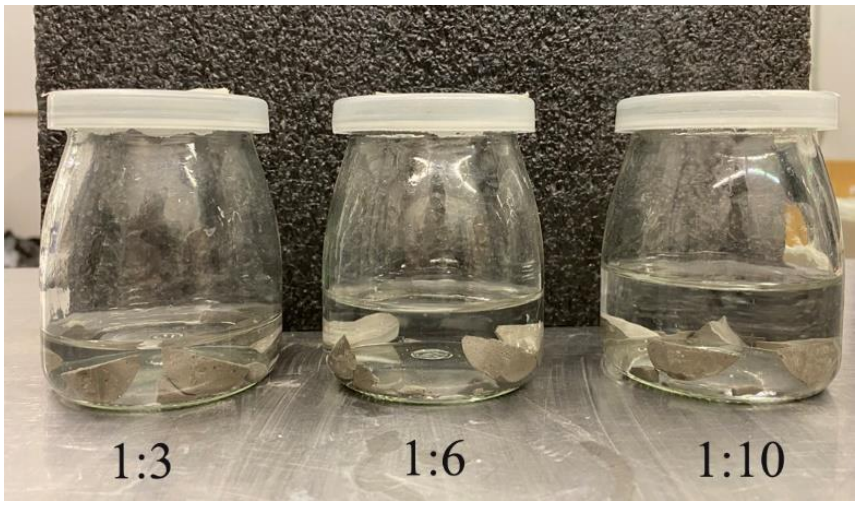

Figure 3.5. Setup to study the effect of sample-to-exposure solution mass ratio

3.1.5. Chloride Binding Test

The process of chloride binding was carried out by exposing samples to chloride solutions for a period of 14 days in sealed capped glass containers, as illustrated in Figure 3.5. The containers were kept in a room with a temperature of 23°C ± 2°C. Throughout the 14 days, the samples were subjected to regular shaking. The rationale behind this method was to ensure that all samples were uniformly exposed to the chloride solution until they reached equilibrium, while avoiding salt precipitation. According to previous studies, a 14-day duration is adequate for the chloride concentration in samples to reach an equilibrium with the chloride concentration in the solution [46, 62, 138].

At the end of the 14-day period, the concentration of chloride in the glass containers was measured by extracting 2 mL of the supernatant solution and analyzing its concentration using an automatic titrator (T5, Mettler Toledo), with 0.05 M $AgNO_3$ being used as the titrant. The titrator used in this study was equipped with a combined silver ring electrode (DMi141, Mettler Toledo),

which is a recommended electrode for argentometric titration of halides in aqueous solutions. Accordingly, the bound chloride concentration was computed using Eq. (3.1):

$$C_b = \frac{(c_i - c_f) \times V \times 35.45}{m_{dry}} \quad (3.1)$$

C_b: bound chloride concentration (mg Cl^-/g paste)

C_i: initial free chloride concentration of the exposure solution (M)

C_f: measured free chloride concentration (M) of solution inside the glass jars after 14 d

V: volume of the exposure solution (mL)

m_{dry} weight of the sample (g), (35.45 is the molar mass of chlorine (g/mol))

Langmuir and Freundlich isotherms, as discussed in detailed in chapter 2 section 2.4.3, are commonly used to model chloride binding results. The experimental results were fitted to these isotherms to determine which one better describes the chloride binding behaviour in the OPC paste samples. The model with the lowest sum of squared errors was chosen as the best fit. The concentrations of free and bound chlorides in this study were expressed in units of M and mg Cl−/g paste, respectively.

3.2. Objective 2: Chloride Binding and Chloride Desorption Capacity of Portland Cement Paste Exposed to Salt Solutions

Figure 3.6 summarizes experimental variables for objective 2. In this objective chloride binding and desorption for OPC cement exposed to three brine solutions with different concentrations was investigated. Cement pastes were prepared with an OPC meeting the Type I/II requirements of ASTM C150 and AASHTO M 85 [185] standards and a water-to-cement ratio of 0.4. This water-to-cement ratio was selected based on preliminary testing to minimize bleeding. The cement and its oxide composition were the same as the cement used in objective 1.

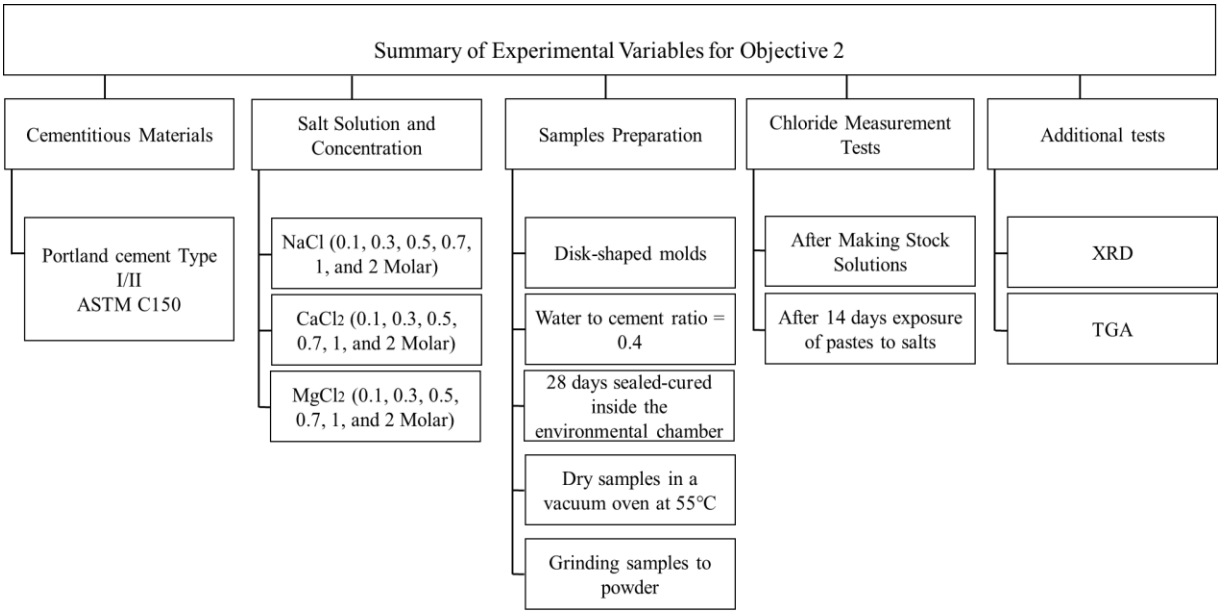

Figure 3.6. Summary of experimental variables for objective 2

American Chemical Society (ACS) -grade $MgCl_2$, $CaCl_2$, and NaCl salts were dissolved in distilled water to make chloride solutions with concentrations of 0.1, 0.3, 0.5, 0.7, 1, and 2 M, respectively. The paste mixing procedure followed ASTM C305 guidelines. Immediately after mixing, the paste was poured into a 100 mm × 200 mm plastic mold and seal-cured at room temperature (20±1°C, 68±33.8°F) for 28 days. Next, the hardened paste was ground into a fine

powder using a custom-made profile grinder and passed through a 150-μm (No. 100) sieve. The ground powder was then used for chloride binding, chloride dissociation, X-ray diffraction (XRD), and thermogravimetric analysis (TGA), details of which are provided in the sections that follow.

3.2.1. Chloride Binding Test

To remove all free moisture from the hydrated cement paste, approximately 600 g of ground OPC paste was dried for 1 week in a desiccator at 50±2°C (122±35.6°F) until no change in mass greater than 0.1% was measured. During this process, beakers containing soda-lime and sodium hydroxide were stored inside the desiccator to minimize carbonation and to keep the relative humidity inside the desiccator below 10%, respectively [71]. Next, 12.5 g of dried ground cement paste was mixed with 37.5 ml of chloride solution (solid-to-liquid ratio of 1:3) in a 250-ml beaker. The materials in the beakers were mixed well, sealed with a low-density polyethylene plastic wrap, and stored in a room at a fixed temperature of 23±1°C (73.4±33.8°F) for 1 week. Previous research has found that chloride concentrations generally stabilize after a week [62]. Upon completion of the exposure period, the solutions were stirred carefully with a glass rod and then vacuum filtered through No.1 Whatman® filter paper. To prevent loss of the chlorides, the filter paper was washed three times with distilled water. The concentrations of the chlorides in the filtrate solutions were determined using a potentiometric titrator (Model T5, Mettler Toledo) as described in section 3.1.5. Two replicates were used for measuring chloride binding.

3.2.2. Chloride Desorption Test

Five replicate beakers containing 12.5 g of dried ground OPC paste were exposed to 37.5 ml of 2 M $MgCl_2$, $CaCl_2$, and NaCl solutions (total of 15 samples). The process of drying the ground OPC paste was the same as the procedure followed in the chloride-binding test. One of the replicates was used as a baseline to quantify the chloride-binding capacity of the paste, while the

other four were used in the desorption analysis. The samples were covered with wrapping plastic and stored at a fixed temperature of 23±1°C (73.4±33.8°F) for 1 week.

The concentrations of the baseline free chlorides were determined first, similar to the chloride-binding isotherm testing, described in section 3.2.1. In addition, the pH of the solutions was measured using a pH meter (SevenCompact, Mettler Toledo). Then, 5, 10, 15, and 20 ml (0.17, 0.34, 0.51, and 0.68 fl oz) dilute nitric acid (1:1) was added to the remaining four beakers, respectively. This step was repeated for all three salts. The suspensions were stirred well with a glass rod and left to sit overnight. After that, the suspension was filtered, as discussed for the binding test, and the pH and concentrations of chlorides in each beaker were measured by potentiometric titration.

Theoretically, if there was no dissociation (i.e., no chlorides dissociated due to a reduction in the pH of the solution), the concentration of chlorides in the new solution (the original salt solution plus added acid) would be lower than in the original solution due to the dilution effect. However, if the chlorides did dissociate and were released into the solution, then ΔC, which is the difference between the adjusted concentration of chlorides in the new solution after the addition of acid and the molar concentration of the free chlorides before the addition of acid, would be positive. ΔC can be expressed using Eq. (3.2):

$$\Delta C = C_a \left(\frac{V_{f+a}}{V_f} \right) - C_f \tag{3.2}$$

C_a: molar concentration of chlorides after the addition of acid

V_f: volume of added 2 M chloride solution (ml),

V_{f+a}: volume of the chloride solution plus the added acid (ml)

The plot of ΔC values for each concrete sample versus their corresponding pH values represents the chloride desorption isotherm of that sample.

3.2.3. Analytical Tests

X-ray diffraction (XRD) and thermogravimetric analysis (TGA) were carried out on representative ground paste samples before and after exposure to 0.7 M and 2 M NaCl, $CaCl_2$, and $MgCl_2$ solutions. In addition, post-exposure reaction products and phase changes within the samples after adding 25 ml of 1 molar nitric acid were characterized using XRD and TGA. The XRD recording was performed using a Bruker D8 Discover DaVinci. The X-ray tube functioned at 40 kV with a current of 40 mA. The diffraction patterns were recorded in the 2θ range of 10°–70° and analyzed using the Bruker DIFFRAC EVA software (version 5.1.0.5) loaded with the Crystallography Open Database (COD) [191, 192].

TGA was performed using the Q500 Thermogravimetric Analyzer (TA Instruments), as shown in Figure 3.5. The TGA tests were carried out in a nitrogen gas atmosphere at temperatures of 50–500°C and a heating rate of 20°C/min to monitor the mass loss owing to the dehydroxylation of Friedel's salt. A digital microscope was used to investigate the extent of damage owing to chloride attack and acidic corrosion after chloride binding and desorption tests, respectively.

3.3. Objective 3: Chloride Binding and Chloride Desorption Capacity of Cementitious Materials Containing Fly Ash, Slag, and Silica Fume

In this objective, the chloride binding capacity and then chloride desorption in cementitious materials containing three SCMs including fly ash, slag, and silica fume were investigated. The study also examined the impact of pH changes on the disassociation of bound chloride. Figure 3.7 displays a summary of experimental variables for this objective.

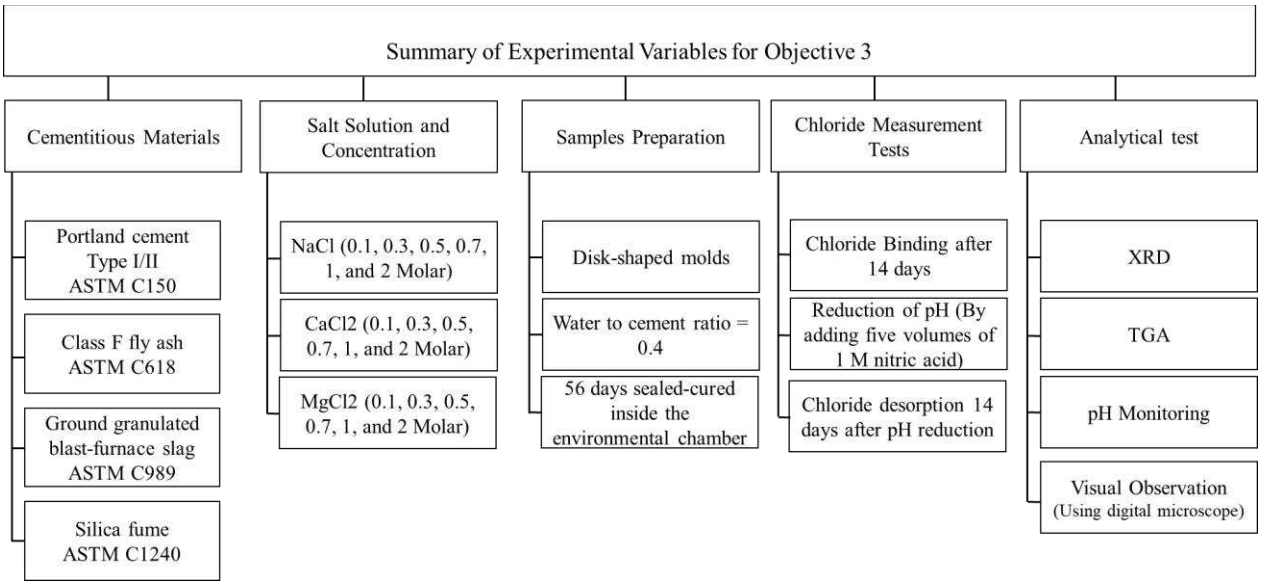

Figure 3.7. Summary of experimental variables for objective 3

OPC conforming to the ASTM C150 [184] and AASHTO M 85 [185] specifications for Type I–II Portland cement, and three supplementary cementitious materials, namely Class F fly ash (FA), slag (SG), and silica fume (SF), were used as binders in this study. Table 3.2 shows the cementitious materials chemical compositions.

Table 3.2. Chemical composition of cementitious materials

	SiO_2	Al_2O_3	Fe_2O_3	CaO	MgO	SO_3	Na_2O	K_2O	LOI
Cement Type I/II	19.24	3.80	2.75	59.05	1.5	2.49	0.17	0.60	9.90
Fly ash	54.24	18.16	10.42	7.37	1.46	1.30	1.24	2.71	1.13
Slag	31.40	15.70	0.40	37.70	8.60	2.50	–	–	0.60
Silica	95.40	0.90	1.30	0.90	1.40	–	–	–	1.70

3.3.1. Mix Design Proportions

Table 3.3 presents the mix design proportions used in this study. The investigation focused on the chloride binding and desorption characteristics of various cementitious systems, utilizing paste samples. These samples were cast with a water-to-binder ratio (w/b) of 0.4, following the guidelines of ASTM C305, utilizing a 5-liter mortar mixer. Post-mixing, the samples were poured into cylindrical disc-shaped molds, each measuring 33 mm in diameter and 15 mm in depth.

Table 3.3. Summary of mix design proportions for pastes

Mix Number	Cementitious Material	SCM Replacement Level with Type I/II (%)	Mix Label
1	Type I/II	0 (100% Type I/II)	Reference (OPC)
2	Type I/II + Fly ash	15% Fly ash	FA 15
3	Type I/II + Fly ash	30% Fly ash	FA 30
4	Type I/II + Slag	25% Slag	SG 25
5	Type I/II + Slag	50% Slag	SG 50
6	Type I/II + Silica	5% Silica	SF 5
7	Type I/II + Silica	10% Silica	SF 10

Upon removal from their molds, the samples were stored in Ziplock bags and kept in an environmental chamber, where they underwent a curing process under the same conditions (25°C and 95% RH) for a duration of 56 days. Then, the samples were dried in a vacuum oven at 55°C until a constant weight was achieved.

Figure 3.8 displays a sample set up for pastes containing fly ash for binding and desorption tests when samples are exposed to NaCl, $CaCl_2$, and $MgCl_2$ solutions with concentrations of 0.1, 0.3, 0.5, 0.7, 1, and 2 Molars. Seven different pastes were used and a total of 462 disk samples were used for this objective. More than 500 titrations were performed to measure the chloride concentrations in solutions.

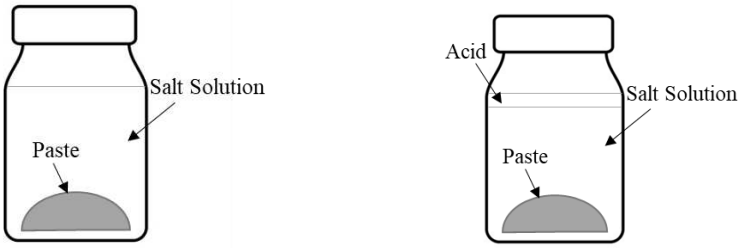

Figure 3.8. Experiment setup for binding (left) and desorption tests (right)

3.3.2. Chloride Binding Test

Three chloride salt solutions, sodium chloride (NaCl), calcium chloride ($CaCl_2$), and magnesium chloride ($MgCl_2$), were prepared in six targeted concentrations: 0.1, 0.3, 0.5, 0.7, 1, and 2 M. Initially, reagent-grade salts of NaCl, $CaCl_2$, and $MgCl_2$ were solubilized in distilled water to achieve a solution with a chloride concentration of 2 M. This resultant solution was then methodically diluted to yield solutions at the desired concentrations. The paste samples were subjected to 60 ml of chloride solutions for a duration of 14 days, contained within sealed glass vessels at a controlled ambient temperature of 23°C ± 2°C. For each chloride concentration, two samples were evaluated. Figure 3.9 shows a simplified chloride binding testing procedure.

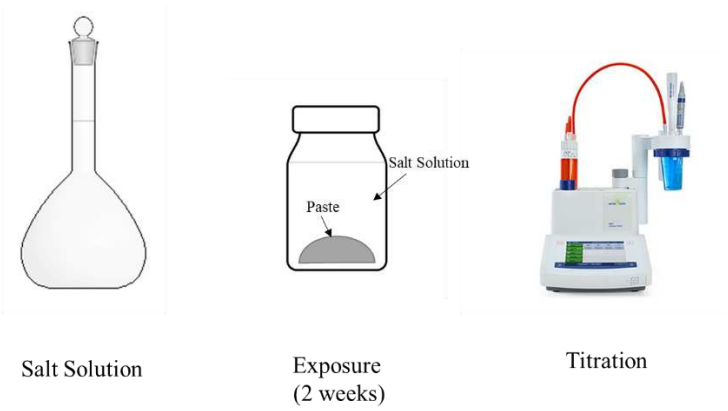

Figure 3.9. Chloride binding testing procedure

The concentration of free chloride in the exposure solution was quantitatively determined using an automatic chloride titrator (Model T5, Mettler Toledo). In total, two hundred and fifty-two samples, comprising two replicates per each of the seven mixes, across six different chloride solutions and three distinct salts, were utilized in the chloride binding experiments. The bound chloride concentration was calculated using Eq. (3.3):

$$C_b = \frac{(c_i - c_f) \times V \times 35.45}{m_{dry}} \tag{3.3}$$

C_i: Initial chloride concentration of the exposure solution (M)

C_f: Measured free chloride concentration (M) after 14 days

V: Volume of the exposure solution (ml)

m_{dry}: Sample's oven-dried weight (g), and 35.45 is the molar mass of chlorine (g/mol)

C_b: Bound chloride concentration (mg Cl^-/g paste)

3.3.3. Chloride Desorption Test

To evaluate the release of bound chlorides in samples subjected to low-pH environments, an initial set of ten replicate paste samples from each mix was exposed to 2 M salt solutions for a period of 14 days. This procedure paralleled the chloride binding method previously described.

Following the two-week exposure period, the pH of the equilibrated solutions was determined at room temperature using a pH meter. Nitric acid (70%) with a density of 1.400 g/mL and a molar mass of 63.01 g/mol was used to prepare nitric acid solutions. 1M nitric acid in volumes 5, 10, 15, 20, and 25 ml were added to the containers to reduce their pH. Prior to each measurement, the pH sensor was calibrated with a standard buffer solution at a pH of 9 to minimize measurement inaccuracies. Figure 3.10 summarizes the desorption testing procedure.

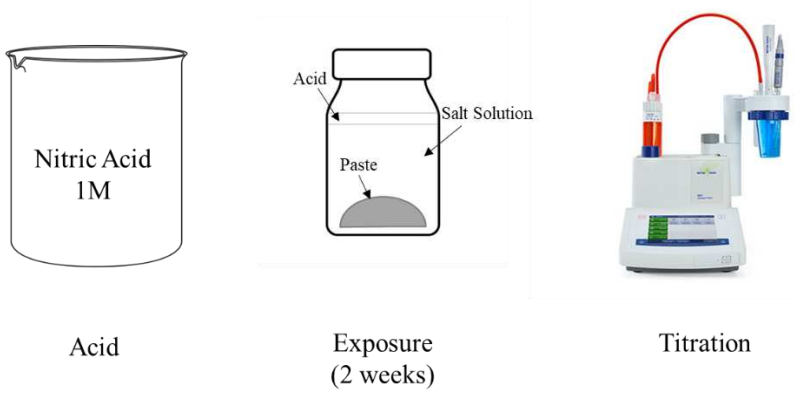

Figure 3.10. Chloride desorption testing procedure

After adding acid to samples, the samples were capped to prevent evaporation and left for two weeks at room temperature until the pH reached an equilibrium. During this period, the evolution of the pH of each solution was monitored periodically. The concentration of free chlorides after chloride desorption was measured using an automatic chloride titrator, and the

concentration of released bound chlorides due to the drop in the pH of the solution was calculated using Eq. (3.4):

$$C_{released} = \frac{(c_d - c_f) \times V_c \times 35.45}{m_{dry}} \quad (3.4)$$

C_d : Measured free chloride concentration (M) 14 d after the addition of acid

C_f: Free chloride concentration (M) after the binding period

V_c: Corrected final volume of solution (ml), which accounts for the volume of added acid to 60 ml chloride solution

m_{dry}: Sample's oven-dried weight (g).

$C_{released}$: Released bound chloride concentration (mg Cl^-/g paste);

It should be noted that the determination of nitric acid concentration was meticulously executed through a series of experiments on Ordinary Portland Cement (OPC) samples, which had been exposed to a 2M NaCl solution. For this purpose, OPC paste samples, previously immersed in a 2M NaCl solution for two weeks, were treated with varying concentrations of nitric acid, ranging from 0.5M to 3M, in different volumes.

The pH of these mixtures was rigorously monitored for a duration of one week. Results from these experiments revealed that the 1 M concentration of nitric acid was most effective in achieving a desirable pH range when equilibrated with the solution. Therefore, 1 M nitric acid was chosen as the ideal concentration to reduce the pH, aiding in the accurate assessment of the desorption properties of various blended paste samples.

3.3.4. Analytical Measurements

The analytical tests, including XRD and TGA, are the same as explained in the methods for objective 2, (section 3.2.3). The same sampling process and measurement parameters were used. Figure 3.11 shows the main equipment used in the objective 3.

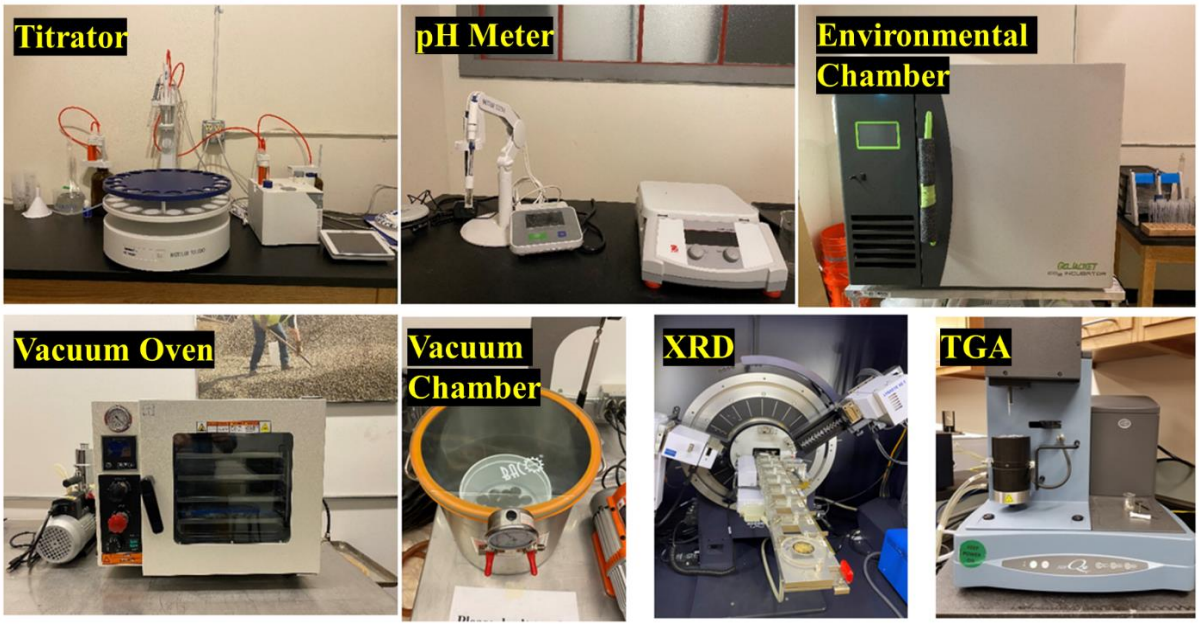

Figure 3.11. a) Titrator b) pH meter c) environmental chamber d) Vacuum oven e) Vacuum chamber f) XRD equipment g) TGA equipment

3.4. Objective 4: pH Change in Cement Pastes Containing Portland Cement and Fly ash Exposed to Salt Solutions and Carbonation

Figure 3.12 provides a summary of experimental variables for objective 4. The primary goal was to evaluate the combined effects of carbonation and salt solution exposure on pH reduction of cementitious systems. Type I/II Portland cement per ASTM C150 [184] AASHTO M 85 [185] standards and fly ash as per ASTM C618 were used to cast paste samples. The fly ash replacement level was 15%. The water to cement ratio was 0.4, similar to the water to cement ratio used in the previous objectives to allow for comparison to prior results. 100 by 200 mm cylinders were used to cast samples. Samples were mixed as per ASTM C305, and samples were demolded after 24 hours. Paste samples were moisture cured in saturated lime water as specified in test method C109/C109M for 56 days. Then samples were removed, and water washed before exposure to salt solution.

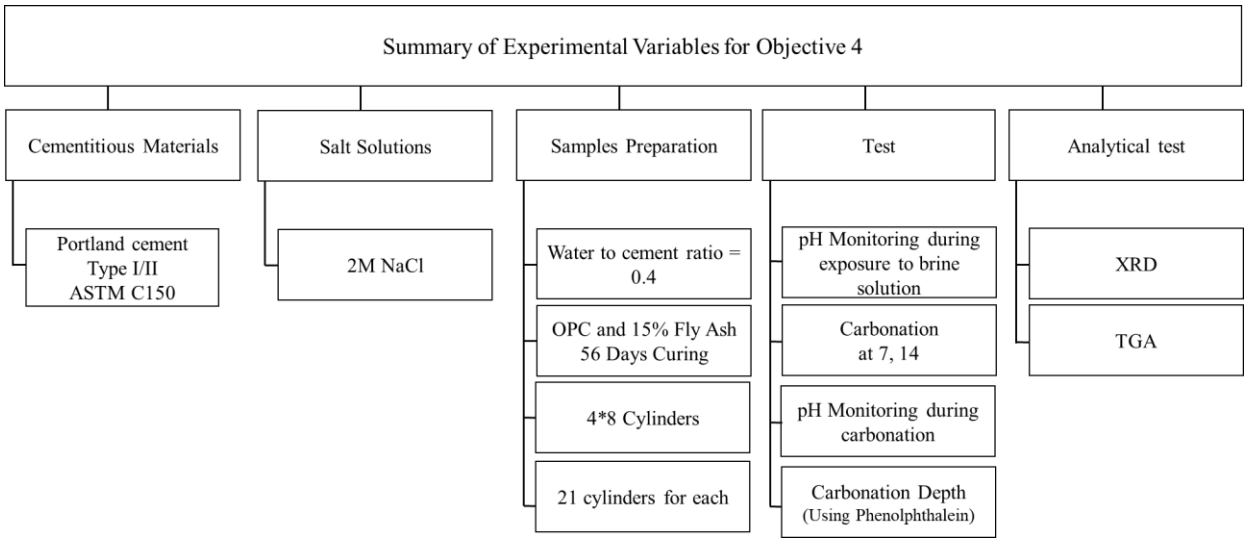

Figure 3.12. Summary of experimental variables for objective 4

3.4.1. Sample Preparation

Using a masonry saw, 50 mm (2 in) from both the top and bottom of the samples were trimmed off. The primary reason for trimming the top and bottom portions of the cylinders is related to the compaction process. Typically, more water tends to accumulate in the top section of a cylinder due to compaction. And the bottom portion of the cylinder often contains heavier particles. The center portion of the cylinder is more uniform. Next, super clear epoxy resin was used to coat the circumference of the cylinders to ensure salt solution penetrates only from the top and bottom surface not cylinder sides. After the epoxy was applied, the samples were left to set for 24 hours. Figure 3.13 displays a schematic drawing of the sample preparation before exposure to NaCl salt solution.

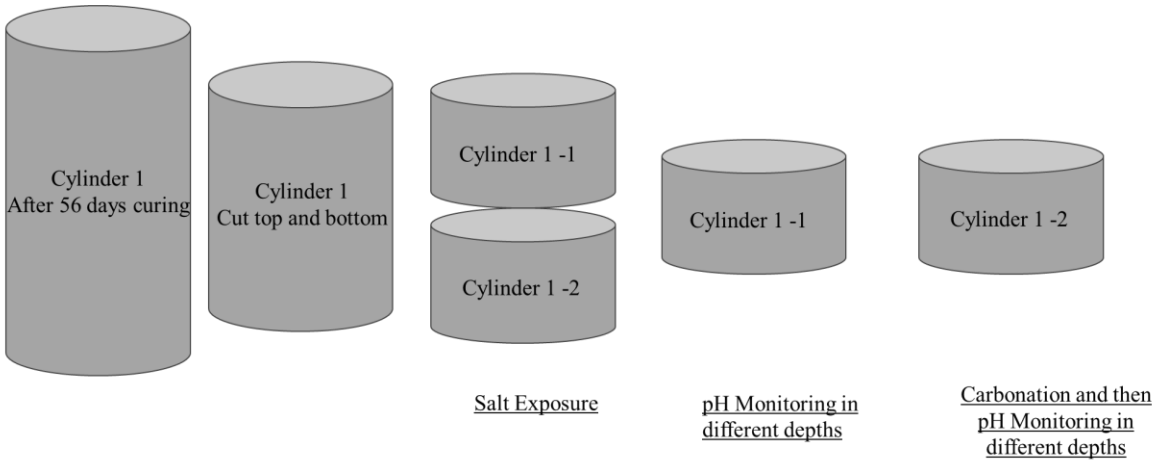

Figure 3.13. Sample preparation before exposure to NaCl solution and carbonation

3.4.2. Chloride Exposure

After cutting and coating, samples were placed in an oven for 6 hours at a temperature of 100°F to ensure uniform saturation levels before introducing them to the brine solution. Next, samples were immersed in 2 M NaCl solution for up to 35 days and the pH of samples were monitored at specified periods (10, 20, 35 days). This concentration was used based on the

previous objective's testing and the exposure time of 35 days was selected to as recommended by ASTM C1556. The preparation of the 2 M NaCl solution was the same as described in objectives 2 and 3.

3.4.2.1. pH Monitoring During Chloride Exposure

An Ohaus pH meter (Starter 300) with a resolution of 0.01 was utilized for pH monitoring. Before measurements, the pH-meter was calibrated using a 3-point calibration method. Certified commercial buffers with pH of 4.01, 7.00, and 10.01 were used for calibration. To date, there is no standard method to assess the pH level of paste, mortar, and concrete [16, 193]. In this thesis, for pH monitoring, ex-situ which is also known as suspension methods were utilized. First, Holes of varying depths were drilled in each cylinder as shown in Figure 3.14. and powder samples were collected separately from each. Three samples were taken for each depth and age. In total, 36 pH measurements (3 samples × 3 depths × 4 ages) were conducted during the exposure to the salt solution over a period of 35 days, as shown in Figure 3.15.

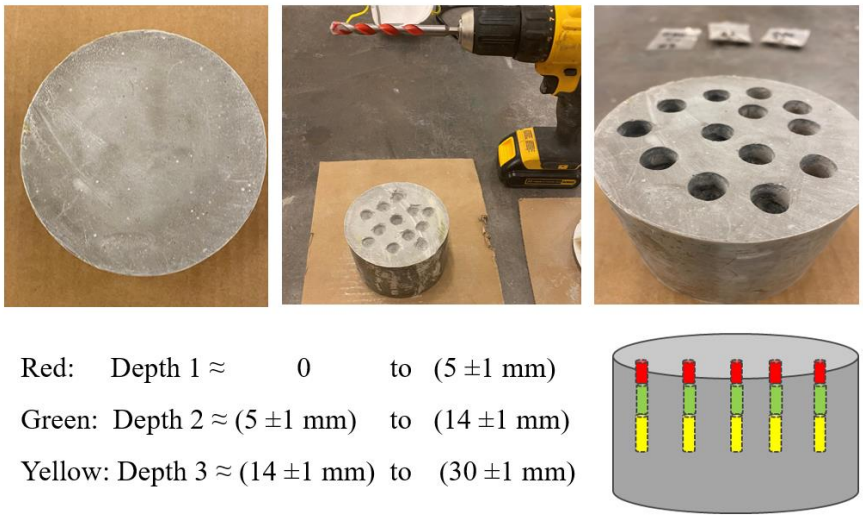

Figure 3.14. Taking powder from different depth of cylinders for pH measurements (the different colors represent sample collection for the different depths)

The powders were immersed in deionized water for 2 hours, after which the pH was measured. The pH measurement using ex-situ leaching, the method that used in this thesis is fast, simple, practical [193], and comparable with other more accurate laboratory measurements [16, 194]. It should be reminded that in this thesis the powder taken from different depth of a sample immersed in DI water for 2 hours and then equilibrated suspension was transferred to conical tubes and pH measured using a pH electrode (Ohaus pH meter). The suspension did not filter to remove any errors, as the main reason for filtration is that the existing suspended particles in the suspension may decrease the pH probe lifespan and the filtering process do not significantly and meaningful impacts the pH reading [193]. To make sure the room temperature and solution temperature do not impact the pH readings, the temperature was monitored and was in the range of 22 ±1ºC. Figure 3.15 illustrates the pH measurement in this study.

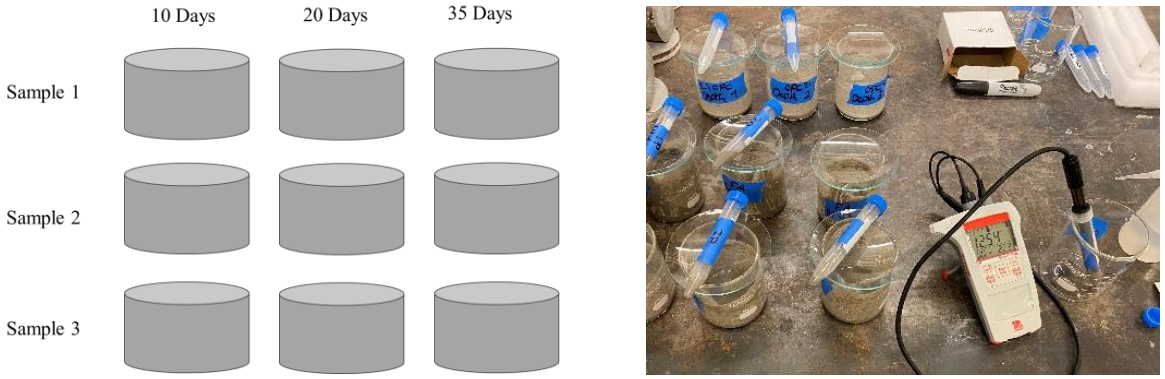

Figure 3.15. pH measurements during NaCl solution exposure

3.4.3. Accelerated Carbonation Test

Following the 35-day period, the samples were transferred to a carbonation chamber for the carbonation test. The temperature in the chamber was 21± 1 °C and the relative humidity was kept between 65% to 70%. Samples were kept in the chamber for up to 14 days to facilitate the accelerated carbonation. The pH was monitored for 4 weeks and compositional changes were

investigated using TGA and XRD for two weeks. Figure 3.16 shows the carbonation setup in this investigation.

Figure 3.16. Exposure to carbon dioxide (carbonation test)

3.4.3.1. pH Monitoring During Carbonation

At defined intervals samples were removed from the chamber and powder form four depth were taken, as shown in Figure 3.17. The pH was measured as described in 3.4.2.1. Three sample were used for each measurement and the average and standard error reported.

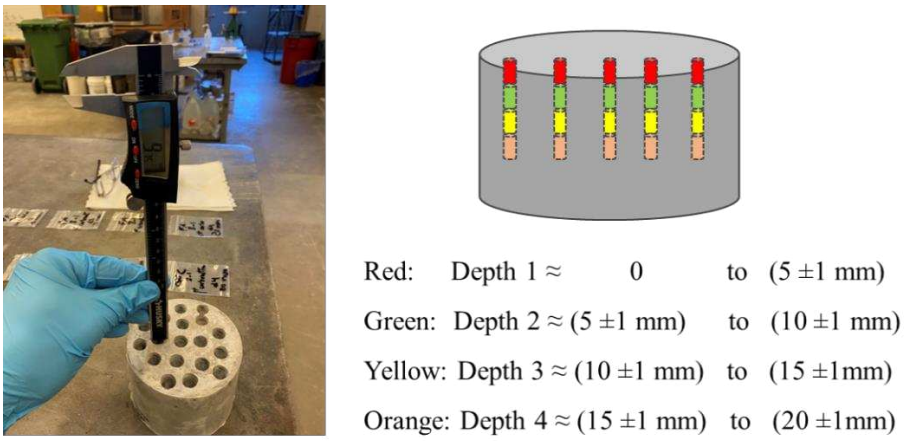

Figure 3.17. Taking powder from four depths of carbonated paste (colors represent depths)

3.4.4. Analytical Tests

The analytical test including XRD and TGA are the same as explained in the methods for objective 2 and 3. It should be noted that the same sampling process and measurement parameters have been used. The XRD analysis was performed using DIFFRAC.EVA software and peaks analyzed using PDF5+ database. The TGA analysis was done utilizing TA Instruments software, TRIOS Version 5.1.1.

Chapter 4 : Results and Discussion

This chapter presents and discusses results obtained from the experimental tests described in the previous chapter. Four separate yet related investigations were performed and in this chapter the results are presented according to the objectives. It is important to note that these results for first three objectives have been published as four peer-reviewed journal papers in Elsevier and ASCE Journals. The necessary permissions to republish these sections have been obtained and submitted to the Colorado State University Graduate School and ProQuest.

4.1. Objective 1: Investigate the Factors Impacting Chloride Binding Measurements

The results and discussion presented in this section were first published in journal of *Construction and Building Materials, Volume 409, Page 134067, "Investigating the effects of testing protocol factors on chloride binding capacity in cementitious materials", Copyright Elsevier (2023)* [195]. In this objective, the impact of various factors on chloride binding measurements was examined. These factors included:

i) Three different saturation levels (0%, 50%, and fully saturated)

ii) Four exposure solutions with varying chemical compositions

iii) Three sample forms (disk, crushed, and powder)

iv) Three solid-to-exposure solution mass ratios (1:3, 1:6, and 1:10)

4.1.1. Effect of Degree of Saturation (DoS) on Chloride Binding

Previous investigations requiring chloride binding measurement have mostly employed Nilsson's equilibrium method, which involves exposing dried samples to brine solutions. These test procedures do not accurately reflect real-life conditions. The transport characteristics of concrete vary based on saturation level [196]. Previous findings [197, 198] showed that the

chloride diffusion coefficient steadily increases with the degree of saturation and reaches the highest values at fully saturation level.

Figure 4.1 depicts the chloride binding results for samples with varying degrees of saturation. The results indicate that as the saturation state of the samples increased, a greater amount of chloride binding was observed. In comparison, the oven-dried specimens exhibited significantly lower chloride binding capacity compared to samples that were partially or vacuum-saturated. The binding capacity of a cementitious system is expressed as the rate of change (derivative) bound with respect to free chloride. Figure 4.1b shows the binding capacity associated with the Langmuir isotherm (derivative of the Langmuir isotherm with respect to free chloride).

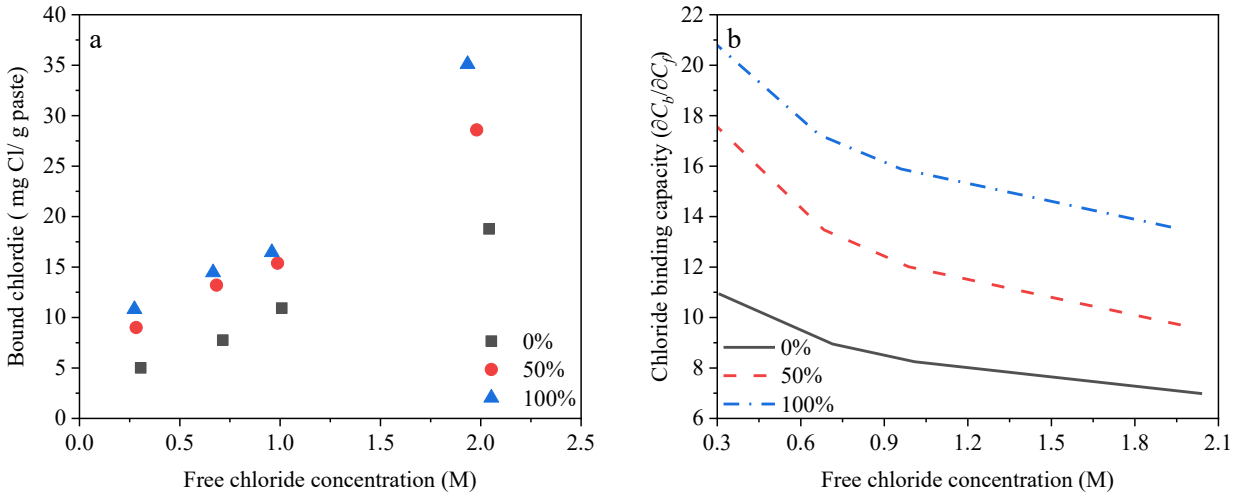

Figure 4.1. (a) Chloride binding and (b) chloride binding capacity at varying saturation levels

According to Figure 4.1a, at lower concentrations of free chlorides, the vacuum-saturated sample exhibited approximately 20% and 115% more bound chloride content than the partially saturated and oven-dried samples, respectively. This trend remains consistent even at higher chloride concentrations (e.g., 2 mol/L), where the vacuum-saturated sample showed 22% and 85% more bound chloride content than the partially saturated and dried samples, respectively.

Figure 4.1b displays the chloride binding capacity at varying saturation levels. The results reveals that the binding capacity was higher for fully saturated samples than dry samples. The results indicate that the rate at which the chloride binding capacity decreased was influenced by the concentration of free chlorides. However, this decrease is not consistent. As shown in Figure 4.1b, the decline in the slope of the chloride binding capacity is more pronounced until approximately 0.7 mol/L, after which it exhibits a shallower linear decline. This can be explained by two factors. Firstly, at lower chloride concentrations, there is a higher ratio of available binding sites to chloride ions, allowing more sites for chlorides to bind with cement hydrates. Secondly, due to the limited capacity of cementitious systems to bind chlorides, when additional chlorides are introduced, they may not always find available binding sites, resulting in a slower rate of chloride binding.

The decrease in the ability of the samples to bind chloride ions as the saturation level decreases can be attributed to two primary reasons; firstly, when the samples become less saturated, there are fewer water-filled pores that allow the movement of chlorides within the samples. Second, the interface between the solid components of the samples and the pore solution is reduced at lower saturation levels. This decrease in transport channels and interface limits the access of chlorides to binding sites within the samples.

Another reason contributing to lower chloride binding as a result of reduced saturation is the increased competition between Cl^- and OH^- for binding sites. The zeta potential of C–S–H in OPC paste is generally less than -10 mV [199, 200]. To compensate for the negative charges of C–S–H at the pore wall surfaces, calcium and other positively charged cations establish an ionic bond with the negatively charged silanol sites, forming what is known as the Helmholtz layer [162, 201],

named after Hermann von Helmholtz, who was the first to propose a model for the electrical double layer (EDL) at the interface between a solid and an electrolyte [202] as shown in Figure 4.2.

According to Helmholtz's model, the EDL consists of two layers: the inner layer, known as the Helmholtz layer, and the outer diffuse layer. The Helmholtz layer is a region immediately adjacent to the solid surface where ions are strongly attracted and adhere to the surface [203, 204]. Beyond the Helmholtz layer lies the diffuse layer [204]. This region is less densely packed with ions and contains a mixture of counterions and co-ions (ions with the same charge as the surface). With an increase in the positive charge density at the Helmholtz layer, the zeta potential of pore walls shifts to a positive value, which can selectively attract chlorides or hydroxyl ions.

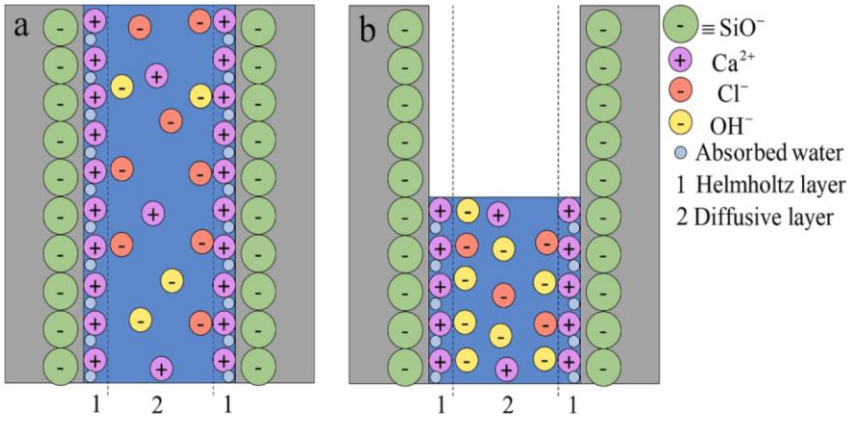

Figure 4.2. Helmholtz model of the EDL for (a) a saturated pore, (b) an unsaturated pore

It should be noted there is a competition between Cl^- and OH^-, among others, to bind with the positively charged hydration sites [58, 201, 205]. Since the pH of the pore solution is typically above 13, a decrease in the saturation level of the sample leads to an increase in the concentration of OH^- within the pore solution [199]. This results in more OH^- being adsorbed onto the C–S–H surface, reducing available binding sites for Cl ions and leading to reduced chloride binding.

These findings highlight the importance of considering the saturation state of samples prior to chloride exposure, a factor that has often been overlooked in previous literature. Previous studies have predominantly utilized Luping and Nilsson's equilibrium method, which involves exposing completely oven-dried samples to brine solutions that do not accurately represent real-world conditions. Concrete elements in service usually experience varying degrees of saturation, influenced by factors such as location and season. It is uncommon to come across completely dried concrete elements that are exposed to solutions containing chloride ions. Consequently, estimating the chloride binding capacity of cementitious systems based on dried samples significantly underestimates their actual binding capacity.

4.1.2. Effect of Exposure Solution on Chloride Binding

Figure 4.3 displays the outcomes of the chloride binding experiments using different solutions. The results indicate that, at chloride concentrations of 0.3 and 2 mol/L, the solution containing calcium, potassium, and sodium ions demonstrated the lowest level of chloride binding. In contrast, the pure NaCl solution and the solution with calcium and potassium ions displayed the highest levels of chloride binding at 0.3 mol/L. However, at 2 mol/L chloride concentration, the NaCl solution exhibited significantly higher chloride binding compared to the solution containing calcium and potassium ions. Interestingly, the solution containing only calcium ions exhibited a consistently similar behavior to the pure NaCl solution.

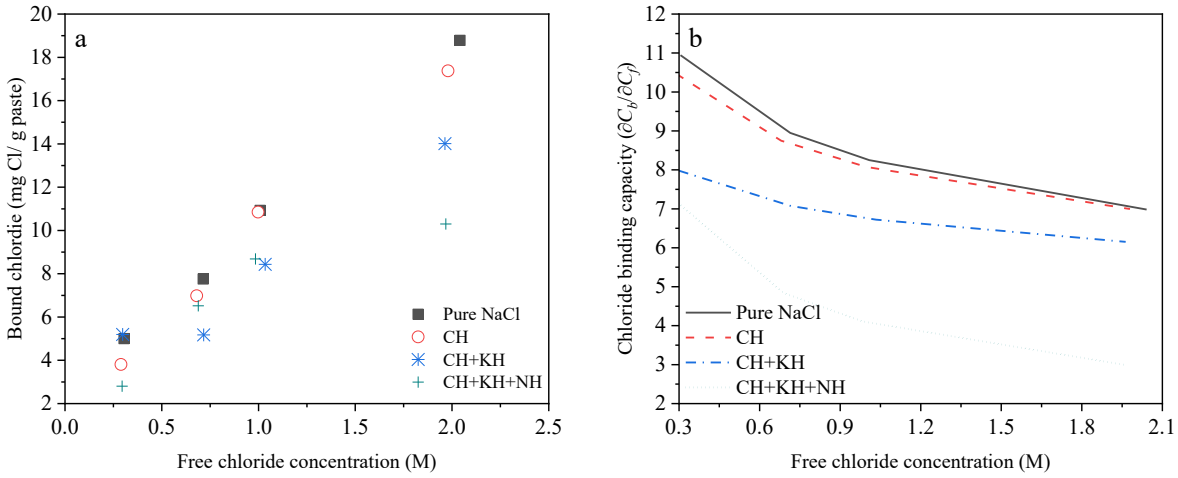

Figure 4.3. (a) Chloride binding and (b) chloride binding capacity in different solutions

Figure 4.3b demonstrates a general trend suggesting a relationship between the number of ions added to the chloride solution and the chloride binding capacity of the system. As more ions, especially sodium hydroxide, were introduced to the chloride solution, the overall chloride binding capacity of the system decreased.

The binding capacity of calcium-silicate-hydrates and AFm phases such as mono-sulfate aluminate, hydroxy-AFm, mono-carbonate-AFm, and hemicarbonate-AFm compounds is influenced by the presence of other ions and the pH level of the solution [136]. For instance, Hemstad et al. [64] conducted a study where they demonstrated that reducing the pH of the pore solution from 13 to 12 increased the chloride binding in cement pastes. This increase in chloride binding was associated with higher amounts of chlorides in the AFm-phases. However, further lowering the pH below 12 resulted in a decrease in the chloride binding capacity due to the dissolution of AFm phases [83].

The pH values of multi-ionic exposure solutions used in this study are shown in Figure 4.4. Among the three solutions, the (CH + KH + NH) solution exhibited the highest pH values at all

chloride concentrations, followed by (CH + KH) and CH solutions. The chloride binding results of cement paste in these solutions, as shown in Figure 4.3a, followed the reverse pattern in which the CH solution showed the highest bound chloride and the (CH + KH + NH) solution had the lowest bound chloride. These findings align with the results reported by Hemstad et al. [83].

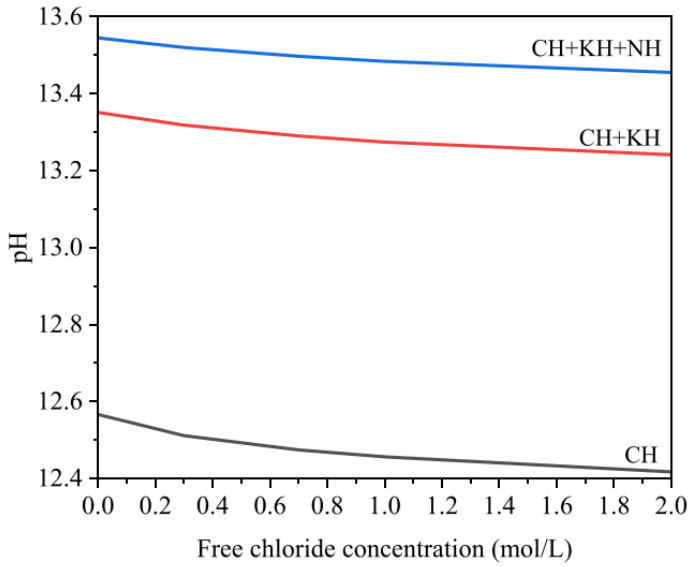

Figure 4.4. pH of exposure solutions at various chloride concentrations

The addition of more ions to water can also increase the ionic strength of the solution, which can impact the capacity of cement pastes to bind chlorides. Ionic strength is a measure of the concentration of ions in a solution, calculated by summing the products of the concentrations of each ion multiplied by the square of its charge. Figure 4.5a presents the ionic strength of four solutions, expressed in mole per kg of water (mol/ kgw) at various chloride concentrations. The PHREEQC software [206] was utilized to predict the ionic strength of these solutions. Since three of the four solutions in this study were saturated with calcium hydroxide, the Pitzer model, known for its suitability in modeling high ionic strength solution speciation, was employed [207].

According to Figure 4.5a, at any given chloride concentration, the ionic strength of the four solutions follows this order: (CH + KH + NH) > (CH + KH) > CH > pure NaCl solution. For instance, at a chloride concentration of 2 mol/L, the ionic strength of (CH + KH + NH) was 27 % higher than that of the pure NaCl solution. Moreover, at the same chloride concentration, the chloride binding of OPC pastes in the (CH + KH + NH) solution was 133 % lower than in the pure NaCl solution. This suggests that the ionic strength of the chloride solution can significantly impact the chloride binding of cement pastes.

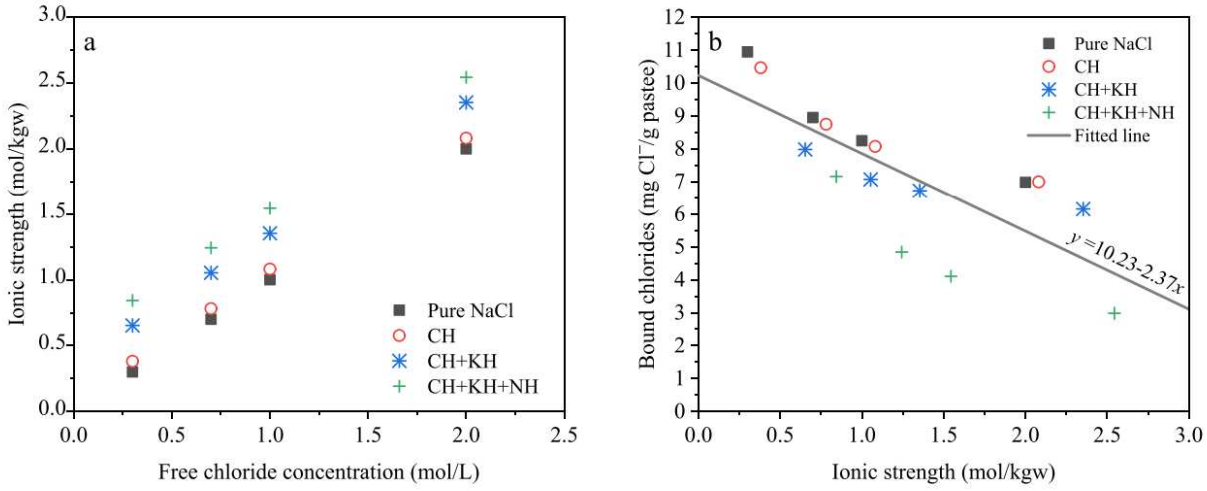

Figure 4.5. (a) Estimated ionic strength of four exposure solutions at different chloride concentrations, (b) the relationship between ionic strength of salt solution and bound chloride content

Figure 4.5b displays the relationship between the estimated ionic strength of the four solutions and the corresponding measured chloride binding. The results demonstrate a relatively significant inverse relationship (Pearson's r = -0.77) between the ionic strength of the exposure solution and the bound chloride content within the cement pastes. This inverse relationship can be attributed to increased competition between the ions in the solution and chlorides for available binding sites. In simpler terms, when the ionic strength of the solution is higher, there are more

ions present that can compete with chlorides to bind to the cement paste, resulting in a reduced chloride binding capacity.

4.1.3. Effect of Solid-to-Liquid Mass Ratio on Chloride Binding

In Figure 4.6, the chloride binding contents and capacities were examined for different solid-to-liquid (SLR) ratios of 1:3, 1:6, and 1:10. The results indicate that there were no notable differences in the amount of bound chloride when the samples were exposed to low chloride concentrations (i.e., < 0.5 mol/L). At higher chloride concentrations, the paste samples exposed to SLRs of 1:3 and 1:6 exhibited similar performance. In contrast, a significant increase in chloride binding was observed in samples exposed to an SLR of 1:10.

Figure 4.6b, shows that for SLR values of 1:3 and 1:6, the binding capacity reaches a plateau at higher concentrations of free chlorides, indicating that the samples reached equilibrium with the exposure solution. In contrast, samples exposed to an SLR of 1:10 exhibit a steeper downward linear trend up to a free chloride concentration of 0.7 mol/L, followed by a slight reduction thereafter. Notably, in this case, no indications of reaching equilibrium are evident, indicating that the binding capacity of the samples subjected to an SLR of 1:10 exhibits a continuous increase in chloride binding even beyond the 2 mol/L threshold of maximum chloride concentration employed in this study.

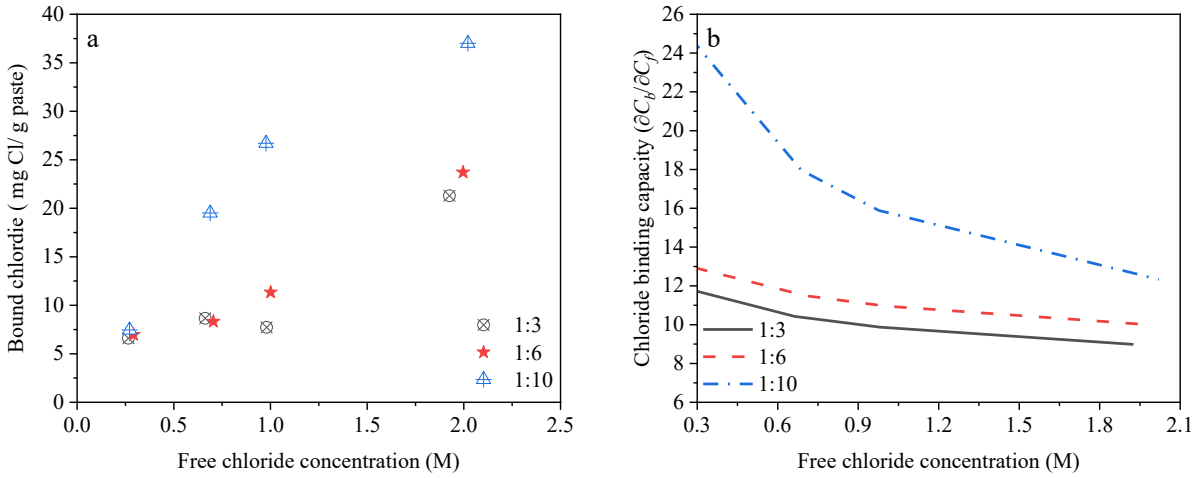

Figure 4.6. (a) Chloride binding and (b) chloride binding capacity at diverse SLR ratios

Figure 4.6b shows two distinct slopes. The first relates to low free chloride concentration i.e. free chloride concentration less than 0.7 M and the second one is associated with high free chloride concentration i.e. free chloride concentration greater than 0.7 M. Figure 4.6b reveals that the chloride binding capacity of pastes exposed to higher chloride concentrations is considerably higher than chloride binding capacity at low free chloride concentration. The same trend was observed for the chloride binding capacity, where the values were 9.87, 10.96, and 15.89 mg/g paste/M for the 1:3, 1:6, and 1:10 SLRs, respectively, at a free chloride concentration of 1 M. In other words, the results show that the volume of the exposed solution, even at the same concentration, influences the number of chloride ions, affecting the chloride binding results.

The observed increase in chloride binding for the SLR of 1:10 can be attributed to several factors. Firstly, the larger volume of chloride solution necessitates a greater number of moles of chlorides to maintain a constant concentration. Consequently, under the assumption of unchanged conditions, there were higher moles of chloride ions available per unit mass of concrete in SLR of 1:10. This increased availability of chlorides enhances the likelihood of chloride binding to the cement hydration products. Secondly, the increased water volume potentially improves the overall

mobility of chloride ions within the paste's pores, facilitating their efficient transport towards the reactive sites. Thirdly, the larger volume of water may dilute the pore solution of the paste, resulting in a decreased ionic strength within the pores. Previous research has demonstrated that such reduced ionic strength contributes to an increased self-diffusion of water [67], which in turn can increase the probability of a greater number of chlorides reaching the binding sites within the paste's pores.

These results suggest that although sample surface area plays a critical role in providing binding sites for chlorides, the amount of chlorides per unit mass of sample is also playing a critical role in this matter and should not be taken for granted. Currently, there is limited research available in this specific domain. Further investigation is warranted to comprehensively understand the intricate mechanisms underlying the observed increase in chloride binding, particularly regarding the interplay between exposure solution volume, chloride ion transport, dilution effects in pore solution chemistry, and the resulting impact on binding interactions within the concrete matrix.

4.1.4. Effect of Sample Shape on Chloride Binding

Figure 4.7 depicts the quantity of bound chloride in disk-shaped, crushed, and powder samples at varying free chloride concentrations ranging from 0.3 to 2 M. The results indicate that grinding the samples into powder resulted in the highest chloride binding capacity compared to the crushed and disk-shaped specimens. This is attributed to the higher available surface area and particles for chloride ions to physically or chemically absorb on cement hydration products.

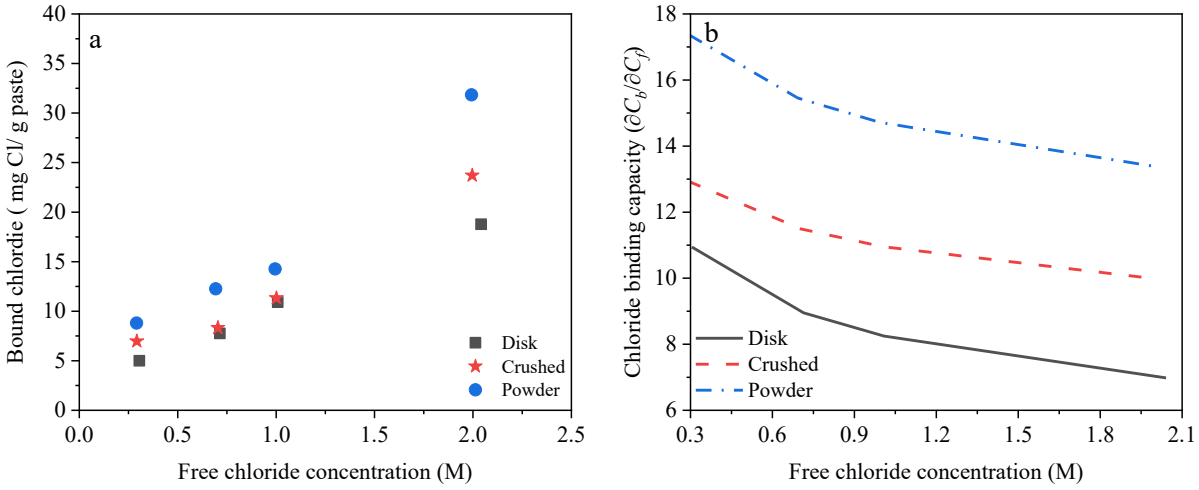

Figure 4.7. (a) Chloride binding content and (b) chloride binding capacity in different sample forms

Although the chloride binding content of crushed and disk-shaped specimens remained relatively similar at free chloride concentrations up to 1 mol/L, a significant difference was observed at higher chloride concentrations. At 2 mol/L free chloride concentration, the bound chloride contents were approximately 18.8, 23.70, and 31.83 mg/g paste for disk-shaped, crushed, and powder specimens, respectively.

The findings indicate that the powder form of the samples showed significantly higher chloride binding capacity than the other forms, regardless of the free chloride concentration. For example, at a free chloride concentration of 1 M, the chloride binding capacity for disk-shaped, crushed, and powder samples were 8.25, 10.96, and 14.72 mg/g paste/M, respectively.

4.1.5. Chloride Binding Isotherms

Langmuir and Freundlich isotherms given in Eqs. (6) and (7) were fitted to the experimental data to calculate their parameters (α and β), followed by the calculation of the residual sum of squares (RSS) for each fit. Table 4.1 displays the calculated parameters and RSS for all samples.

Table 4.1. Calculated Langmuir and Freundlich parameters

Parameter	Factor	Langmuir Isotherm			Freundlich Isotherm		
		α_L	β_L	RSS	α_F	β_L	RSS
Shape	Disk	13.72	0.25	1.60	10.83	0.76	0.78
	Crushed	13.31	0.07	11.72	12.67	0.87	10.06
	Powder	17.94	0.07	19.80	17.01	0.86	16.77
Saturation	0	13.72	0.25	1.60	10.83	0.76	0.78
	50%	23.94	0.35	13.19	17.38	0.69	6.98
	100%	23.80	0.18	31.15	20.29	0.78	23.23
L/S Ratio	1:3	11.18	0.02	24.55	11.44	0.86	22.85
	1:6	13.31	0.07	11.72	12.67	0.87	10.06
	1:10	38.70	0.53	6.79	24.21	0.65	18.52
Solution	NaCl	13.72	0.25	1.60	10.83	0.76	0.78
	CH	12.94	0.24	0.63	10.21	0.79	0.75
	CH+KH	8.91	0.13	0.95	7.83	0.86	0.82
	CH+KH+NH	15.40	0.94	1.35	7.57	0.54	3.12

The findings indicate that the Langmuir and Freundlich isotherms yield comparable estimations within the chloride concentration range investigated in this study. Table 4.1 indicated that calculated RSS for Freundlich isotherm was lower than Langmuir isotherm in most cased, therefore, the Freundlich parameters (α_F and β_F) should be utilized to compute the chloride binding capacity. It is crucial to highlight that the Freundlich isotherm tends to overestimate the binding capacity when chloride concentrations are extremely low (<0.1 mol/L). Consequently, it is advisable to employ the Langmuir isotherm for that particular range.

4.1.6. Summary of Main Findings (Objective 1)

The absence of standardized testing protocols for chloride binding results in variability and errors when estimating actual binding capacity. To mitigate this issue and establish a more reliable approach with practical applications, several recommendations should be considered:

1- To enhance test result accuracy and extend the applicability of chloride binding tests, it is important to define a normal saturation level for samples to accurately replicate real-life scenarios. This can be achieved by obtaining samples from a structure located in a similar environment or by using precipitation data to estimate the average saturation level of concrete. If a normal saturation level is unknown, the authors suggest testing the chloride binding isotherm at three different degrees of saturation, allowing the results to be extrapolated to conditions within that range.

2- The chemical composition of the chloride solution should correspond to the pore solution chemistry of the sample under study. Avoid saturating the solution with calcium, sodium, and potassium ions, as it can lead to an underestimation of the chloride binding results. One approach to achieving this is by obtaining a representative pore solution using the pore-press technique.

3- It is important to select sample shapes that resemble real-world conditions to obtain more realistic estimates of chloride binding capacity in actual concrete structures. Solid samples can provide a better estimation of chloride binding capacity as they more accurately resemble field conditions.

4- The solid-to-liquid mass ratio should be selected based on precipitation data relevant to the field conditions.

5- Finally, researchers are recommended to report all testing parameters related to the degree of saturation of samples, the chemical composition of the exposure solution, sample shape and surface area, and the solid-to-liquid mass ratio when testing the chloride binding of cementitious systems.

4.2 Objective 2: Investigate the Chloride Binding and Desorption Capacity for OPC Cement

The results and discussion presented in this section were first published in journal of *Construction and Building Materials, Volume 312, Page 125415, "pH-dependent chloride desorption isotherms of Portland cement paste", Copyright Elsevier (2021)* [66]. This objective studied pH-dependent chloride desorption isotherms for OPC paste exposed to $MgCl_2$, $CaCl_2$, and NaCl solutions as the most common de-icers. In addition, we investigated which empirical isotherm better suits the chloride binding of OPC paste, and whether the amount of bound chloride is influenced by the cation-type (Ca^{2+}, Mg^{2+}, Na^{+}) of brine solution.

4.2.1 Chloride Binding Isotherms

To identify the appropriate binding isotherm that could mimic the nonlinear binding behavior of the chlorides in these samples, the Langmuir and Freundlich isotherms were fitted to the experimental results by means of nonlinear least-squares analysis. Figure 4.8b indicates the binding capacity of each sample based on the estimated α and β parameters for the Langmuir isotherm given in Table 4.2.

Table 4.2. Langmuir and Freundlich parameter estimates

	Langmuir Isotherm			Freundlich Isotherm		
Solution	α_L	β_L	RSS	α_F	β_F	RSS
$MgCl_2$	43.64	1.12	13.74	19.30	0.51	31.56
$CaCl_2$	30.52	0.35	21.11	21.69	0.71	24.44
NaCl	23.44	1.31	2.80	9.62	0.47	1.20

Table 4.2. shows the residual sum of squares (RSS) for each fit and the corresponding parameter estimates associated with the isotherms. The results presented in Table 4.2. indicate that, in all cases except for NaCl, the Langmuir isotherm had a smaller RSS and provided a better fit to the experimental data. Numerous researchers have investigated chloride binding isotherms. Cao et

al. [68] studied chloride binding for OPC cement paste exposed to NaCl solutions with diverse concentrations ranging from 0.1 M to 3 M. They reported a non-linear relationship between bound and free chloride and cited that both Langmuir and Freundlich models fit experimental results well. A review of the effects of external chloride on chloride binding in cement-based materials by Yuan et al. [208] reveals that considering a linear correlation between free and bound chloride is an oversimplification. They also pointed out that a Langmuir isotherm corresponds very well with experimental results at low chloride concentrations. Thomas et al. [114] also noted that free and bound chloride have a non-linear relationship. They pointed out that for concrete samples containing diverse binder types exposed to NaCl solution, the Freundlich isotherm was better fitted to experimental results than the Langmuir isotherm.

Figure 4.8a illustrates the relationship between the concentrations of bound and free chlorides for the ground OPC paste samples exposed to three different salt solutions. Figure 4.8a shows that the chloride-binding capability of the OPC paste was greatly influenced by the cation type of the chloride and its magnitude, with the decreasing order $Ca^{2+} > Mg^{2+} > Na^{+}$. This pattern can be explained by the role that the cation type of chloride solutions played in altering the pH of the solution and the structure of C–S–H. When NaCl reacts with cement hydration products, sodium hydroxide forms which is a strong base, leading to increases in the pH of the pore solution. An increase in the pH of the pore solution leads to an increase in the solubility of Friedel's salt and thus a decrease in the number of bound chlorides. When $CaCl_2$ reacts with cement hydration products, Ca^{2+} can contribute to the development of more C–S–H, which can take up more chlorides from the solution and release H^{+} back to the solution in return, leading to a reduction in the pH of the solution [131]. The calcium in the salt solutions fosters the formation of the Cl-AFm phase (Friedel's salt), which is the chemical form of bound chloride. Similarly, the presence of

Mg^{2+} can lead to the formation of brucite and an increased Ca/Si ratio in the C–S–H gel, which in turn can increase the chloride uptake capability of the C–S–H [82].

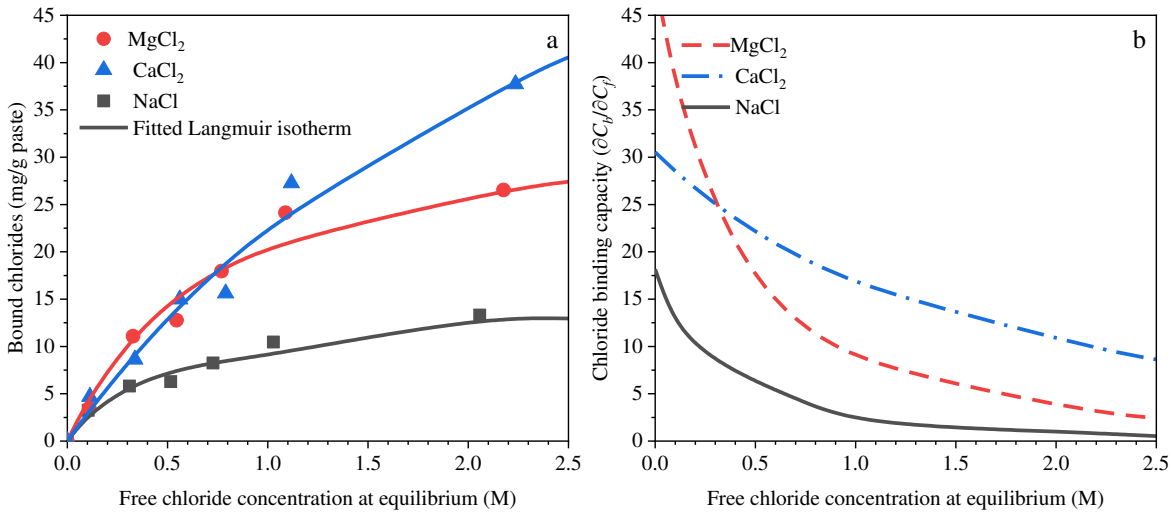

Figure 4.8. (a) Chloride binding isotherm of OPC paste exposed to various salts; (b) Chloride binding capacity OPC paste exposed to various salts

An examination of Figure 4.8b reveals that, at low free-chloride concentrations (i.e., free chloride < 0.3 M), the binding capacity of the ground OPC paste samples exposed to $MgCl_2$ was higher than for $CaCl_2$ and NaCl. For example, at free chloride = 0.1 M, the binding capacities of $MgCl_2$, $CaCl_2$, and NaCl were 38.5, 28.2, and 11.8 mg/g paste/M, respectively. At higher free-chloride concentrations, however, the OPC paste sample appears to have a higher binding capacity when exposed to $CaCl_2$. For example, at a 2 M chloride concentration, the chloride-binding capacity of the OPC sample exposed to the $CaCl_2$ solution was 10.91 mg/g paste/M free chloride, which was 179% higher than for the $MgCl_2$ solution and approximately 991% greater than that of the NaCl solution, which has the binding capacity of 1.00 mg/g paste. The chloride binding results aligns wells with previous finding with De Weerdt et al. [82] that reported a higher chloride binding quantities for cement paste exposed to $MgCl_2$ followed by $CaCl_2$ and NaCl solutions. Previous

findings were reported a higher chloride binding quantities when free chloride concentration increased [68, 132].

4.2.2. XRD and TGA Results After Exposure to Brine Solutions

Figure 4.9 shows the XRD patterns for ground cement samples immersed in 0.1 M and 2 M $MgCl_2$, $CaCl_2$, and NaCl solutions prior to the addition of nitric acid. At a molarity of 0.1 (Figure 4.9a), the main phases observed in all three salt solutions were Friedel's salt, portlandite, and calcite. However, when the molarity increased to 2 (Figure 4.9b), the detected phases were affected by the type of cation. It has been reported that immersing OPC paste in high-concentration salt solutions causes calcium to leach out of portlandite and C-S-H, leading to a reduction in the Ca/Si ratio of the cementitious system [209]. This can be seen in Figure 4.9b, where the portlandite intensities for 2 M $CaCl_2$ were extensively reduced. Moreover, for 2 M $MgCl_2$, no visible sign of portlandite was detected, and, instead, brucite was observed. Figure 4.9 shows that Friedel's salt was detected between 11.1° and 11.9° 2θ, which agrees with previous reports [124, 210].

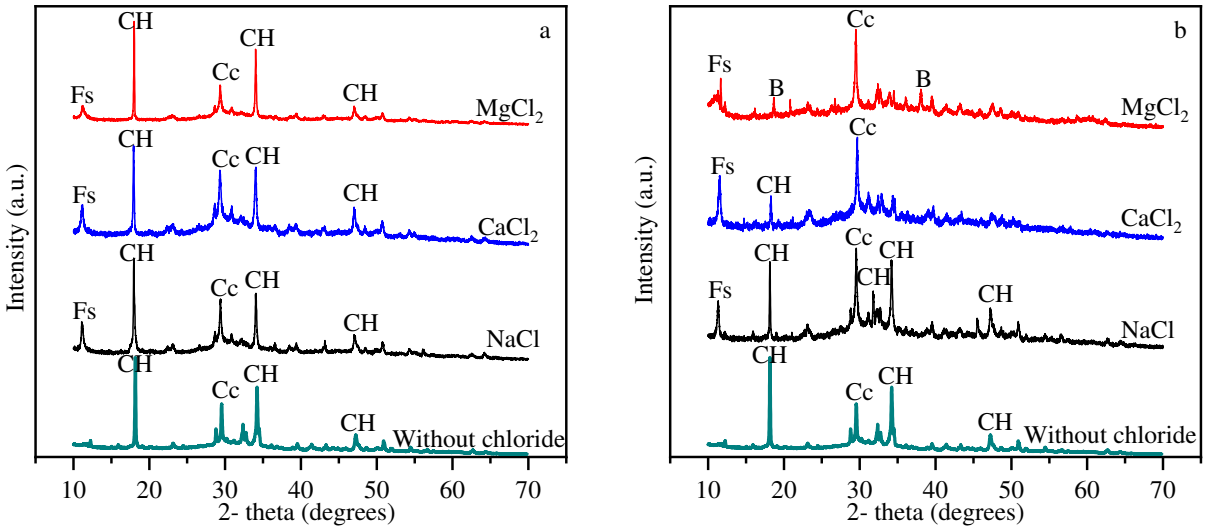

Figure 4.9. XRD patterns of ground OPC paste samples after chloride binding period (a) 0.1 M chloride solution; (b) 2 M chloride solution (Fs: Friedel's salt, CH: portlandite, B: brucite, Cc: calcite)

The results indicate that an increase in the concentration of chlorides from 0.1 M to 2 M led to an increase in the Friedel's salt intensity and a decrease in portlandite intensities. The intensity of Friedel's salt was influenced by the type of cation, and $CaCl_2$ caused the highest intensity. Ca^{2+} can dissolve portlandite and reduce the pH of the pore solution, which in turn can increase the risk of reinforcement corrosion in concrete. Therefore, while $CaCl_2$ salt can bind more chloride with cement hydrates, forming Friedel's salt, $CaCl_2$ salt is considered to be more harmful to concrete than NaCl [211] due to the reduction of pH.

The DTG plots obtained from TGA tests for the OPC pastes exposed to salt solutions before exposure to nitric acid are shown in Figure 4.10. DTG curves show the rate at which mass changes in relation to temperature, such as the percentage of mass loss per degree Celsius. These reveal four significant mass losses, corresponding to ettringite at 85 to 210℃ [212], Friedel's salt at 235 to 375℃ [124, 210, 213], portlandite at 385 to 460℃ and calcite at 540 to 720℃. Figure 4.10 shows a reduction in the amount of portlandite in solute with a molarity of 2 compared to 0.1 M that is in good accordance with the discussion provided above and data that has been reported by other researchers [209].

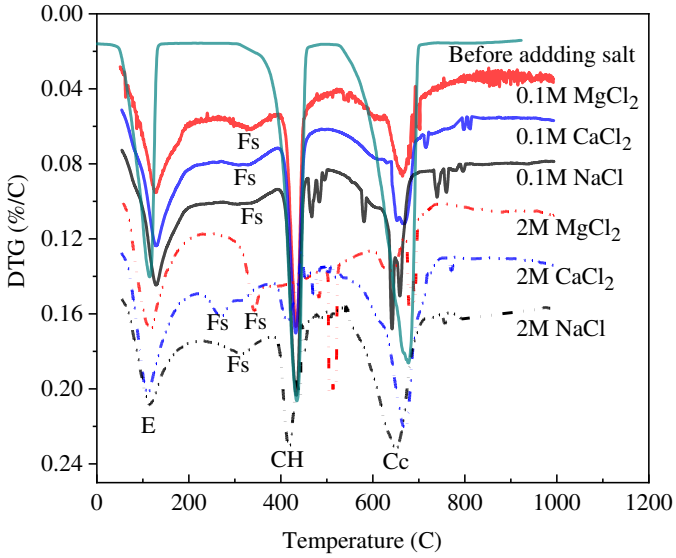

Figure 4.10. DTG curves of ground OPC paste samples after chloride binding period (E: ettringite, Fs: Friedel's salt, CH: portlandite, Cc: calcite)

It should be noted that, in $MgCl_2$ solutions, it is challenging to clearly separate the peaks associated with C-S-H from M-S-H, and the peaks associated with Friedel's salt from brucite because their corresponding peaks are mostly overlapping [214]. The Friedel's salt mass-loss values for ground cement paste immersed in 0.1 M $MgCl_2$, 0.1 M $CaCl_2$, and 0.1 M NaCl were 2.21, 2.75, and 1.40%, respectively, which agree with the XRD results, confirming that more chlorides from $CaCl_2$ salt are available to bind with cement hydrates. The same trend was reported in [78, 215]. A comparison of the DTG curves of the 0.1 M and 2 M solutions shows the presence of more of Friedel's salt in the 2 M solutions. The Friedel's salt mass-loss values for the OPC samples immersed in 2 M $MgCl_2$, 2 M $CaCl_2$, and 2 M NaCl were 3.63, 3.53, and 2.71%, respectively.

4.2.3 Chloride Desorption Results

Figure 4.11a shows how the pH of the exposure solution changes with the addition of nitric acid. It is important to note that the pH values reported in Figure 4.11 were measured after no further reaction between the acid and the cement paste sample was visible (i.e., typically after 12 hours). Upon the addition of nitric acid to an exposure solution, the equilibrium state of the solution is disturbed, and the pH of the solution drops significantly, followed by a gradual increase in the pH.

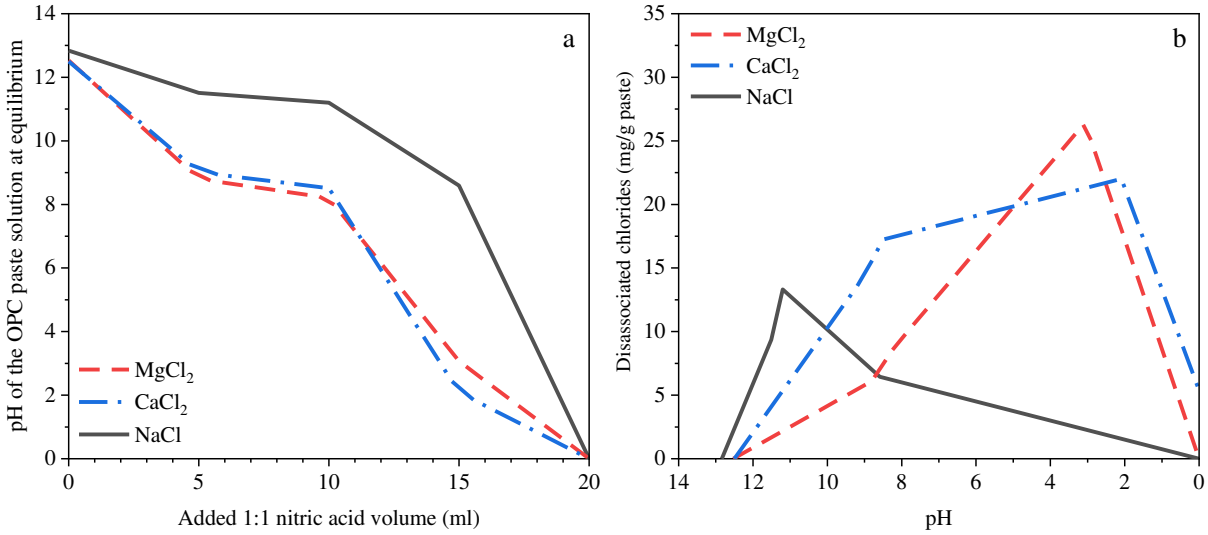

Figure 4.11. (a) The volumetric influence of nitric acid on the pH of the OPC solution at equilibrium; (b) the influence of pH on chloride disassociation of bound chlorides

As the pH decreases, the hydrated cement compounds undergo hydrolytic decomposition. At pH values below 12.6, portlandite is the first constituent that starts to decompose, followed by C-S-H and calcium aluminate hydrate [216]. At pH values below 4, aluminum hydroxide reacts further to form aluminum nitrate, and at pH values below 2, the acid can dissolve the calcium alumino-ferrite phases to form calcium nitrate and iron hydroxide [172].

Figure 4.11b shows the concentration of dissociated chlorides as a function of the pH of the exposure solution. The general trend in this figure indicates that the pH-dependent chloride

desorption isotherm is nonlinear and can be divided into two upward and downward parts. Soon after the addition of nitric acid, the bound chlorides dissociated to a certain degree and were released into the exposure solution, which corresponds to the increasing trend in the desorption isotherm curve in Figure 4.11b. During this phase, the concentration of the free chlorides in the exposure solution increased. With the further addition of nitric acid, the trend of the desorption isotherm shifts to a downward direction, which is an indication of chloride uptake from the exposure solution. During this phase, the concentration of free chlorides in the exposure solution was reduced. At a pH of 0, almost all the dissociated chlorides were taken up from the solution, as discussed in more detail below.

Figure 4.11b also shows that the pH at which the maximum chloride dissociation occurred was influenced by the cation type of the chloride. For example, in the sample exposed to the NaCl solution, the maximum value of chloride dissociation was 13.31 mg/g paste, which occurred at a pH of 11.2, whereas in the samples exposed to $MgCl_2$ and $CaCl_2$, the maximum values of the dissociated chlorides were 26.54 and 22 mg/g paste, at pH values of 3.07 and 2.09, respectively. These results suggest that the breakdown of physical or chemical chloride bonds in the ground cement paste exposed to the $MgCl_2$ and $CaCl_2$ solutions required a lower pH value, and therefore it can be assumed that they had developed a stronger bond compared to the NaCl solution. Another interesting finding was the rate of dissociation, which was influenced by the cation type of the chloride and had the decreasing order NaCl > $MgCl_2$ > $CaCl_2$. A comparison of Figure 4.8a and Figure 4.11b indicates that almost all the bound chlorides in the $MgCl_2$ and NaCl solutions were dissociated at the peak points, whereas only 58% of the bound chlorides in the $CaCl_2$ solution were dissociated and released into the exposure solution. These results agree with the previous

assumption that cement hydrates form a stronger bond with the chlorides in $CaCl_2$ solution than in NaCl solution.

In general, the final products of the reaction between nitric acid and cement paste are expected to be calcium salt (i.e., calcium nitrate), water, hydrogels of silica, aluminum, and ferric oxide [216]. The authors hypothesized that these precipitated calcium salts and hydrogels could absorb some of the free chlorides from the exposure solution, resulting in the downward trend in the chloride desorption isotherm that appears in Figure 4.11b. The formation of similar gel-like products during chloride extraction by nitric acid has been reported by several previous authors. For example, Lolivier [217] reported the formation of gelatinous silica during chloride extraction from hardened concrete, while Ahmed and Trejo [218] found whitish gypsum-like products, rich in calcium, sulfur, and alumina, during chloride extraction from calcium aluminate and calcium sulfoaluminate paste samples containing admixed chlorides.

Some researchers have suggested that boiling the solution after the addition of nitric acid is a required step to make sure all the chlorides are extracted [219]. However, “total” chloride extraction using nitric acid and the boiling method has been debated and needs further investigation [220, 221]. Note that boiling is recommended when the purpose of the test is to determine the concentration of total chlorides in a hardened cementitious sample [220, 222], but this was beyond the scope of the present study.

The chemical compositions of the hydrogels produced after the addition of 20 ml (0.68 fl oz) nitric acid were obtained by means of X-ray fluorescence analysis and are shown in Table 4.3. These hydrogels were mainly composed of calcium, and contained noticeable concentrations of chlorides and sulfides, which agrees with the hypothesis discussed above, that hydrogels can

absorb chlorides. In addition, there was a fair amount of Fe^{3+}, possibly in the form of iron hydroxide, in the hydrogels, which would explain their brownish colors.

Table 4.3. Chemical composition of hydrogels (%)

Solution	Na^{+}	Mg^{2+}	Al^{3+}	Si^{2+}	P^{3-}	S^{2-}	Cl^{-}	K^{+}	Ca^{2+}	Fe^{3+}
$MgCl_2$	0.00	1.91	0.01	0.18	0.18	3.40	18.74	0.56	71.44	3.06
$CaCl_2$	0.00	0.24	0.45	0.31	0.16	6.91	13.09	0.47	76.60	1.43
NaCl	1.06	0.29	0.58	0.37	0.19	6.71	15.64	0.52	69.32	4.73

4.2.4. XRD and TGA Results After pH Reduction

Figure 4.12 shows the diffraction patterns after the addition of nitric acid to the OPC samples immersed in 0.1 M and 2 M $MgCl_2$, $CaCl_2$, and NaCl solutions. A comparison of Figure 4.12 with Figure 4.9 highlights that adding nitric acid and reducing the pH of the solution can significantly affect the phases detected. Portlandite is the first hydration product starting dissolution when acid attacks concrete and the pH value is lower than 12.6. The final products of the reaction between an acid and cement paste hydrations are expected to be calcium salts, and the type of acid does affect the resulting calcium salt [223]. As can be seen in Figure 4.12, the recorded diffractions are dominated by calcium nitrate. Moreover, Friedel's salt has been removed. The XRD results also show that, after adding nitric acid to ground OPC samples, a gypsum phase is present. This can, in part, be caused by the instability of ettringite at low-pH values, and its subsequent decomposition into alumina hydroxide and gypsum [216, 224].

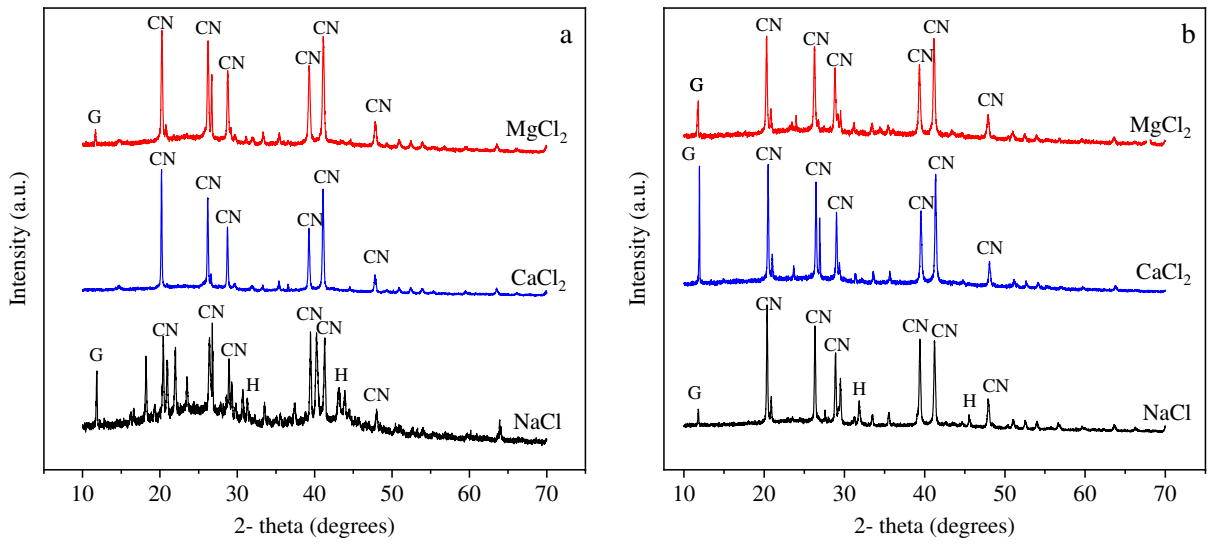

Figure 4.12. X-ray diffraction patterns of ground OPC pastes immersed in salt solutions after adding (1:1) nitric acid (a) 0.1 M; (b) 2 M (G: gypsum, CN: calcium nitrate, H: halite)

The DTG curves for the ground pastes exposed to varying salt solutions after the addition of nitric acid are shown in Figure 4.13. It should be noted that some data, including from the 0.1 M NaCl and 2 M $CaCl_2$, were lost due to data collection problems. As can be seen in Figure 4.13, after adding nitric acid, a very negligible amount, if any, of Friedel's salt was present. After the addition of 20 ml (1:1) nitric acid, the pH of the solutions reached close to 0, which led to decalcification and the dissolution of Friedel's salt.

The DTG curves (Figure 4.13) indicate that gypsum and calcium nitrate were the two main phases. Gypsum decomposition is observed in a temperature range of 100 to 165°C; more precisely, based on the literature, it occurs around 140°C, although the exact temperature range varies and is influenced by the heating rate and the type of vessel used [212]. The second notable mass loss was related to calcium nitrate, which happened at around 460 to 620°C, after adding the acid [225]. As discussed in the first part of this section, portlandite becomes unstable at this very low pH, and the main phase is calcium nitrate, as confirmed by XRD (Figure 4.12). The calcium

nitrate mass-loss values for the 0.1 M $MgCl_2$, 0.1 M $CaCl_2$, 2 M $MgCl_2$, and 2 M NaCl were 35.94, 36.37, 29.41, and 36.04%, respectively.

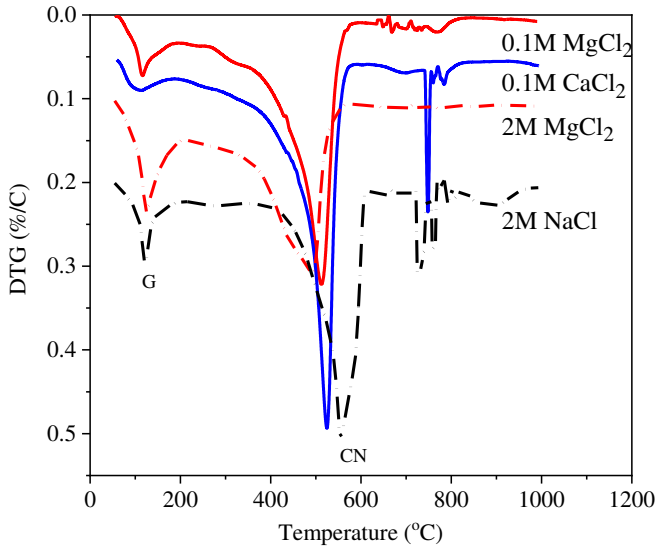

Figure 4.13. DTG curve of OPC paste immersed in salt solution after the addition of nitric acid (G: gypsum, CN: calcium nitrate)

4.2.5. Summary of Main Findings (Objective 2)

In this objective, we first investigated the chloride-binding behavior of ground OPC paste exposed to $MgCl_2$, $CaCl_2$, and NaCl solutions, and then we devised a testing procedure to develop and study pH-dependent chloride desorption isotherms of ground OPC paste. It was hypothesized that samples that develop a strong chloride binding can better resist a low-pH environment and release fewer chlorides into the concrete pore solution. Here a summary of primary outcomes:

1- It was found that the Langmuir isotherm is better suited to the chloride binding of ground OPC paste compared to Freundlich isotherm.

2- The quantity of bound chloride is predominantly influenced by the cation-type of chloride in the decreasing order $CaCl_2$ > $MgCl_2$ > NaCl.

3- The drop in the pH of the exposure solution, initially resulted in the total dissociation of the bound chlorides from the $MgCl_2$ and NaCl salts. However, only 58% of the bound chlorides from the $CaCl_2$ solution could be dissociated as a result of the reduced pH of the exposure solution.

4- Friedel's salt formation which represents the chemically bound chloride was influenced by the type and concentration of the salt solution.

4.3 Objective 3: Investigation on the chloride binding capacity and desorption for cementitious systems containing SCMs

The results and discussion presented in this section were first published in journal of *Construction and Building Materials, Volume 370, Page 130667, "Chloride desorption mechanisms of cement pastes containing fly ash", Copyright Elsevier (2023)* [153] and American Society of Civil Engineering (*ASCE) journal of Materials in Civil Engineering, Volume 35, Issue 12, "Effect of pH on Desorption of Bound Chlorides in Cement Pastes Containing Granulated Blast-Furnace", Copyright American Society of Civil Engineering (ASCE) (2023)* [226]. In this objective, we comprehensively investigated the properties of blended cement incorporating three principal supplementary cementitious materials (SCMs): fly ash (at 15% and 30% replacement levels), slag (at 25% and 50% replacement levels), and silica fume (at 5% and 10% replacement levels). Initially, these blended cements were subjected to exposure in three different brine solutions (NaCl, $MgCl_2$, and $CaCl_2$) to assess their chloride binding capacity. Subsequently, the pH of the system was systematically altered through the addition of varying amounts of nitric acid. At each specified pH level, we conducted a detailed analysis of chloride desorption and the associated changes in chemical composition. To facilitate a clear and coherent presentation of our findings, the results for each type of SCM are discussed separately.

4.3.1. Chloride Binding and Desorption Capacity for Blended Cement Containing Fly Ash

4.3.1.1. Hydration Characterization of Binary Blended Cement Pastes

Adding fly ash (FA) to an OPC system promotes pozzolanic reactions, in which portlandite is consumed to form C–S–H gel [227, 228]. Figure 4.14 shows the XRD spectra of OPC, FA15, and FA30 pastes that were cured for 56 d. The intensity of the portlandite peaks decreased with the inclusion of FA because it was consumed to produce C–S–H. For instance, the intensity of the

portlandite peak around 18 degrees for OPC is 0.899, which is reduced to 0.842 and 0.833 in FA15 and FA30, respectively. At the next portlandite peak, around 29 degrees, the intensities in OPC, FA15, and FA30 are 0.336, 0.258, and 0.213, respectively. Ettringite, tetra calcium aluminoferrite (C_4AF), monocarbonate, ferrite, portlandite, calcite, and belite were also detected.

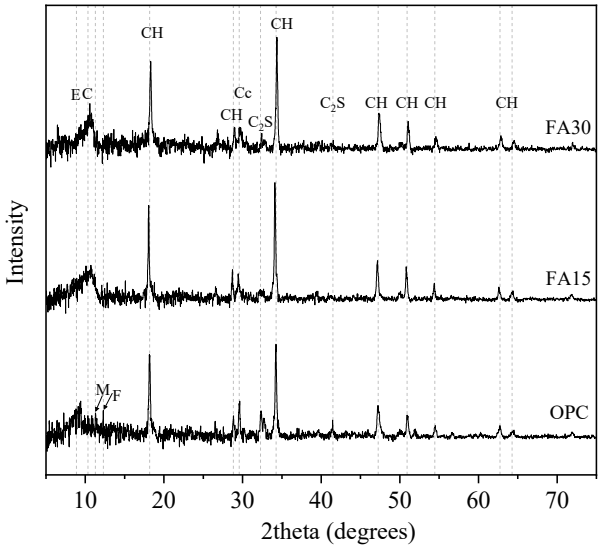

Figure 4.14. XRD spectra of 56-d paste samples containing fly ash (E: Ettringite, C: C4AF, M: Monocarbonate, F: Ferrite, CH: portlandite, Cc: Calcite, C_2S: Belite)

The results are in agreement with previous investigations that studied microstructures of blended cement pastes containing fly ash [229, 230]. Figure 4.15 shows TGA and DTG results for blended cement pastes containing fly ash. In the TGA tests and DTG analysis, two significant dips were observed at around 100°C and 450°C, which are attributed to ettringite and portlandite, respectively [212]. Only small amounts of monocarbonates were observed in the DTG of FA-bearing samples, with a dip at around 280°C. Figure 4.15 shows the reduction in the magnitude of the portlandite further decreases with an increased level of FA replacement, indicating a lower mass loss associated with portlandite due to pozzolanic activity [231]. The TGA results show that the mass loss percentage related to portlandite in OPC was 4.86%, dropping to 4.09% and 3.43%

in the FA15 and FA30 pastes, respectively. Compared to the previous studies, the same phases and reduction in mass loss of the portlandite by incorporation of fly ash compared to OPC were reported by Kocak et al. [230] and Leklou et al [232].

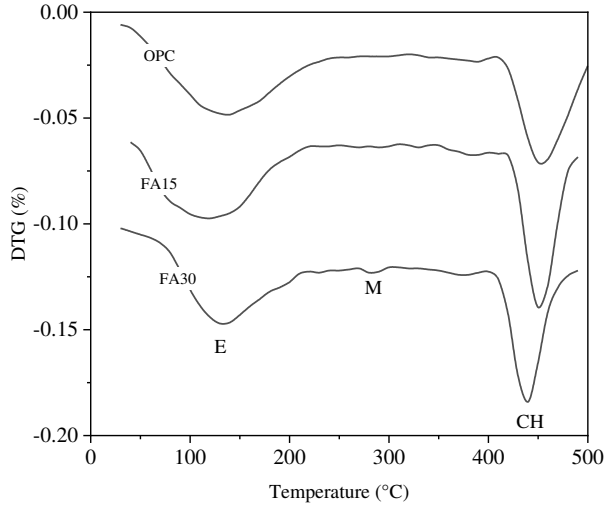

Figure 4.15. DTG analyses of 56-d hydrated paste samples containing fly ash (E: ettringite, CH: portlandite, and M: Monocarbonate)

4.3.1.2. Chloride Binding of Blended Pastes Containing Fly Ash

Figure 4.16 illustrates the relationship between the free and bound chloride concentrations in three systems containing OPC and FA. In most cases, the relationship between free and bound chlorides is nonlinear. The Langmuir and Freundlich isotherms were fit to the experimental results to identify the binding isotherm that best mimics the nonlinear binding behavior of the chlorides in these samples. Table 4.4 shows the residual sum of squares (RSS) of the fits and the corresponding parameter estimates associated with each isotherm. The Langmuir isotherm was a better fit for the chloride binding in paste samples in the NaCl and $MgCl_2$ solutions, whereas the Freundlich isotherm was a better fit for the $CaCl_2$ solutions.

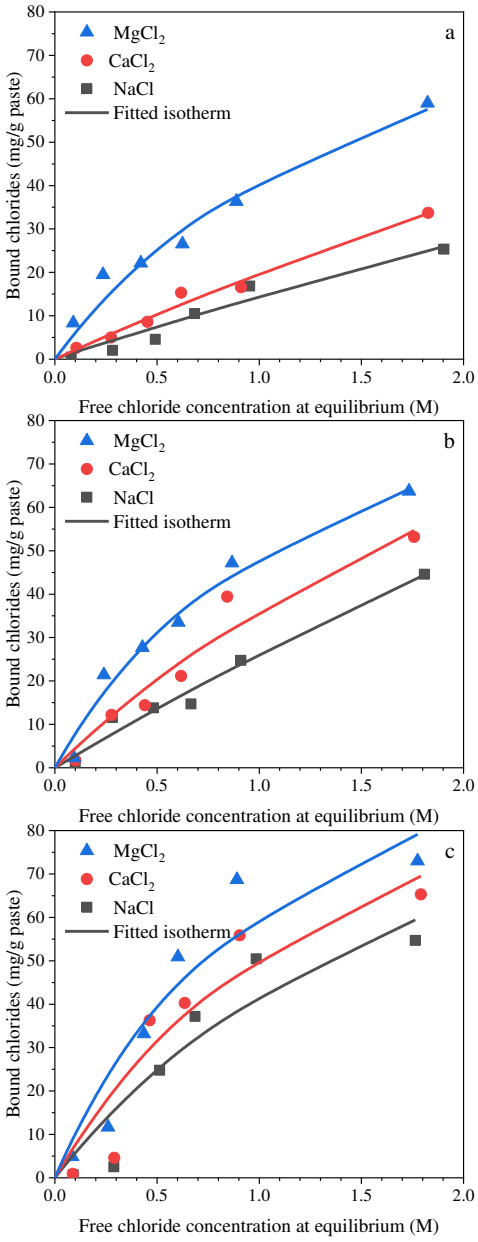

Figure 4.16. The chloride binding isotherms of OPC+ fly ash paste exposed to NaCl, $CaCl_2$, and $MgCl_2$ (a) OPC; (b) FA15; (c) FA30

Table 4.4. The estimated parameters of the Langmuir and Freundlich isotherms

System	Solutions	Langmuir Isotherm			Freundlich Isotherm		
		α_L	β_L	RSS	α_F	β_L	RSS*
OPC	NaCl	15.32	0.06	23.46	14.07	0.98	23.67
	$CaCl_2$	21.60	0.10	10.96	19.43	0.91	11.01
	$MgCl_2$	65.98	0.60	58.94	69.60	0.64	22.86
FA15	NaCl	28.40	0.09	28.27	25.90	0.91	27.17
	$CaCl_2$	46.63	0.28	95.65	35.00	0.82	117.39
	$MgCl_2$	87.16	0.78	53.24	46.64	0.64	99.87
FA30	NaCl	61.99	0.48	323.73	39.99	0.76	419.70
	$CaCl_2$	84.09	0.65	419.63	48.20	0.69	572.24
	$MgCl_2$	114.39	0.88	389.67	57.38	0.62	626.58

*RSS: Residual sum of squares

Figure 4.16 shows that the cation of the salt played a significant role in the chloride binding capacity of the OPC pastes. The solubility of Friedel's salt is dependent on pH [233] and an increase in pH can increase the solubility of Friedel's salt. Therefore, the lower chloride binding in NaCl solution can be attributed to its higher pH and reduced chemical binding capability. One reason for a higher bound chloride content in $CaCl_2$ is the contribution of the aqueous Ca^{2+} to the development of more of the C–S–H phase with an increased Ca/Si molar ratio, which in turn can adsorb more chloride ions. The presence of aqueous Mg^{2+} can lead to an increased Mg/Si molar ratio, promoting the formation of magnesium silicate hydrate (M–S–H), which has a detrimental impact on the porosity and integrity of the paste samples. The higher porosity due to formation of M-S-H means more chloride ions can ingress, resulting in a higher chloride binding quantity.

Figure 4.16 also reveals that replacing a portion of OPC with FA improved the overall chloride binding of the system. For example, in a 2 M NaCl solution, replacing a portion of the OPC with 15% and 30% FA increased the number of bound chlorides by 176% and 216% compared to their OPC counterparts. The same trend was observed in $CaCl_2$ and $MgCl_2$ solutions.

The increased chloride binding due to the inclusion of FA resulted from the higher Al_2O_3 content of FA. Based on the chemical composition of FA, Table 3.2 in chapter 3, it has nearly 4.8 times greater Al_2O_3 content than OPC which can help the formation of more AFm phases in hydration production [107]. Higher AFm content facilitates the formation of chloride-bearing AFm compounds such Friedel's salt ($C3A.CaCl_2.10H_2O$), which are the primary forms of chemically bound chlorides, leading to a higher capacity in FA-containing pastes.

In addition, the XRD and TGA results confirmed that the inclusion of FA promoted pozzolanic reactions, which resulted in the consumption of portlandite to form C–S–H, an increase in Al-rich phases and AFm, and finally, a reduction in ettringite [228]. A higher amount of C-S-H gel in the paste is beneficial because it can increase the possibility of physical chloride binding [61]. Therefore, more chlorides physically or chemically reacted with hydration phases, leading to a higher chloride binding capacity.

4.3.1.3. Chloride Desorption of Blended Pastes Containing Fly Ash

The pH of the exposure solution is one critical factor that can influence the rate of chloride desorption in cementitious samples. The pH values of the 2 M NaCl, $CaCl_2$, and $MgCl_2$ solutions used in this study for chloride binding were 6.8, 9.4, and 8.7, respectively. When the paste samples were each immersed in 60 mL of salt solutions, the pH gradually increased during the exposure period due to the leaching of portlandite, which in turn increased the pH buffering capacity of the solution. After keeping the paste samples in salt solutions for 2 weeks, the average pH increased gradually to 12.2 and 11.4 in the NaCl and $CaCl_2$ solutions, respectively. The average pH kept constant at 8.7 for the $MgCl_2$ solution.

Figure 4.17 shows the pH of the exposure solutions measured at different times during the desorption period. The results show that after nitric acid was added, even at low volumes, the pH of the exposure solution dropped significantly for a few minutes and then slowly increased.

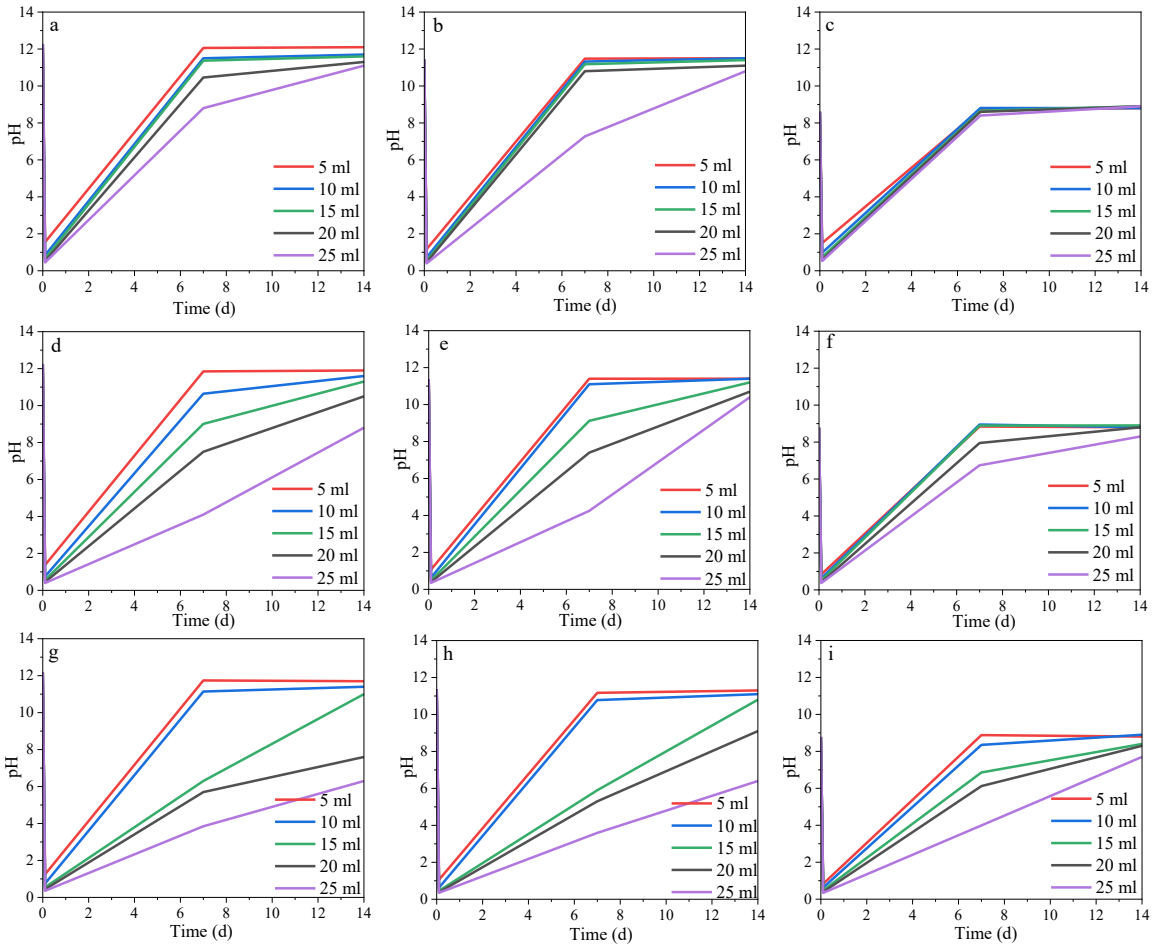

Figure 4.17. pH evolution after adding different volumes of acid. (a) OPC-NaCl; (b) OPC-$CaCl_2$; (c) OPC-$MgCl_2$; (d) FA15-NaCl; (e) FA15-$CaCl_2$; (f) FA15-$MgCl_2$; (g) FA30-NaCl; (h) FA30-$CaCl_2$; (i) FA30-$MgCl_2$

With time, the increased pH confirms the buffering capacity of paste samples due to the reaction between portlandite and nitric acid. Comparing the subplots in Figure 4.17 suggests that the rate of pH increase is closely related to the volume of acid added to the solution. The exposure solution reached equilibrium much faster when a smaller volume of nitric acid was added. For example, after adding 5 mL of acid to the salt solutions, the pH plateaued after about a week. When

a larger volume of acid was used, binders containing higher percentages of fly ash (FA30) had lower pH than OPC because their portlandite content was lower.

Figure 4.18 shows the percentage of released bound chlorides in samples exposed to various volumes of acid. For OPC pastes, Figure 4.18a shows that adding 5–10 mL of acid led to a significant release of bound chlorides: nearly 87%, 92%, and 86% of bound chlorides were released in the NaCl, $CaCl_2$, and $MgCl_2$ solutions, respectively. The number of chloride ions released from the pastes after adding 10 mL of nitric acid yielded similar results. Among the various salt solutions, the released bound chloride contents after 5–10 mL of acid was added to NaCl, and $MgCl_2$ solutions were almost the same or lower than that of $CaCl_2$. Nevertheless, the released bound chloride content declined with the further addition of acid.

In the FA15 pastes (Figure 4.18b), adding acid in volumes of 5–10 mL released more than 90% of the bound chlorides in the NaCl solution, followed by the $CaCl_2$ (nearly 80%) and $MgCl_2$ (nearly 60%) solutions. The further addition of acid decreased the percentage of released bound chlorides. However, in most cases, a higher release of bound chlorides was observed in the NaCl solution than in the other two solutions. Similarly, in the FA30 pastes (Figure 4.18c), the release of bound chlorides in the NaCl solution was more than 87% at all acid volumes, considerably higher than the other two salt solutions. When the FA replacement level increased from 15% to 30%, there were no noticeable changes in the percentage of released bound chlorides in the NaCl and $MgCl_2$ solutions. However, the percentage of released bound chlorides in $CaCl_2$ was reduced, especially within the 5–10 mL range of added acid.

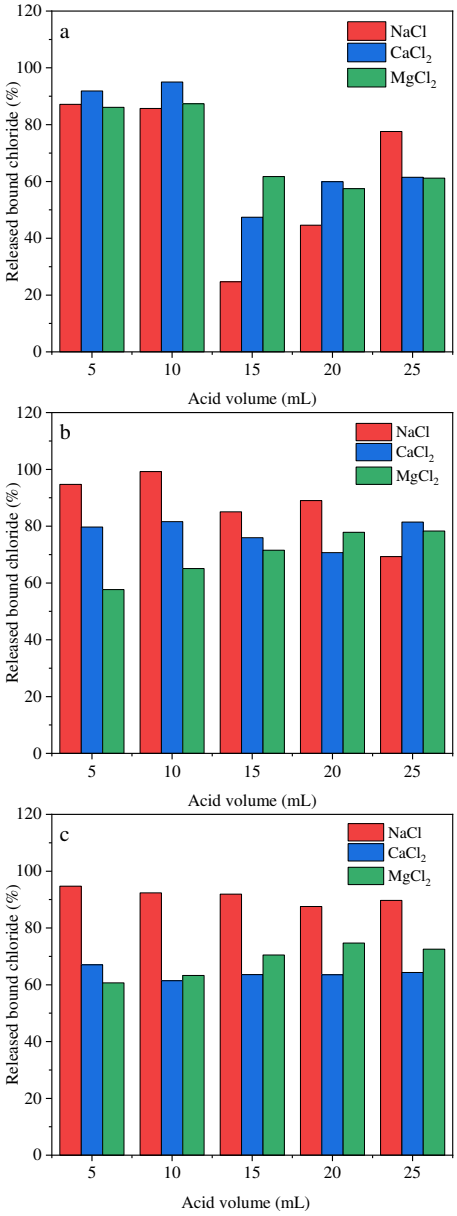

Figure 4.18. The released bound chlorides after 2 weeks of exposure to nitric acid in samples containing (a) OPC; (b)FA15; and (c) FA30

4.3.1.4. XRD Analysis of Chloride Desorption Products

An XRD analysis was performed to investigate the influence of acid exposure on the crystallographic structure and the composition of the paste samples. Figure 4.19 compares the XRD spectra of OPC pastes collected before and after exposure to 25 mL of nitric acid. The

intensity of the portlandite peaks was weaker after acid addition due to the leaching of calcium hydroxide to buffer the pH.

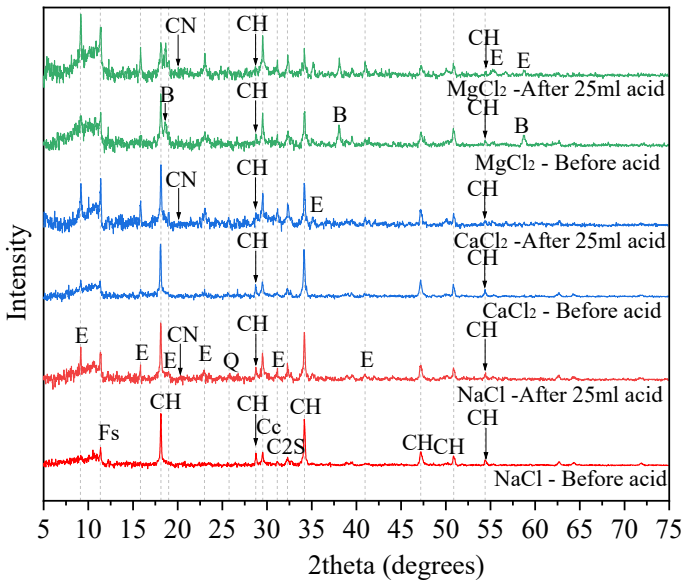

Figure 4.19. The XRD spectra for OPC samples before and after exposure to 25 mL of acid. The samples were first exposed to 2 M salt solutions (Fs: Friedel's salt, CH: portlandite, Cc: calcite, C2S: belite, E: ettringite, B: brucite)

The XRD results show that a considerable amount of ettringite, an expansive crystalline phase, was present after the acid attack due to the dissolution of AFm phases, such as monosulfate (C3A. $CaSO_4 \cdot 12H_2O$) [175]. The peak associated with Friedel's salt located at around 11.3 degrees after exposure to 25 mL of acid suggested that some bound chlorides could not disassociate due to the drop in the pH. These bound chlorides either formed a stable bond that could not be broken at such low pH or resulted from new chemical chloride binding on the subsurface layers of the pastes. As the pH of the solution stabilizes, the available chloride ions in the solution can ingress through the damaged layer and form physical or chemical bonds with the hydration products on the sublayers. A visual inspection of the pastes (see Figure 4.20) confirmed that a considerable portion of the inner parts of the pastes remained intact even after exposure to 25 mL of acid; therefore, it is highly probable that they could bind chlorides.

Another possible reason for the presence of Friedel's salt in the paste samples (Figure 4.19) is that since the samples were dried before they were exposed to the chloride solution, chlorides entered the pastes via capillary action and formed chemical or physical bonds with the inner hydration products. Since the paste samples were exposed to chloride solution for 2 weeks, it can be assumed that they were partially saturated when acid was added to the solution. Therefore, it is acceptable to assume that diffusion governed the acid ingress into the paste. Since acid diffusion slows considerably when the acid loses its strength as it moves through an alkaline environment, the inner parts of the paste sample may not have been exposed to the acid; therefore, the bound chlorides in those parts remained unaffected. Figure 4.20 shows the cross sections of FA30 pastes exposed to 25 mL of acid for 2 weeks, confirming that the inner parts of the paste specimens were intact. This hypothesis was confirmed by the presence of Cl-AFm in the XRD spectra of the paste after acid was added.

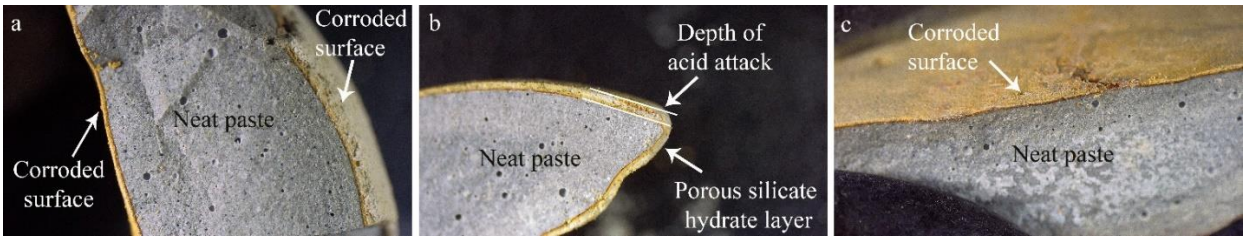

Figure 4.20. Cross-sectional images of FA 30 samples after exposure to 25 mL of nitric acid in (a) NaCl; (b) $CaCl_2$; and (c) $MgCl_2$ solutions

Figure 4.21 shows the XRD spectra of the FA-bearing samples before and after exposure to nitric acid. Similar to the OPC results, the presence of ettringite and calcium nitrate after exposure to acid was observed in the XRD spectra. In the FA15 and FA30 pastes exposed to $MgCl_2$, the portlandite peak intensity, especially around $2\theta = 18$ degrees, was reduced. Moreover, the portlandite peaks in FA30 have lower intensities than FA15 before and after acid exposure, indicating pozzolanic reactions occurred due to the higher replacement level of FA. Another

noticeable point in Figure 4.21 is the presence of brucite peaks in pastes immersed in $MgCl_2$ before acid addition at around 18.7, 38.1, and 58.8 degrees, and their attenuation after exposure to nitric acid. The reaction between brucite and nitric acid forms a highly water-soluble salt, magnesium nitrate; this reaction is the leading cause of such an attenuation.

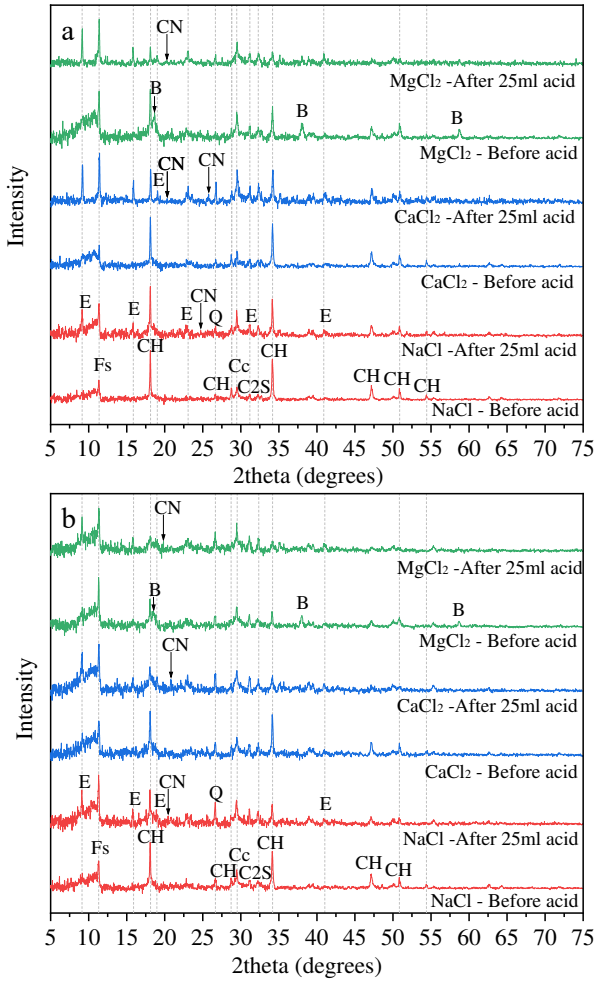

Figure 4.21. XRD spectra of FA samples before and after exposure to 25 mL of acid. Samples were first exposed to 2 M salt solutions. (a) FA15; (b) FA30 (Fs: Friedel's salt, CH: portlandite, Cc: calcite, C2S: belite, E: ettringite, B: brucite)

Additional XRD measurements and analysis were performed on the damaged surface layer of OPC paste samples exposed to 25 mL of nitric acid to determine the chemical composition and

identify the phases formed on the surface of these samples after exposure to salts and nitric acid (Figure 4.22).

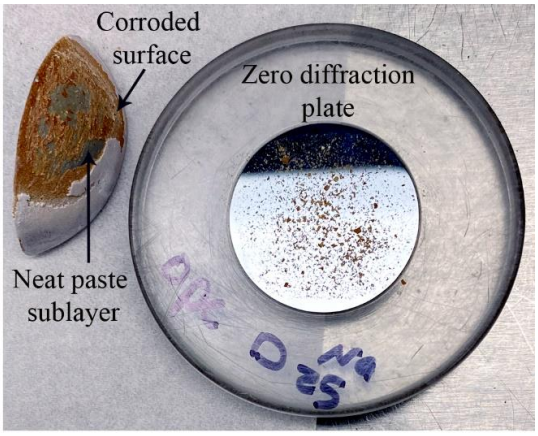

Figure 4.22. Sample preparation for testing the chemical composition of corroded layer (OPC paste exposed to 25 mL of added acid)

Figure 4.23 shows the prominent brucite peak in samples exposed to $MgCl_2$. Brucite can form due to a reaction between portlandite and $MgCl_2$. In addition, quartz, gibbsite, gypsum, and calcium nitrate were detected.

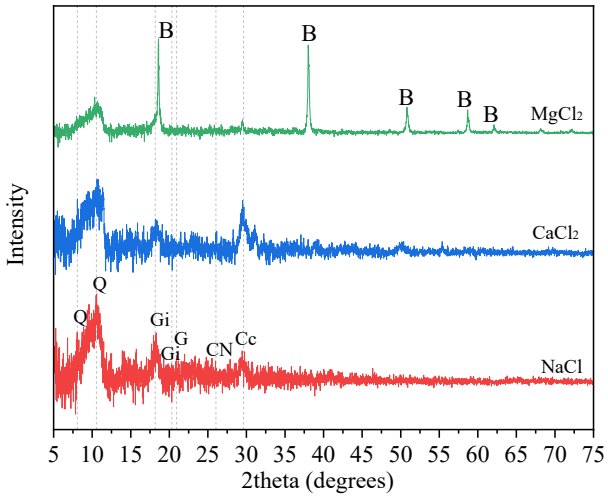

Figure 4.23. The XRD spectra of the corroded layer of the OPC paste exposed to 25 mL of acid (Q: quartz, Gi: gibbsite, G: gypsum B: brucite, CN: calcium nitrate)

The XRD spectra indicated that the corroded layer of the samples exposed to the NaCl and $CaCl_2$ solutions was somewhat amorphous and composed mainly of quartz. The brownish color of the corroded layer may be due to the presence of iron in the altered layer, as previously reported in [175]. However, there were no iron-containing crystalline phases in the XRD spectra.

4.3.1.5. TGA Analysis of Chloride Desorption Products

Figure 4.24 compares the DTG results for the OPC paste samples exposed to salt solutions before and after acid exposure. The DTG results show three significant mass losses, corresponding to ettringite at 85 to 210℃ [212], Friedel's salt at 235 to 375℃ [124, 210, 213], and portlandite at 385 to 460℃. The results indicate considerably shallower dips for portlandite after acid exposure, resulting from the leaching of portlandite from the paste matrix. While the second dip in Figure 4.24 at 350°C is labeled as Friedel's salt, due to the reactions between cement hydrates and nitric acid, other phases such as brucite may have formed that have a similar dehydroxylation temperature to Friedel's salt. The reported decomposition temperature ranges by Scrivener et al. [212] for Friedel's salt (250°C to 400°C), brucite (around 400°C), aluminum hydroxide (around 270°C), magnesium silicate hydrates (around 270°C and 400°C) overlap, which makes it very challenging to distinguish their mass losses in TGA curves. The presence of Friedel's salt in the DTG curves supports the XRD results.

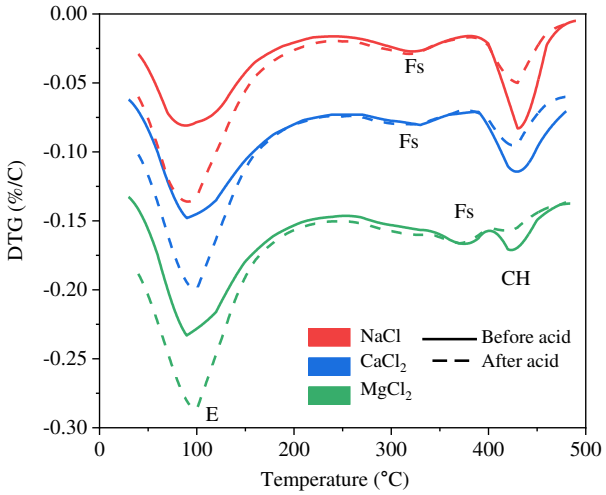

Figure 4.24. DTG results for the OPC sample before and after 25 mL of acid addition

Figure 4.25 displays the DTG curves of specimens containing FA. The dips associated with Friedel's salt before and after acid addition did not change in the samples exposed to NaCl and $CaCl_2$. The explanation provided for the presence of Friedel's salt in the OPC samples is valid for other binders, including FA15 and FA30. These dips probably represent Friedel's salt on the subsurface layer. The magnitude of the dips associated with Friedel's salt after the acid was added to the samples exposed to $MgCl_2$ solution was not as pronounced as before acid exposure. This decrease can be attributed to the lower pH of the $MgCl_2$ solution compared to the other two solutions before and after the acid was added, leading to more Friedel's dissolution.

The mass fraction of Friedel's salt in paste samples was determined based on Eq. (4.1):

$$m_{Fs} = \frac{M_{Fs}}{6M_{H_2O}} m_{H_2O} \tag{4.1}$$

m_{Fs}: mass fraction of Friedel's salt

m_{H2O}: mass loss (% wt.) of the primary layer of water obtained from TGA

M_{FS} and M_{H2O}: molar mass of Friedel's salt (561.3 g/mol), and water (18.02 g/mol)

The m_{H2O} for Friedel's salt can be determined from the TGA by subtracting the results for the paste which was not exposed to salt from the pastes which were exposed to salt in the temperature range in which Friedel's salt was observed.

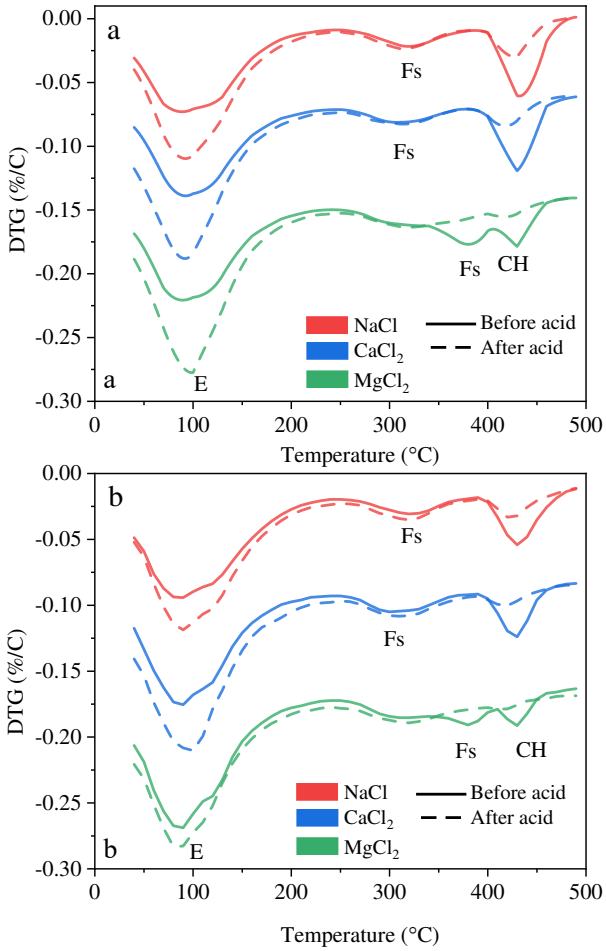

Figure 4.25. DTG results of fly ash-containing samples before and after exposure to 25 mL of nitric acid (a) FA15 and (b) FA30

Table 4.5 summarizes the mass fraction of Friedel's salt between 240 and 420°C before and after acid exposure, calculated based on Eq. (20). The mass fraction of Friedel's salt was the highest in the $MgCl_2$ solution, followed by the $CaCl_2$ and NaCl solutions, which agreed well with the chloride binding results and the XRD spectra. In the NaCl and $CaCl_2$ solutions, the mass of Friedel's salt slightly increased after the acid was added. However, in the $MgCl_2$ solution, the trend was reversed after adding 25 mL of acid.

Table 4.5. Measured mass fraction of Friedel's salt in a temperature range of 240 to 420°C before and after adding 25 mL of acid

Sample	Friedel's salt mass fraction (% wt.)					
	Before exposure to acid			After exposure to acid		
	NaCl	$CaCl_2$	$MgCl_2$	NaCl	$CaCl_2$	$MgCl_2$
OPC	4.14	3.41	5.89	4.36	4.64	5.00
FA15	3.84	3.77	7.14	5.23	4.31	7.01
FA30	3.37	4.25	8.79	4.45	4.78	5.9

4.3.1.6. Visual Inspection of Samples After Chloride Desorption Test

An acid attack can dissolve and leach acid-susceptible constituents, mainly calcium hydroxide, from the cement paste, resulting in increased capillary porosity, loss of cohesiveness, and eventually loss of strength [178]. Additionally, the decalcification of cement paste generates intense tensile stresses on the surfaces of paste samples, leading to the formation of cracks [234].

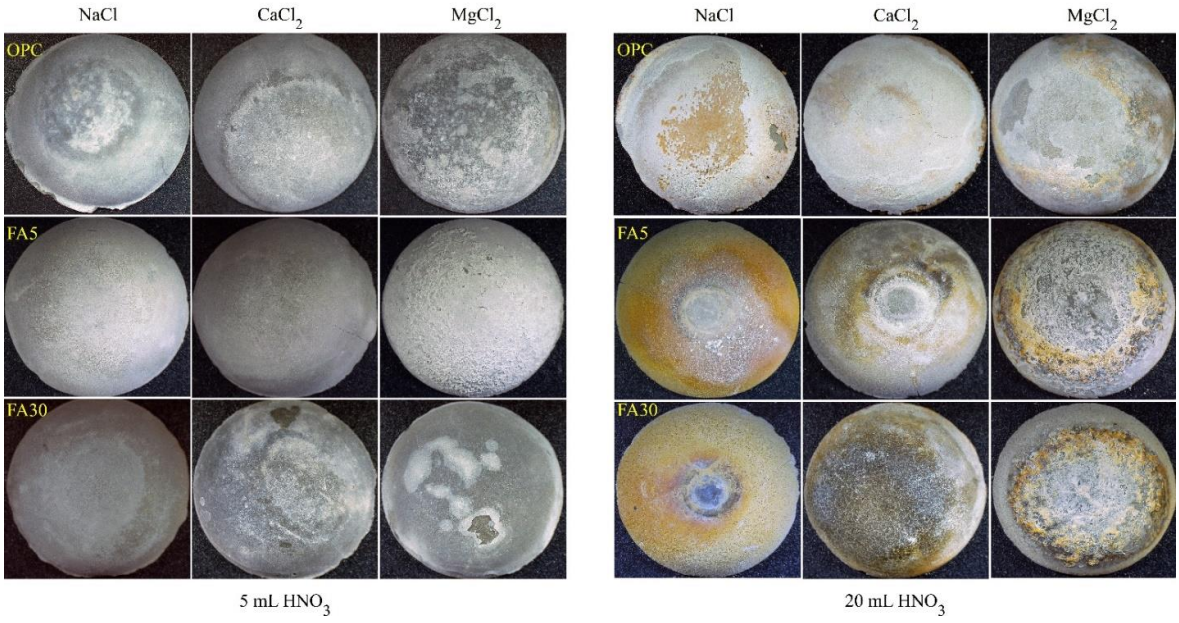

Figure 4.26. Images after 2 weeks of exposure to 5 mL (left) and 20 mL (right) nitric acid

Based on visual observations of the surface cracks under a microscope, the pastes in this study showed no significant damage after 2 weeks of exposure to 5 and 10 mL of nitric acid. However,

the extent of the damage increased with an increase in the volume of added acid and took the form of bleaching, surface corrosion, and surface grazing or cracking. For example, samples exposed to 5 and 20 mL of acid for 2 weeks are shown in Figure 4.26.

Figure 4.27 shows salt crystallization on the surface and within the generated cracks. The considerable amounts of crystalized salts and other residual materials could potentially create an expansive pressure within the cracks, leading to more internal damage. The reason is that when the brine solution evaporates, the salts start precipitating and crystallizing in confined spaces of cracks. Under this condition, salt crystallization can generate stress on the crack walls. The direct measurement of the force exerted by a growing crystal is challenging, however, there is some evidence in the literature [235]. After acid was introduced to the system, the reaction between nitric acid and portlandite produced calcium nitrate, which is highly soluble. The whitish layer observed on the surface of samples immersed in 2 M $MgCl_2$ and exposed to nitric acid can be explained as the precipitate of magnesium sulfate formation.

Figure 4.27. Salt crystallization on the surface and within the cracks of dried samples after immersing them in salt solution followed by acid exposure.

4.3.2. Chloride Binding and Desorption Capacity for Blended Cement Containing Slag

4.3.2.1. The Phase Composition of Slag-Blended Pastes

The reactivity of blended cement pastes containing GGBFS is mainly governed by the chemical composition and degree of crystallinity of GGBFS [227, 228, 236]. Figure 4.28a shows the XRD scans of OPC and GGBFS-blended pastes cured for 56 d. Portlandite was the most dominant phase detected in all samples. The results show a reduction in the portlandite peak intensity with the incorporation of GGBFS. The inclusion of GGBFS consumes portlandite to form C–S–H gel [32, 33]. Other detected phases were ettringite, tetracalcium aluminoferrite, monocarbonate, calcite, and belite.

Figure 4.28 shows the DTG plots of pastes cured for 56 d. Ettringite and portlandite had primary dips observed at approximately 100°C and 450°C, respectively [212]. The results showed that increasing the replacement level of GGBFS reduced the portlandite content, in good agreement with the XRD results. Based on TGA results, the portlandite mass loss percentage was 4.86% in OPC, 3.42% in SG25, and 2.51% in SG50.

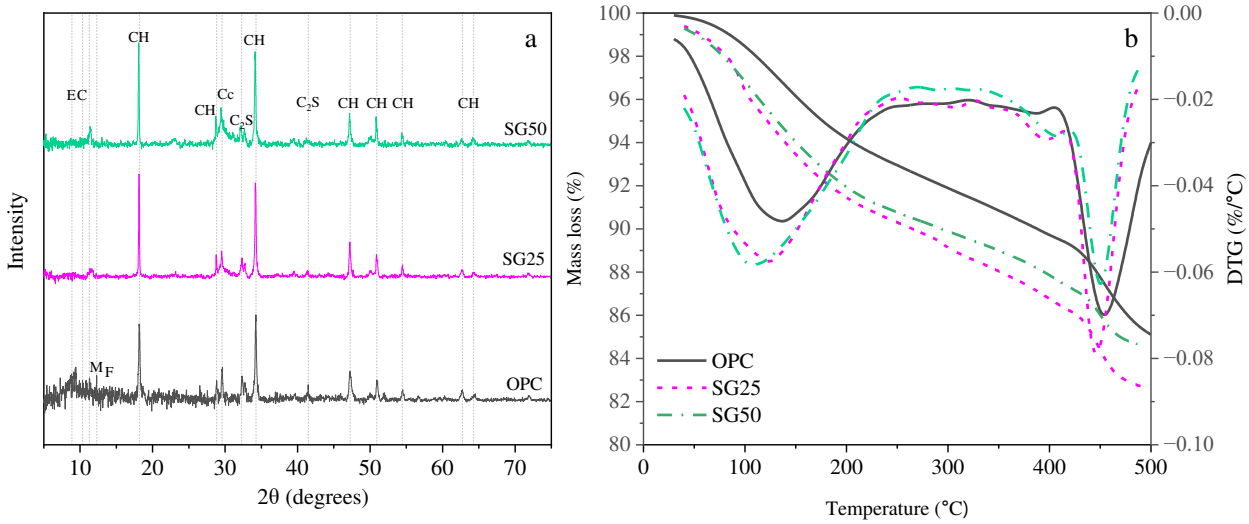

Figure 4.28. (a) The XRD patterns of hydrated pastes. (b) Mass loss and DTG curves of hydrated pastes (E: Ettringite, M: Monocarbonate, F: Ferrite, CH: portlandite, Cc: Calcite, C2S: Belite)

4.3.2.2. Chloride Binding of Slag-Blended Pastes

Figure 4.29 shows the experimental data (symbols) for free and bound chloride concentrations and the fitted Langmuir isotherms (lines) for the OPC and GGBFS-blended pastes. The results show a non-linear relationship between the free and bound chlorides. The estimated parameters and the residual sum of square errors (RSS) comparing Langmuir and Freundlich isotherms for these pastes are shown in Table 4.6.

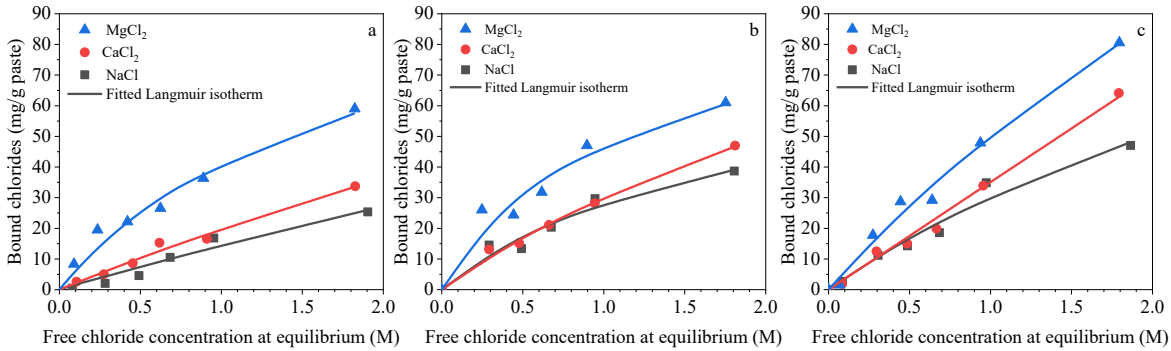

Figure 4.29. The experimental data and fitted Langmuir isotherm of OPC and GGBFS pastes exposed to NaCl, CaCl2, and MgCl2 solutions (a) OPC; (b) SG25; and (c) SG50

Table 4.6. The fitting parameters of Langmuir and Freundlich isotherms

System	Solutions	Langmuir Isotherm			Freundlich Isotherm		
		α_L	β_L	RSS	α_F	β_L	RSS
OPC	NaCl	15.32	0.06	23.46	14.07	0.98	23.67
	$CaCl_2$	21.60	0.10	10.96	19.43	0.91	11.01
	$MgCl_2$	65.98	0.60	58.94	69.60	0.64	22.86
SG25	NaCl	44.73	0.59	32.88	25.14	0.49	70.66
	$CaCl_2$	38.16	0.26	9.29	29.47	0.78	5.29
	$MgCl_2$	92.19	0.95	98.72	45.38	0.54	73.98
SG50	NaCl	37.54	0.24	45.82	29.23	0.82	55.16
	$CaCl_2$	35.06	0	22.74	34.41	1.06	17.40
	$MgCl_2$	59.57	0.18	52.55	49.17	0.85	51.54

4.3.2.3. Influence of Slag on Chloride Binding

The binding results in Figure 4.29 show that regardless of the cation of the salt, the inclusion of slag led to more chloride binding than that of the pure OPC paste. For example, the SG25 and SG50 pastes exposed to a NaCl solution showed approximately 53% and 56% higher bound chloride contents than the OPC. The same trend was observed for pastes exposed to $CaCl_2$ and $MgCl_2$ solutions. The higher chloride binding capacity of SG25 and SG50 can be attributed to increased pozzolanic reactions in the GGBFS-blended samples, leading to the further consumption of portlandite to form more C–S–H gel [228, 237], which can physically bind chlorides. Moreover, GGBFS contains a slightly higher amount of Al_2O_3 than OPC, and Al_2O_3 can produce more AFm and AFt phases during hydration [238]. AFm phases can bind chemically with chlorides to form Friedel's salt [239]. Al can also bind with C–S–H and increase the Si/Al ratio, which increases the ability of the C–S–H phase to uptake chloride ions [228].

4.3.2.4. Influence of Salt Cation on Chloride Binding and pH of the Exposure Solutions

Figure 4.29 shows that the salt cation greatly affects the chloride binding capability of cement pastes. These results agree with the previous finding that $MgCl_2$, followed by $CaCl_2$, has a higher affinity to bind with cement hydration products than NaCl [82, 111, 128]. Arya [111] have attributed the higher binding capacity of $MgCl_2$ to the faster diffusion of chlorides in this salt. It has been suggested that chlorides diffuse more rapidly because their steady-state diffusion in divalent cations is faster than in monovalent cations [240]. However, there is no consensus on this matter. Other researchers, such as Hansson [241], have reported faster chloride diffusion for NaCl, followed by $CaCl_2$ and $MgCl_2$. Increased chloride binding of $MgCl_2$ could also be due to the higher ionic strength of the $MgCl_2$ solution, which affected the rate of chemical reactions between the chlorides and cement hydrates [242].

The type of salt cation can also influence the pH of the salt solutions and the concrete pore solution. Experimental results showed that the pH of 2 mol/L NaCl, $CaCl_2$, and $MgCl_2$ solutions were 6.9, 6.7, and 5.8, respectively. When the paste samples were immersed in 60 mL of salt solution, the pH gradually increased during the exposure period, mainly due to the leaching of portlandite and the corresponding effect on pH buffering. After the paste samples were exposed to salt solutions for 2 weeks, the pH reached close to 12.3, 11.4, and 8.8 in the NaCl, $CaCl_2$, and $MgCl_2$ solutions, respectively. These results agree with previous investigations that have reported that the pH of the concrete pore solution decreased in the presence of $CaCl_2$ and $MgCl_2$ [82, 124, 128]. When NaCl is dissolved in water, it undergoes dissociation into Na^+ and Cl^- ions. The Na^+ ions do not participate in any reaction with water and thus do not have any impact on the pH of the solution. Chloride ions, on the other hand, can react with water to produce hypochlorous acid (HOCl), a weak acid that has little effect on pH [243]. Conversely, the dissolution of $CaCl_2$ and $MgCl_2$ can lead to liberation of hydrogen ions, causing the pH to become lower [244, 245]. The solubility of Friedel's salt is pH dependent and rises with increased solution pH [129]. Thus, an increase in the pH of the pore solution dissolves chemically bound chlorides, reducing the overall number of bound chlorides [111, 128, 129].

Another underlying reason that $MgCl_2$ and $CaCl_2$ can bind more chlorides is the development of more C–S–H phases in samples exposed to aqueous Ca^{2+} and Mg^{2+}. Ca^{2+} from calcium-bearing salts contributes to the formation of more C–S–H, which can then take up more chlorides from the solution. Mg^{2+} from magnesium-bearing salt produces four changes that enhance chloride binding capacity. First, it reacts with portlandite; second, it forms brucite and $CaCl_2$; third, it increases the Ca/Si ratio in the C–S–H gel; and fourth, it reacts with C–S–H to form M–S–H and magnesium oxychloride [66, 82, 246]. De Weerdt, Colombo [82] have reported that a

higher Ca/Si ratio in C–S–H, as a result of exposure to $MgCl_2$, increases the chloride binding of the C–S–H phase.

4.3.2.5. Chloride Desorption of Slag-Blended Cement

4.3.2.5.1. Evolution of pH Under Acid Attack

To study the evolution of pH in the salt solutions after acid was added, the pH was recorded at three different points: immediately (instantaneous pH), 7, and 14 days after the acid was added. Figure 4.30 shows time evolution of pH for pastes containing slag at different acid volume to paste mass (A/P) ratios. The results indicated that immediately after adding nitric acid to the salt solution, the pH dropped significantly, but due to the chemical reaction between the acid, salt solution, and paste hydrates, especially the portlandite, the pH increased slowly over time.

After nitric acid was introduced to the system, it reacted with the aqueous ions from the salt, forming highly water-soluble $NaNO_3$ in the NaCl solution, $Ca(NO_3)_2$ in the $CaCl_2$ solution, or $Mg(NO_3)_2$ in the $MgCl_2$ solution, all of which can react with water to produce strong bases such as NaOH, $Ca(OH)_2$, and $Mg(OH)_2$, respectively [247]. These reactions can slightly increase the pH of the solution. Nitric acid can also react with cement hydration products, such as portlandite, to form calcium nitrate, further increasing the pH [171]. The decalcification of a paste as a result of this reaction will continue as long as enough portlandite and nitric acid are available. The samples immersed in NaCl solution had a higher pH, followed by those in $CaCl_2$ and $MgCl_2$. The lower pH value in the $CaCl_2$ and $MgCl_2$ solutions is due to the formation of complexes such as $[Ca(H_2O)_6]^{2+}$ and $[Mg(H_2O)_6]^{2+}$, which create a positive charge density on the Mg and Ca ions, which releases protons into the solution and consequently lowers the pH of the solution [248].

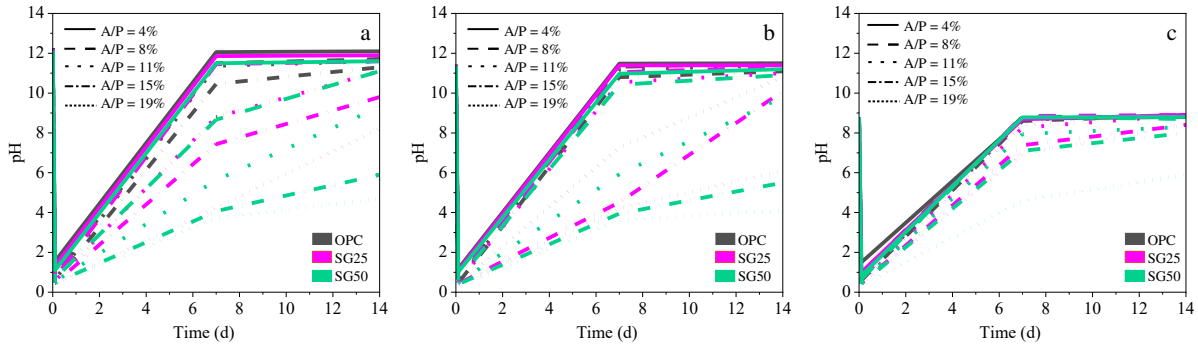

Figure 4.30. Time evolution of pH for pastes containing slag at different acid-to-paste sample mass (A/P) ratio. (a) NaCl; (b) $CaCl_2$; (c) $MgCl_2$

Figure 4.30 also shows that the rate of change of the pH after adding acid is significantly influenced by increase the A/P ratio. For example, when samples were exposed to 5 mL of nitric acid, it took roughly 6 days or less for the pH to equilibrate and revert to the initial pH. However, when more acid was added (e.g., A/P ratio 19%), the solutions barely reached equilibrium–after 14 days, the pH values were still significantly lower than the initial pH.

In both SG25 and SG50 pastes, A/P in range of 4% and 8% resulted in a higher pH in NaCl, followed by $CaCl_2$ and $MgCl_2$. However, further addition of acid reduced the pH in the NaCl and $CaCl_2$ solutions considerably. The SG50 in Figure 4.30 pastes showed a lower pH range than the SG25 pastes, especially at A/P of 11% and higher, which can be attributed to its lower portlandite content. For instance, in all salt solutions at A/P of 15% the pH of SG50 was under 8 and increasing the A/P to 19% caused the pH to drop below 6. Independent of the salt, increased GGBFS replacement reduced the ability of the paste sample to buffer the pH of the solution under acid attack, suggesting that GGBFS-blended paste is less resistant to nitric acid attacks than OPC. This lack of resistance could be due to the presence of less portlandite, which can act as a neutralizing agent to buffer the pH in the GGBFS system.

4.3.2.5.2. Release of Bound Chlorides Under Acid Attack

Figure 4.31 compares the concentration of free chlorides at the end of the chloride binding period with that after the desorption period. The results show that acidifying the solutions slightly increased the concentration of free chlorides in the exposure solution. In other words, adding acid reduced the pH, which led to a partial release of bound chlorides and increased the concentration of free chloride ions in the exposure solution. In most cases, the highest desorption of bound chlorides was observed when the A/P ratios were 4% and 8%.

The pH of the solution critically affects the severity of the acid attack on paste samples. As explained in the previous section, when a small volume of acid was added to the exposure solution, the pastes and solutions buffered the sudden pH drop much faster than when a larger volume of acid was added. Nitric acid attacks the hydration products on the surface of samples first, producing soluble salts and forming an altered porous surface layer with numerous cracks. As a result of this, some of the bound chlorides on the surface of the pastes are released and returned to the exposure solution. However, the interlayer progression of the acid attack in paste samples depends on the pH, that is, whether sufficient acid is available.

These results suggest that when the pH of the exposure solution returns to approximately the pH before acid was added, the desorption process can be either stopped or slowed down considerably, and as a result, the chloride binding process is reinitiated. At this stage, some of the free chlorides in the exposure solution can penetrate the porous damaged surface layer and form physical and chemical bonds with the underlying neat paste layers. This hypothesis is supported by the reduced difference in the concentration of free chlorides before and after adding higher volumes of acid, as shown in Figure 4.31.

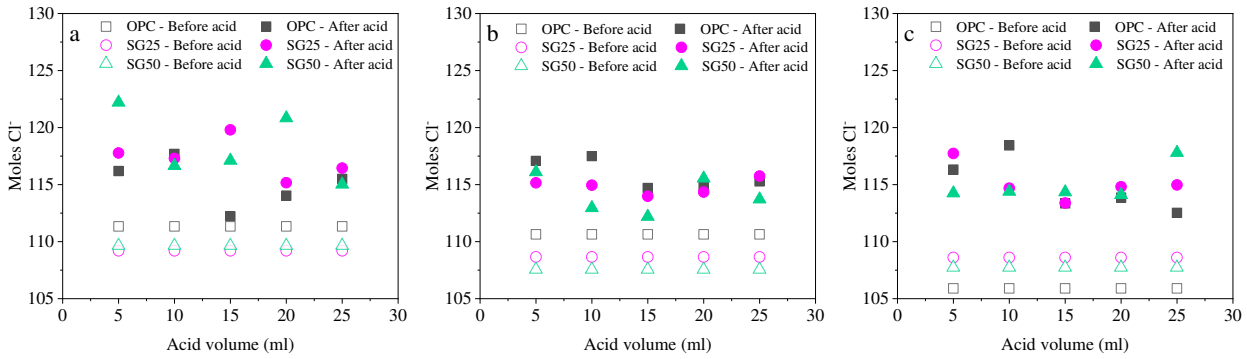

Figure 4.31. Measured moles of free chlorides salt solutions before and after adding nitric acid. (a) NaCl, (b) $CaCl_2$, and (c) $MgCl_2$

Figure 4.32 shows the percentage of released bound chlorides at the end of the chloride desorption period at different A/P ratios. The lower percentage of released bound chlorides means a lower free chloride concentration in the pore solution, which reduces the risk of chloride-induced corrosion. Figure 4.32 indicates that increasing the slag replacement level from 25% to 50% decreased the average percentage of released bound chlorides in NaCl, $CaCl_2$, and $MgCl_2$ solutions by 7.8%, 28.2%, and 29.4%, respectively.

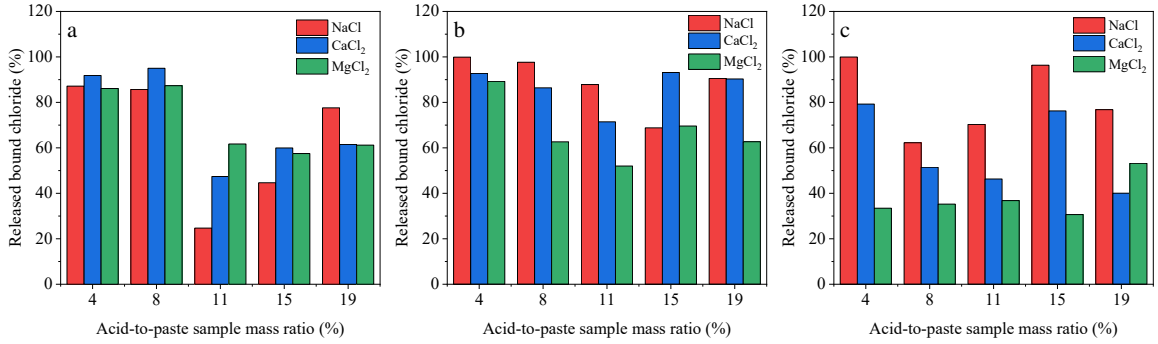

Figure 4.32. The percentages of released bound chlorides after exposure to nitric acid. (a) OPC; (b) SG25; and (c) SG50

The results indicate that the quantity of released chlorides varied depending on the A/P, with the highest release observed between A/P values of 4 and 8%. In Figure 4.32a, it can be seen that at an A/P of 4% in OPC pastes, 87%, 92%, and 86% of bound chloride were released in NaCl, $CaCl_2$, and $MgCl_2$ solutions, respectively. Similar results were observed at an A/P of 8%. However,

with an increase in A/P, the percentage of released bound chlorides decreased significantly, particularly in NaCl solution at A/P values between 11% and 15%. The lower release of bound chlorides in the NaCl solution can be attributed to its relatively higher pH before and after acid addition compared to other salt solutions. Another possible reason is that an increase in A/P results in a complete alteration of the surface layer of paste samples, leading to the formation of hydrogels that can adsorb some of the free chlorides [66]. Figure 4.32b displays that the highest number of bound chlorides was released in SG25 pastes when they were exposed to $MgCl_2$ and NaCl solutions at an A/P ratio of 4%.

Table 4.7 summarizes the general trends of the impact of slag replacement on the total bound chloride contents and the amount of released bound chlorides following the addition of acid. The incorporation of GGBFS positively impacted chloride capacity before and after acid addition. However, due to the consumption of a considerable amount of portlandite, the pH of the system is more sensitive to change after an acid attack.

Table 4.7. Summary of the effect of GGBFS on chloride binding and chloride desorption in comparison to OPC

System ID	Salt	Δ bound Cl (%)	Δ released Cl (%)
SG25	NaCl	+53	+4
	$CaCl_2$	+38	-9
	$MgCl_2$	+3	-15
SG50	NaCl	+56	+4
	$CaCl_2$	+65	-19
	$MgCl_2$	+35	-28

4.3.2.5. Analytical Results

Figure 4.33 shows the XRD analysis of powdered OPC paste after the chloride binding and chloride desorption experiments. The results showed the presence of Friedel's salt peaks at around

11.3 to 11.4° when the specimens were exposed to salt solutions for 14 d. The presence of Friedel's salt indicates the chemical binding of chlorides with AFm phases. In addition to Friedel's salt, portlandite, ettringite, C_2S, and calcite were also detected. In specimens exposed to $MgCl_2$, brucite ($Mg(OH)_2$), a product of the reaction between portlandite and $MgCl_2$ was identified [246].

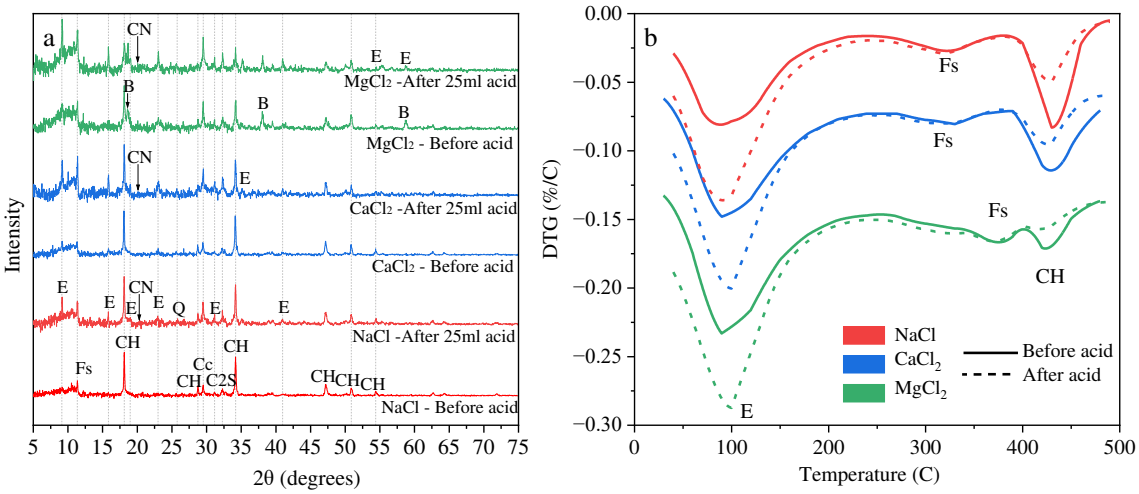

Figure 4.33. The XRD and DTG results for OPC samples before and after exposure to 25 mL of acid (A/P ratio of 19 %). (Fs: Friedel's salt, CH: Portlandite, Cc: Calcite, C2S: Belite, E: Ettringite, B: Brucite)

Figure 4.33 also shows calcium nitrate and portlandite peaks after the samples were exposed to acid, albeit at lower intensities than before exposure. In addition, ettringite peaks, which can be caused by the dissolution of monosulfate ($C3A{\cdot}CaSO_4{\cdot}12H_2O$) were observed [175]. The chemical reaction between the nitric acid and paste can result in portlandite leaching from the surface of the paste to form calcium nitrate [171]. This can cause a considerable shrinkage of the degraded surface, leading to the formation of macro cracks and increased permeability [171, 174]. When chloride ions are present, they can ingress through this highly permeable surface and increase the risk of corrosion.

The presence of Friedel's salt after exposure to nitric acid could be due to two reasons: First, before performing XRD, the paste specimens were ground, and therefore, the reported XRD peaks represent phases from both the exposed surface and the neat core of the specimens, as shown in Figure 4.34. As a part of the preparation process for the chloride binding test, the specimens were dried and then exposed to the salt solution. Therefore, the ingress of chlorides into the core of the specimens was fast and mainly governed by capillary action. It can be assumed that after 14 days of continuous exposure to a salt solution, the specimens reached a partially to fully saturated state. Thus, the acid ingress in these partially or fully saturated specimens was mainly governed by diffusion, which is a slower process than capillary action. Due to the buffering capacity of portlandite, the strength of the acid declines as it penetrates through the hydrated layers of the paste specimens. Therefore, the bound chlorides formed within the core of the sample were either unaffected by the acid or were less exposed to the low-pH environment than those at the surface of the specimen. The second possible reason for the presence of Friedel's salt after exposure to nitric acid is the formation of new chemical bonds between the free chlorides in the solution and the neat paste layer underneath the damaged surface layer.

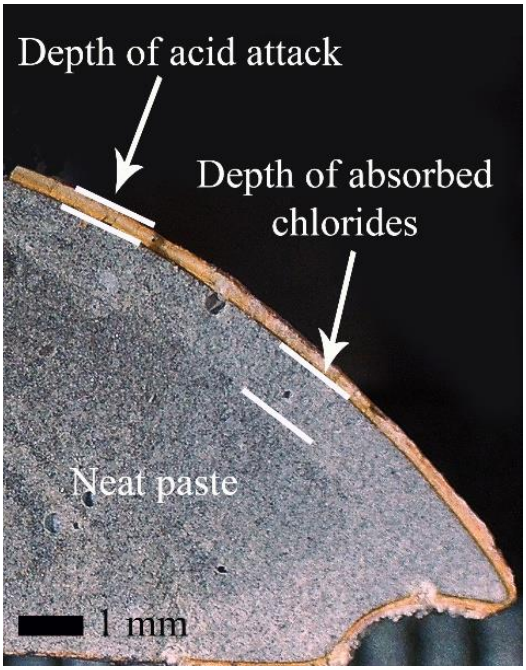

Figure 4.34. Cross-section of OPC paste sample after exposure to chlorides followed by nitric acid

Figure 4.35 displays the XRD analysis of the GGBFS-blended specimens performed after the chloride binding and desorption tests. In general, Friedel's salt formation was observed in all specimens, and its intensity seems somewhat stronger in samples exposed to the $MgCl_2$ solution. The pH of the SG25 paste exposed to a $MgCl_2$ solution before adding acid was around 8.8, which decreased to 6.7 after 1 week of exposure to 25 mL of acid (A/P ratio of 19 %) and returned to 8.4 during the second week. In the SG50 specimens, in which most of the portlandite was consumed during hydration, the solution was more acidic, and the pH was around 5.9 after 2 weeks of exposure to acid.

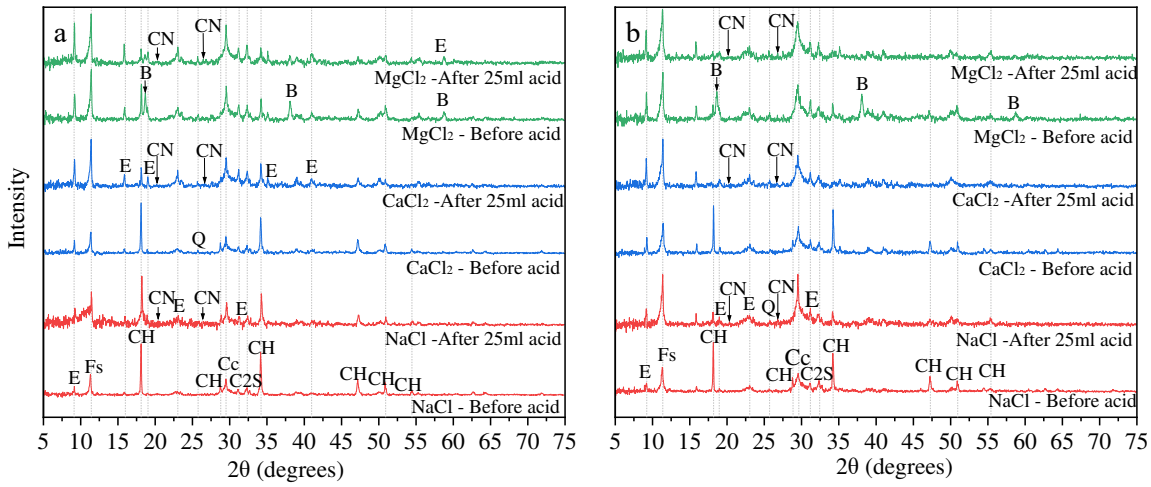

Figure 4.35. The XRD scans of GGBFS-blended specimens before and after exposure to 25 mL of acid (A/P ratio of 19 %). (a) SG25 and (b) SG50 (FS: Friedel's salt, CH: Portlandite, Cc: Calcite, C2S: Belite, E: Ettringite, B: Brucite)

The thermogravimetric analysis of OPC pastes exposed to three salt solutions before and after exposure to acid (Figure 4.36) show three distinguishable dips at 85–210°C (associated with ettringite) [212], 235–375°C (associated with Friedel's salt) [38, 47, 48], and 385–460°C (portlandite) [212]. The presence of Friedel's salt is consistent with the XRD results. Due to the leaching of portlandite and its reaction with nitric acid to form calcium nitrate, shallower portlandite dips were observed after acid exposure.

Comparing the DTG results of SG25 and SG50 in Figure 4.36 with those in OPC (Figure 4.33b) shows noticeably shallower portlandite dips in GGBFS-blended systems. This can be attributed mainly to the consumption of portlandite by a pozzolanic reaction with GGBFS, which forms C–S–H gel. After adding acid, parts of the remaining portlandite are leached out, contributing to the shallower portlandite dip in Figure 4.36.

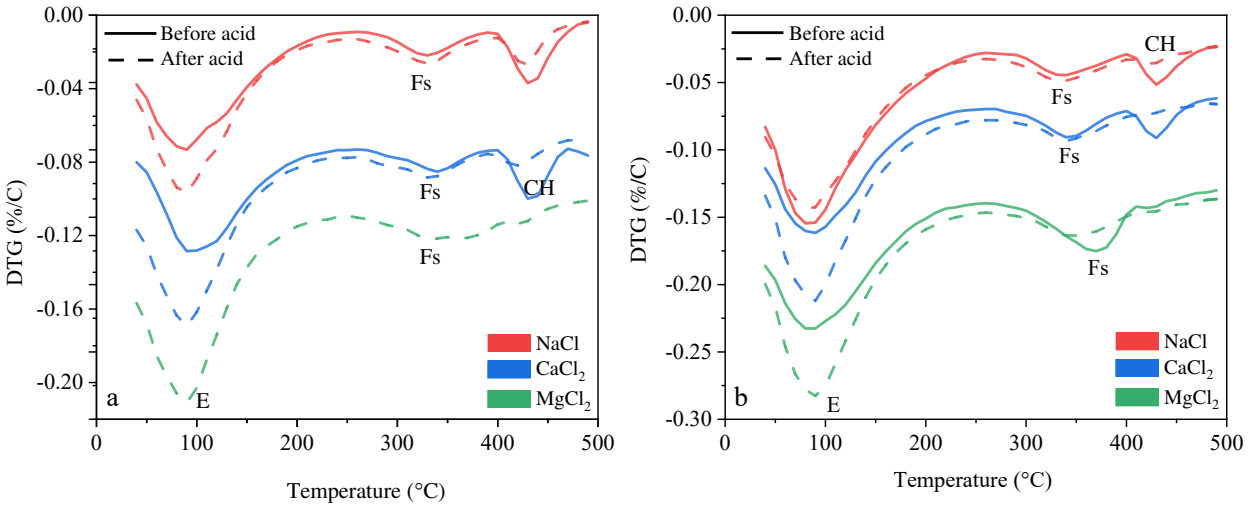

Figure 4.36. The DTG results of GGBFS-containing samples before and after exposure to 25 mL of nitric acid (A/P ratio of 19 %). (a) SG25 and (b) SG50

The mass fraction of Friedel's salt in paste specimens can be determined based on Eq. (4.1). The calculated mass fraction of Friedel's salt based on DTG curves from 240 to 420°C before and after acid exposure is shown in Figure 4.37. The results show that the slag-blended pastes had a higher Friedel's salt content than the OPC. When acid was introduced to the system, Friedel's salt was still detected, indicating that the neat inner layer was able to keep it in place. However, it should be noted that distinguishing between old and new phases formed after acid attack becomes challenging when a paste specimen is exposed to a large amount of acid. This is due to the complex nature of the acid attack and the close decomposition temperatures of the formed phases.

After adding acid to the NaCl solutions, the mass percentage of Friedel's salt decreased slightly from 4.14% to 3.85% in OPC and from 5.04% to 3.60% in the SG25 samples. In the $CaCl_2$ solutions the mass percentage of Friedel's salt slightly increased from 3.41% to 3.74% in OPC and decreased from 4.69% to 4.24% in SG25. However, the OPC pastes showed an increase of Friedel's salt mass percentage from 5.89% to 7.05% in the $MgCl_2$ solution when acid was added. In all

SG50 pastes exposed to the $MgCl_2$ solution, a significant reduction in the mass percentage of Friedel's salt was observed, from 12.89% to 7.09%.

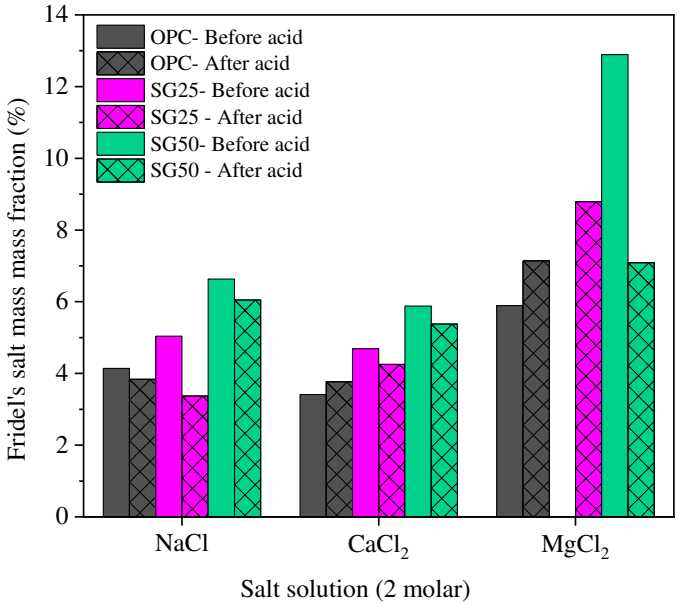

Figure 4.37. The mass fraction of Friedel's salt in paste samples made with OPC and slag

When high volumes of acid were introduced to the system, due to the complex nature of the acid attack on the cement paste, it was hard to differentiate the mass losses for Friedel's salt (250 to 400°C), brucite (around 400°C), aluminum hydroxide (around 270°C), magnesium silicate hydrates (around 270°C and 400°C) because they have close decomposition temperatures [249].

The underlying reason for the presence of Friedel's salt, even after acid was added, can be attributed to pH buffering capacity of portlandite and chloride rebinding by the internal paste layers as discussed in more detail in the XRD results. In addition, because a major portion of the portlandite in SG50 was consumed, this paste had a lower pH and smaller buffering capacity than the OPC and SG25, which could be another factor that contributed to the greater reduction of the Friedel's salt content in SG50 compared to the two other pastes.

Figure 4.38 shows the extent of deterioration in the paste specimens after exposure to 2 mol/L chloride solutions followed by 25 mL of nitric acid (A/P ratio of 19%). The deterioration is in the form of surface cracks, surface corrosion, and pop-outs after exposure. This process resulted in the formation of new products and the dissolution of some hydration products. The primary new phase formed after exposure to the salt solution was Friedel's salt, and both XRD and TGA results confirmed this after the chloride binding period. In addition, brucite and $Mg_3(OH)5Cl{\cdot}4(H_2O)$ can also form in samples exposed to $MgCl_2$, which are observed as a whitish substance on the surface of the specimens [246]. However, nitric acid attacks on the OPC and GGBFS-blended pastes resulted in the dissolution of portlandite and C–S–H and the formation of calcium nitrate, which is highly soluble in water at room temperature [171, 174]. The brownish color of the corroded layer may be due to the presence of iron in the damaged layer, as previously reported by Gutberlet et al. [175].

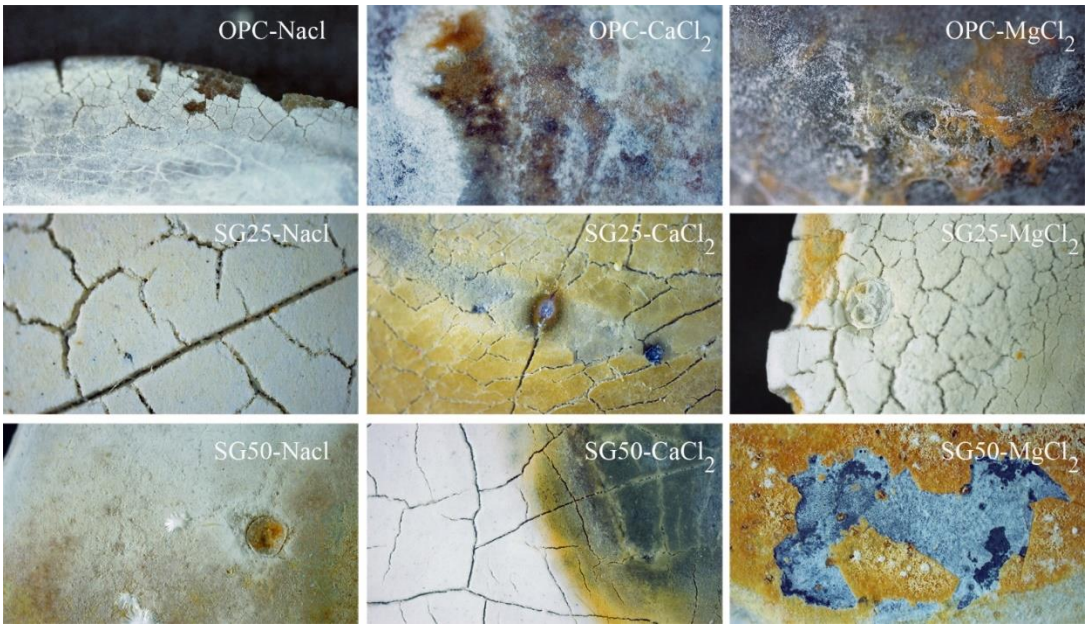

Figure 4.38. The extent of deterioration of OPC and GGBFS-blended paste specimens after exposure to 2 mol/L chlorides and 25 mL 1 M nitric acid (at A/P ratio of 19%) (10X magnification)

4.3.3. Chloride Binding and Desorption Capacity for Pastes Containing Silica Fume

4.3.3.1. Hydration Products Characterization of Pastes Containing Silica Fume

Figure 4.39 shows XRD scans and TGA analysis of OPC and silica fume blended pastes after 56 days of curing before exposure to brine solution. As is obvious from the results, there is no sign of Friedel's Salt (FS). Portlandite (CH) peaks (quantity) decreased in silica fume blend due to the pozzolanic reaction consuming CH to form additional C-S-H gel. The DTG plots are similar and again there is no sign of Friedel's Salt (FS) in samples before chloride exposure.

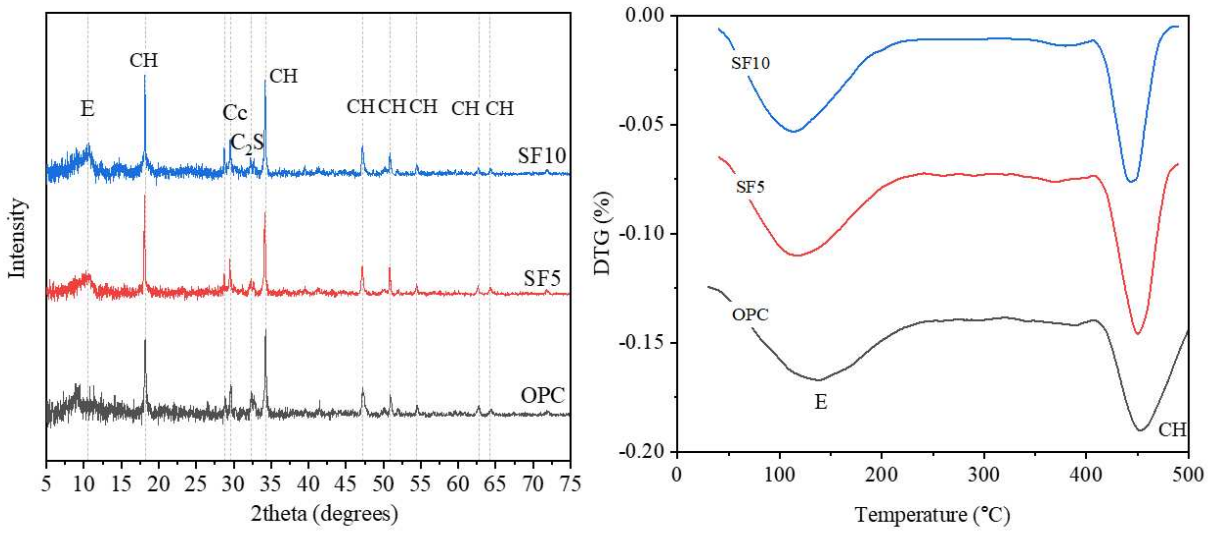

Figure 4.39. (Letft) XRD anf (Right) DTG results of blended pastes before chloride exposure

4.3.3.2. Chloride Binding Capacity of Cement Containing Silica Fume

Chloride binding isotherms of pastes containing 5% and 10% silica fume using experimental results and Langmuir and Freundlich isotherms are calculated and the parameters are shown in Table 4.8. The chloride bindin results are plotted in Figure 4.40.

Table 4.8. Estimated Langmuir and Freundlich isotherm parameters

Mixtures	Langmuir Isotherm			Freundlich Isotherm		
	α_L	β_L	RSS	α_L	β_L	RSS
SF 5 Na	14.13	0.14	0.45	12.19	0.86	0.24
SF 5 Ca	59.56	2.24	0.37	17.62	0.37	3.31
SF 5 Mg	94.34	2.89	0.07	23.36	0.32	3.73
SF 10 Na	11.97	0.10	4.51	10.95	0.87	3.81
SF 10 Ca	39.14	1.41	0.74	15.52	0.46	3.50
SF 10 Mg	89.84	4.12	4.47	17.08	0.28	1.33

Figure 4.40 illustrates the chloride binding results for pastes containing silica fume (SF 5= 95% OPC + 5% silica fume and SF10 = 90% OPC + 10% silica fume). Regardless of cation type, the incorporation of silica fume resulted in a lower bound chloride compared to OPC paste. For instance, the bound chloride quantity for sample exposed to NaCl solution at molarity of 1 were 16.84 mg/g paste for OPC, 12.14 mg/g paste for SF5, 11.12 mg/g paste for SF10. The same trend in chloride binding results was reported in previous investigations [250, 251] that measured the chloride binding quantities in OPC and silica fume containing pastes.

Another observation was that the inclusion of more silica fume did not result in higher chloride binding results as reported in previous sections for slag and fly ash. The primary reason can be related to the difference in composition of silica fume compared to slag and fly ash. The composition of silica fume, predominantly consisting of SiO_2 (95.40%), is noteworthy for its exceptionally small particle size compared to other SCMs. Empirical data reveals a marked difference in particle size and specific surface area among common SCMs and silica fume: Portland cement averages 14.1 μm in particle size and 360 m²/g in surface area, fly ash at 6.4 μm and 510 m²/g, slag at 20 μm and 721 m²/g, while silica fume is significantly finer with a median particle size of 0.418 μm and an expansive surface area of 17,102 m²/g [229, 252]. The mentioned

compositional differences results in a denser microstructure of cement and concrete and dramatically reduces permeability [253], leading to a considerably lower chance of chloride ions to penetrate and bind with cement hydration products. Another difference between silica fume containing paste and OPC is that the alumina (Al_2O_3) content in silica fume is comparatively lower than that found in OPC, adversely impacting the chloride binding capacity of silica fume containing pastes [61, 62, 76, 79] because the presence of Al_2O_3 helps to form more AFm in hydration products that can chemically bind with chloride ions and forms Cl-AFm phases like Friedel's salt.

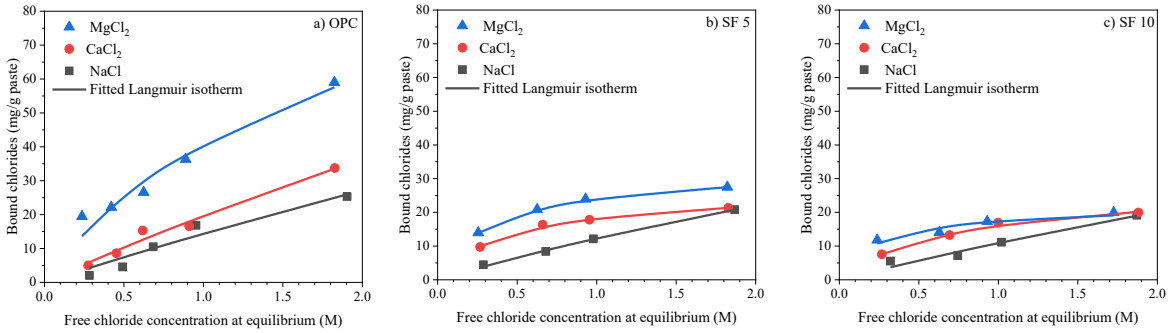

Figure 4.40. Chloride binding results for pastes containing silica fume exposed to NaCl, $CaCl_2$, and $MgCl_2$ (a)OPC, (b) SF5, and (c) SF10

Table 4.9 compares the bound chloride binding quantity of different pastes containing SCMs exposed to salt solutions at a high concentration (2 molar salt solutions). The results reveal that pastes containing silica fume have lower chloride binding capacity compared slag blended and fly ash blended pastes.

Table 4.9. Measured chlorides bdining in mg Cl/ g paste for paste samples containing SCMs when exposed to 2 M salt solutions

Paste type	Chloride binding quantity at the molarity of 2 (mg Cl/ g paste)		
	NaCl	$CaCl_2$	$MgCl_2$
OPC	25.35	33.72	59.00
SG25	36.97	46.43	60.99
SG50	47.03	64.12	80.56
FA15	44.58	47.51	63.73
FA30	54.70	65.28	72.99
SF5	20.82	21.34	27.47
SF10	19.00	19.94	19.92

Silica fume plays a significant role in refining pore distribution and modifying the mineral composition of binders. This modification results in diluted concentrations of tricalcium aluminate (C3A) and tetracalcium aluminoferite (C4AF), which consequently leads to a reduction in chemical binding of chlorides [61]. Previous studies have indicated that the contribution of physical binding to chloride immobilization is not substantial when silica fume is incorporated into the binder [79].

4.3.3.3. Chloride Desorption of Cement Containing Silica Fume

Figure 4.41 displays the release of bound chloride from silica fume-containing pastes when the pH is lowered by adding nitric acid in various mass ratios (A/P ratios) of 4%, 8%, 11%, 15%, and 19%. In both SF5 and SF10 pastes, A/P ratios of 4% and 8% resulted in the significant release of bound chloride, with over 95% being released.

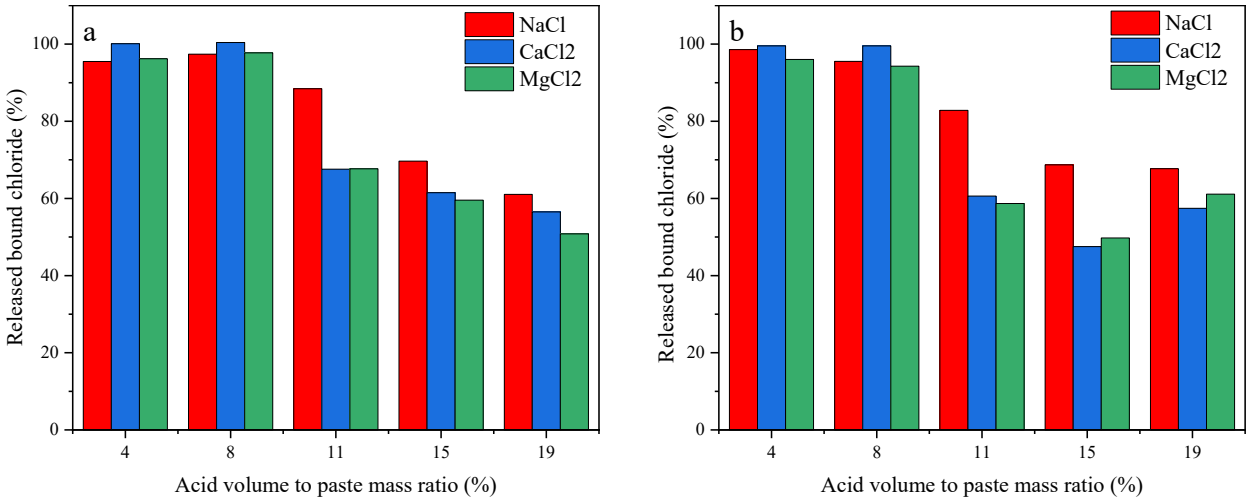

Figure 4.41. Percentages of released bound chlorides after acid addition (a) SF5; (b) SF10

The chloride desorption results indicate that the quantity of released chlorides varied depending on the A/P ratio, with the highest release observed at lower A/P ratio. Figure 4.41 shows that at the highest A/P ratio of 19%, the percentages of released bound chlorides in SF5 is around 61% in NaCl, 56% in $CaCl_2$, and 51% in $MgCl_2$. The same trend is observed for SF5 pastes at A/P ratio of 15% where NaCl showed the highest chloride desorption and $CaCl_2$ and $MgCl_2$ have similar and lower chloride desorption amount. The lower percentage of released bound chlorides means a lower free chloride concentration in the pore solution, which reduces the risk of chloride-induced corrosion.

To better understand the underlying reasons for observed results, monitoring the pH change in the systems is critical. Figure 4.42 shows the time evolution of pH for pastes containing SF at different A/P ratios exposed to the three brine solutions. The pH results show that for pastes exposed to NaCl solution with pH reduction at A/P ratios of 4% and 8%, the pH right after acid addition was considerably low, but after a week the pH level quickly reached the point it was before acid addition, around 12. However, at higher A/P ratios the pH level remained low even after a week. For example, at A/P ratios of 15% and 19% the pH levels a week after acid addition

for SF5 paste exposed to NaCl were 9.98 and 4.38, and for SF10 paste exposed to NaCl they were 5.2 and 4.15. The same trend was observed for samples exposed to $CaCl_2$ and $MgCl_2$. Therefore, when more acid volume was introduced to the system (e.g., A/P ratio 19%), pH values during the two-week exposure of pastes to salt and acid were lower than the initial pH.

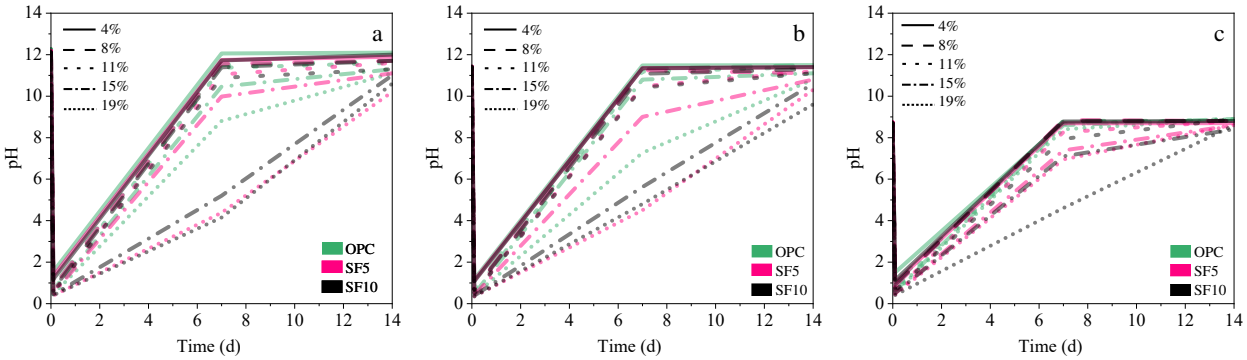

Figure 4.42. Time evolution of pH for pastes containing SF at different A/P ratio. (a) NaCl; (b) $CaCl_2$; (c) $MgCl_2$

The pH observation helps explain the chloride desorption results shown in Figure 4.41. At higher A/P ratios like 11%, 15%, and 19%, as the pH reduction caused by acid attack progresses layer by layer on paste samples, it causes the hydrated phases to dissolve, uncovering the underlying neat layers to the salt solution. If the pH of the solution is still low at this stage, the dissolution of the paste will persist. On the other hand, if the pH is higher, these exposed neat layers may act as sites for increased chloride absorption. Therefore, at higher A/P ratios a lower percentage of bound chloride observed, or in the other word, lower chloride desorption was obtained. Figure 4.43 and Figure 4.44 displays the degree of deterioration on pastes containing silica fume when the A/P ratio increases from 8% to 19%.

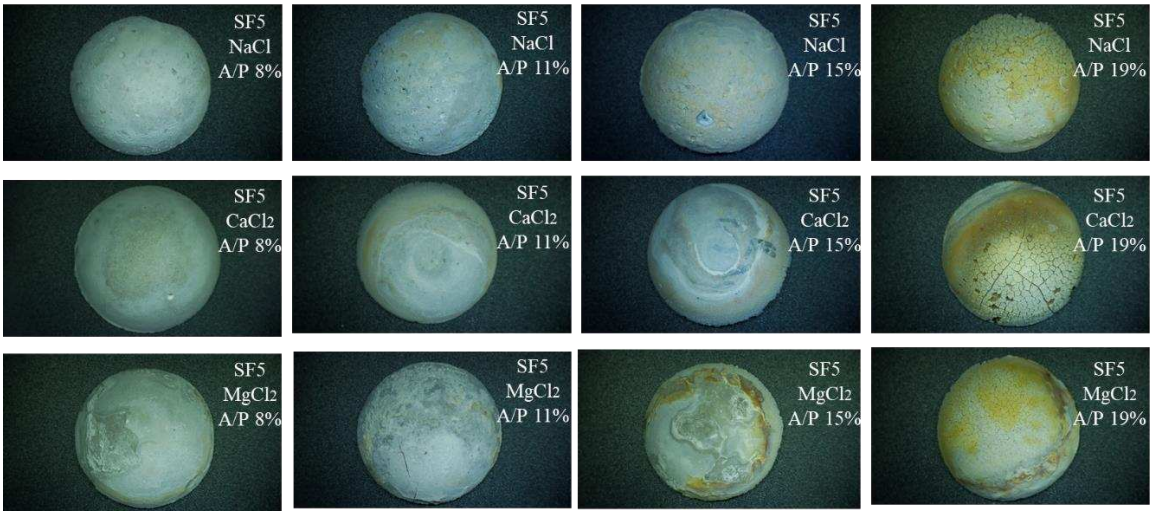

Figure 4.43. SF5 pastes exposed to different A/P ratios

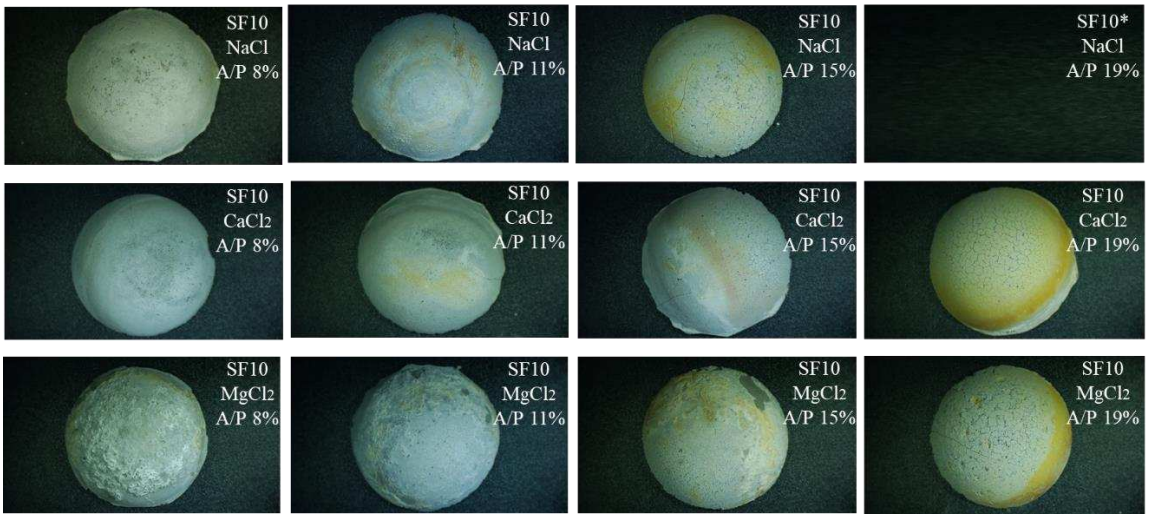

Figure 4.44. SF10 pastes exposed to different A/P ratios (* the image was not available)

As shown in Figure 4.43 and Figure 4.44 at higher A/P ratios like 11%, 15%, and 19% the color change clearly shows the cement hydration products on surface are dissolved. In addition, a very porous layer is formed on top, facilitating chloride penetration as the pH level gradually is equilibrated and stabilized after around a week.

4.3.3.4. Analytical Result for Paste Containing Silica Fume after Brine Solution Exposure and pH Reduction

Figure 4.45 shows XRD scans of SF5 and SF10 after exposure to 2 M brine solution and exposing to 25 mL of acid (A/P = 19%). Similar to other binders, the primary phase prior to the addition of acid was Portlandite, accompanied by the detection of Friedel's salt. As previously discussed, the introduction of acid led to the formation of ettringite and calcium nitrate. The analysis indicates that the Portlandite peaks in pastes containing silica fume remained relatively unchanged following acid addition. This could be attributed to the elevated pH of their exposure solution, which remained above eight even after two weeks of exposure to nitric acid.

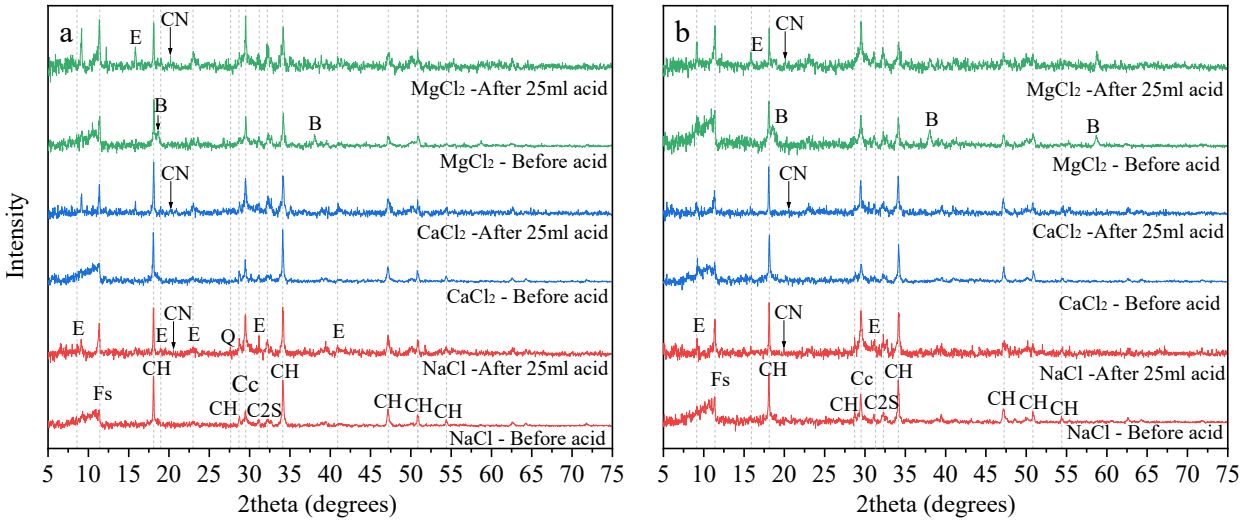

Figure 4.45. XRD scans of silica fume samples before and after exposure to 25 ml acid. Samples were first exposed to 2 M salt solutions. (a) SF5; (b) SF10 (FS: Friedel's salt, CH: Portlandite, Cc: Calcite, C2S: Belite, E: Ettringite, B: Brucite).

Figure 4.46 displays DTG curves for binders with silica fume. The data indicates that exposure to nitric acid had minimal impact on the reduction of Friedel's salt in NaCl and $CaCl_2$ solutions. In contrast, a notable decrease in Friedel's salt content was observed in samples exposed to $MgCl_2$ solution. A comparison of the results before and after acid addition reveals that the level of silica fume substitution did not significantly affect the content of Friedel's salt. However, the

curves show lower dips for Portlandite, which can be attributed to the enhanced pozzolanic reaction and the varying levels of silica fume replacement.

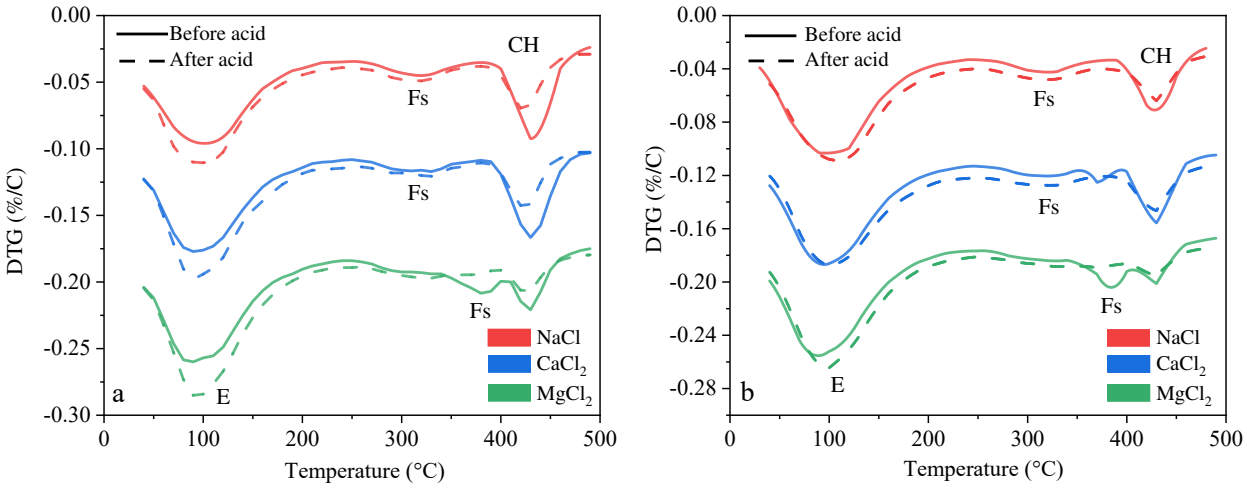

Figure 4.46. DTG results of silica fume-containing samples before and after exposure to 25 ml nitric acid (a) SF5 and (b) SF10

4.3.4.4. Summary of Main Findings on Chloride Desorption Mechanism (Objective 3)

Figure 4.47 shows the proposed mechanisms of acid attack and chloride desorption for pastes containing SCMs. After the nitric acid is added to the salt solution, it reacts with aqueous Na^{+}, Ca^{2+}, and Mg^{2+} ions in the salt solution to produce highly water-soluble $NaNO_3$, $Ca(NO_3)_2$, or $Mg(NO_3)_2$. These soluble salts react with the water, producing NaOH, $Ca(OH)_2$, and $Mg(OH)_2$, which can slightly increase the pH of the exposure solution. Subsequently, acid attacks the surface of the samples, leaching out cement hydrates, leading to surface cracking and creating a porous outer layer mainly composed of silicate hydrates. The number of observed cracks and the thickness of the porous layer increased with an increase in added acid.

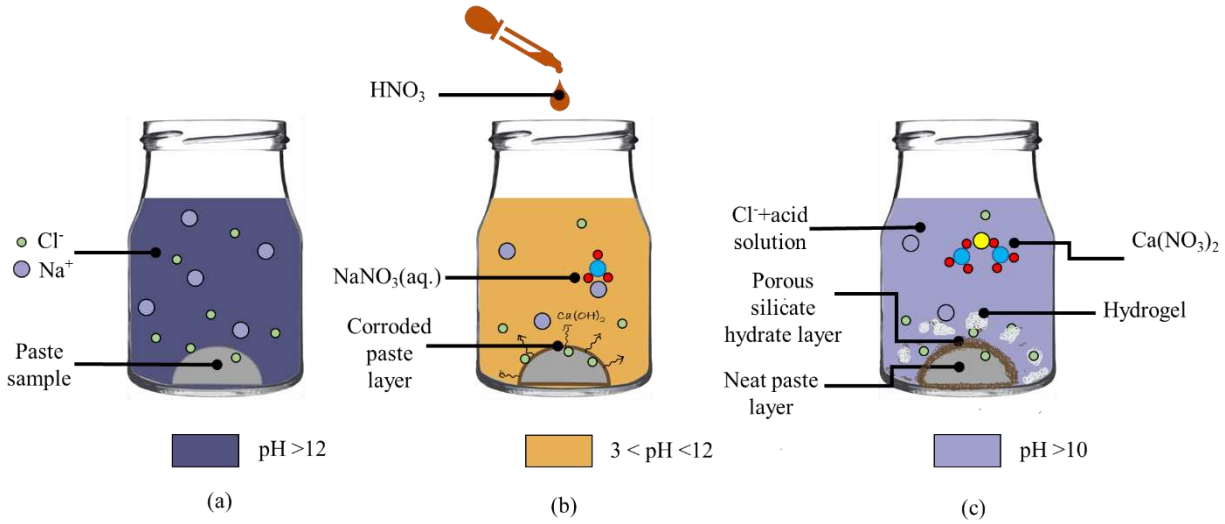

Figure 4.47. A schematic mechanism of the chloride desorption mechanism. (a) a neat paste sample exposed to chlorides for 2 weeks; (b) an instantaneous drop in the pH of the solution after adding nitric acid, which results in the corrosion of the outer layer of the sample; (c) the formation of porous outer silicate hydrate layer and hydrogels capable of absorbing chlorides.

The slow progression of an acid attack on a paste sample can result in the dissolution of hydrated phases, specifically the AFm phases, desorbing the bound chlorides. The dissolution of the outer paste layer also exposes the neat paste sublayers to the salt solution. At this point, if the pH of the solution is still low, the dissolution of the paste continues. Otherwise, the exposed neat sublayer can provide potential sites for chloride binding.

In addition to the reactions discussed above, the leaching of portlandite and silicates and their reaction with nitric acid can produce hydrogels of silica, aluminum, and ferric oxide [171]. Other researchers have reported the formation of a gelatin-like product during chloride extraction tests with acid [66, 148, 217, 218]. These precipitated calcium salts and hydrogels are highly porous and could contribute to chloride binding by absorbing some free chlorides from the exposure solution.

The analytical results showed that the cation of the chloride salt and the FA replacement level play critical roles in controlling the extent of chloride desorption. For example, more than 90% of the bound chlorides were released after adding 5 mL of nitric acid to samples immersed in a NaCl solution. In the $CaCl_2$ solution, regardless of the binder type, the amount of released bound chlorides was relatively lower than that of the NaCl solution. In addition, these results indicate that the percentages of released bound chlorides declined when the replacement level for FA increased from 15% to 30%. In the $MgCl_2$ solution, when 5 mL of acid was introduced to the different solutions, almost 60% of the bound chlorides were released.

There is a difference between the percentage of released bound chlorides and the concentration of available free chlorides after chloride desorption. If two pastes have the same percentage of released bound chlorides, the one with a higher chloride binding content releases more chlorides after desorption and vice versa. For example, the concentration of bound chlorides in OPC paste exposed to 2 M NaCl, $CaCl_2$, and $MgCl_2$ were 25.35, 33.72, and 59 mg Cl/ g paste, respectively. After adding 5 mL of acid to these solutions, the percentages of released bound chlorides were nearly 87% in NaCl, 92% in $CaCl_2$, and 86% in $MgCl_2$. While the percentages of released bound chlorides in NaCl and $MgCl_2$ solution were very close, due to the differences in total binding in these two solutions, the amount of released bound chloride would be 22.10 mg Cl/ g in NaCl and 50.79 mg Cl/ g in $MgCl_2$ solutions. Thus, both the chloride binding and desorption capacity of the system should be considered when designing a durable concrete mixture.

4.4. Objective 4: Synergic Effects of Exposure of Blended Cement Pastes Containing Fly Ash to NaCl Salt Solution and Carbonation on pH and Composition of Pastes

In this objective, the coupled impacts of chloride exposure (2 M NaCl for 35 days) and carbonation (exposure to 20% CO_2 for up to four weeks) on pH and composition of pastes containing OPC (100% cement) and 15% fly ash (85% OPC cement + 15% fly ash) are investigated. The overarching goal was to monitor change in pH and composition of pastes over time to measure the release of bound chloride (chloride desorption) under carbonation.

The average compressive strengths of OPC and FA pastes after 56 days curing in saturated lime solution were 28.8 MPa (4177 psi) and 22.4 MPa (3245 psi), respectively. The FA paste showed around 22% lower compressive strength compared to OPC paste, which is associated with fly ash pozzolanic reactivity. It is well researched that the compressive strength of fly ash containing pastes are lower than OPC cement paste in early ages but as time passes, pastes containing fly ash achieve the same or even surpass the compressive strength of their OPC counterparts [254].

4.4.1. Pastes Composition Before Exposure to NaCl Solution and Carbonation

Figure 4.48 shows the TGA results for OPC and FA pastes right after the curing period and before exposure to NaCl solution and carbonation. Figure 4.48a displays weight loss percentage and Figure 4.48b shows the calculated derivative thermogravimetric (DTG) curve. Figure 4.48 displays three major weight losses (Figure 4.48a) and three main dips (Figure 4.48b). The first weight loss corresponds to ettringite (45 to 140 ºC), the second one is associated with portlandite ($Ca(OH)_2$: CH) (385 to 460 ºC), and the third weight loss corresponds to calcium carbonate ($CaCO_3$) (625 to 750 ºC) [255]. While both pastes have almost the same weight loss up to around 400 ºC, meaning the same ettringite content, after this temperature the overall weight loss

percentage of FA paste is lower than OPC paste. Figure 4.48b reveals the dip associated with portlandite (CH) for OPC is deeper than FA, meaning that the portlandite content in OPC paste is higher than FA paste. The weight loss changes in Figure 4.48a associated with portlandite were 3.55% in OPC paste and 2.79% in FA paste. The main reason for this observation is due to pozzolanic reactivity of fly ash and consumption of a portion of portlandite by fly ash to form C-S-H [254]. The results are in agreement with previous reports by Kocak et al. [230] and Leklou et al. [232].

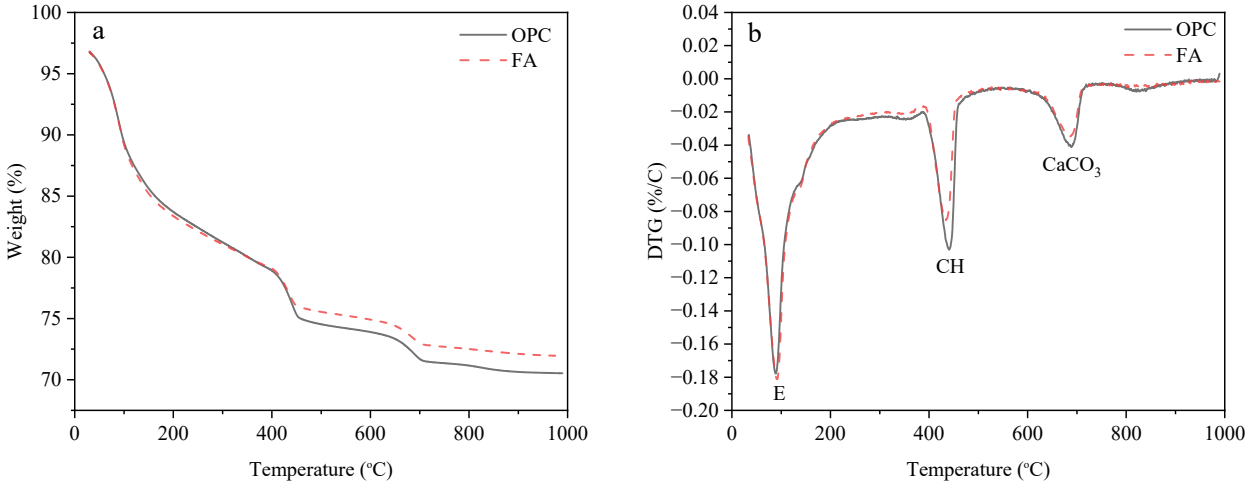

Figure 4.48. TGA results for pastes after moist curing and right before salt exposure a) percentage of weight change b) DTG (E:Ettringite, CH: Portlandite, and $CaCO_3$: Calcium carbonate)

The weight loss associated to $CaCO_3$ in the temperature range of 625 ºC to 720 ºC in OPC paste was 1.91% and in FA paste was 1.49%. $CaCO_3$ contents come from the cement production process due to presence of calcium carbonate (calcite) in the unhydrated cement [255]. The lower $CaCO_3$ content in FA paste is due to fly ash inclusion and lower OPC content.

To further understand the composition of pastes before exposure to chloride and carbonation, XRD tests were performed. Figure 4.49 displays XRD scans of paste before exposure to salt solution. The results showed that the portlandite (CH) was the dominant phase and traces

of ettringite (E) and calcium carbonate (Cc) were detected. It should be noted that the XRD scan was run for an empty sample holder, and the peak that seems to appear around 8 to 11 degrees originates from the sample holder not a real peak from materials. The intensity of the portlandite peak in the FA paste in the range of 45 to 55 degrees is weaker compared to OPC pastes, showing lower content of portlandite due to fly ash pozzolanic reactions. The XRD results support the observations in the TGA tests (DTG curves).

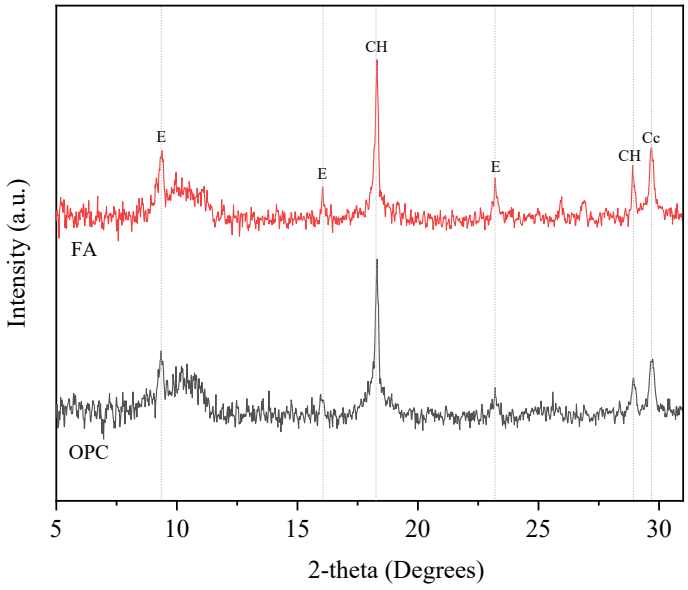

Figure 4.49. XRD traces for pastes after moist curing and right before salt exposure (E: Ettringite, CH: Portlandite, and Cc: Calcium carbonate (calcite))

4.4.2. pH Before Exposure to NaCl Solution and Carbonation

Figure 4.50 displays the average of measured pH in OPC and FA pastes after moist curing and before exposure to the salt solution and carbonation. The pH was measured using in-situ (suspension) method. The average pH in all depths for OPC and FA pastes were 12.98 and 12.95, respectively. The results are in agreement with previous reported pH for non-carbonated cement pastes [16]. As described in the methods section, chapter 3, pH during chloride exposure was monitored at three distinct depths (0 to 5 mm represents the surface layer, 5 to 15 mm, and 15 to

30 mm). As expected, both pastes had a high alkalinity environment which is essential for formation and preservation of a passive layer on the steel in reinforced concrete [16].

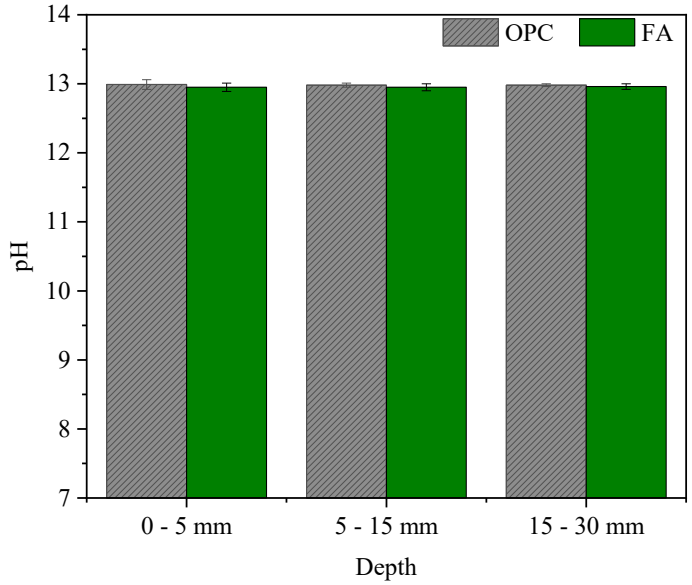

Figure 4.50. pH of pastes after 56 days curing in different depths

4.4.3. Compositional Change After Exposure to NaCl Brine Solution

Figure 4.51 displays DTG curves for pastes (in the surface layer) before and after 35 days exposure to the salt solution. There were no dips in the temperature range of 250 to 390 ºC in the DTG curves which means no signs of Friedel's salt before exposure to the salt solution. The formation of Friedel's salt after exposure to NaCl salt due to chemical reaction of C3A and chloride ions was observed. The Friedel's salt dip was detected in the temperature range of 250 to 390 ºC in both pastes. The weight loss percentage associated with Friedel's salt after 35 days of brine solution exposure was 0.55% in OPC paste and 0.82% in FA paste. In other words, incorporation of fly ash increased the chemical chloride bindings in the form of Friedel's salt formation. The results are in agreement with objective 3 tests that found a higher chloride binding capacity for fly ash containing pastes [153] and previous findings in the literature [19, 71, 126] .

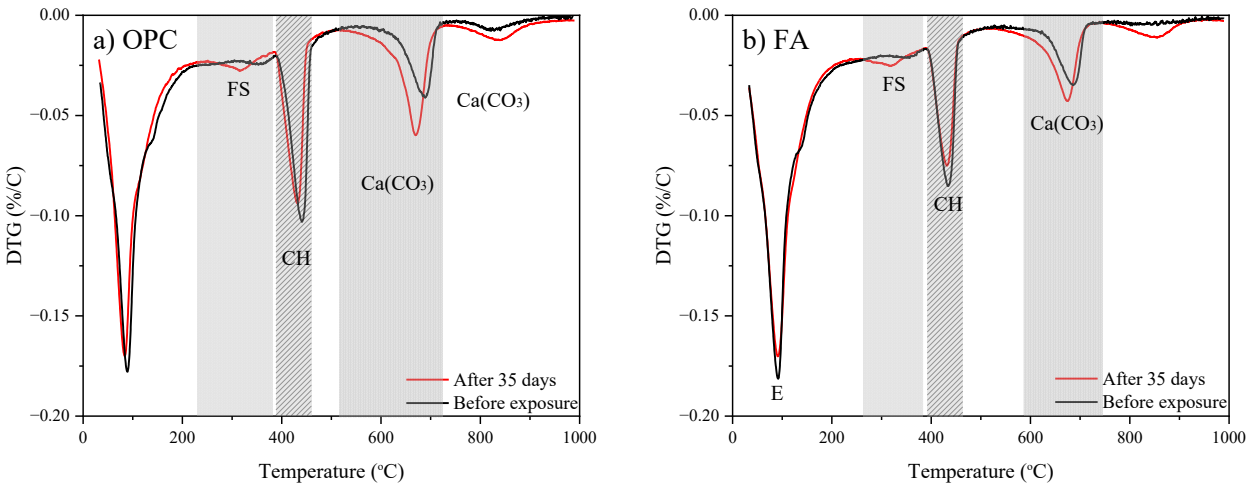

Figure 4.51. DTG plots 35 days after exposure to salt solution in the surface layer a) OPC and b) FA (E:Ettringite, FS: Friedel's salt, CH: Portlandite, and CaCO3: Calcium carbonate (calcite))

Figure 4.51 displays the presence of ettringite (E), portlandite (CH), and calcium carbonate ($CaCO_3$). Figure 4.51 indicated a slightly higher (deeper dips) for $CaCO_3$ in the surface layer after chloride exposure and before carbonation. It is probable that the surface layer may be affected by atmospheric carbon dioxide which concentration is 0.03% to 0.04%. As mentioned in the methods section, after curing, samples were removed from saturated lime solution, saw cut, epoxy coated, dried, and then immersed in salt solution.

Figure 4.52 displays XRD results for OPC and FA paste before immersing samples in 2 molar NaCl solution and after 20- and 35-days of exposure. The results show that the Friedel' salt formed after chloride exposure. The peak associated with Friedel' salt was around 11-12 degrees. As chloride exposure time increases, the higher is the detected peak for Friedel' salt. The results also show that the exposure to NaCl solution increases the quantity of ettringite (E). The reason that ettringite quantity increases when paste is exposed to NaCl solution is that chloride ions react with AFm phases (hydrated calcium aluminates phases) including monosulfate which replace the sulfate. The released sulfate can react with portion of the remaining monosulfate to produce ettringite [256]. The reaction of monocarbonate with chloride ions forms Friedel's salt and the

reaction of monosulfate with chloride ions forms Friedel's salt, however, the monocarbonate is more stable than monosulfate, meaning monosulfate more actively reacts with chloride ions. The XRD results are in good agreement with the DTG curves.

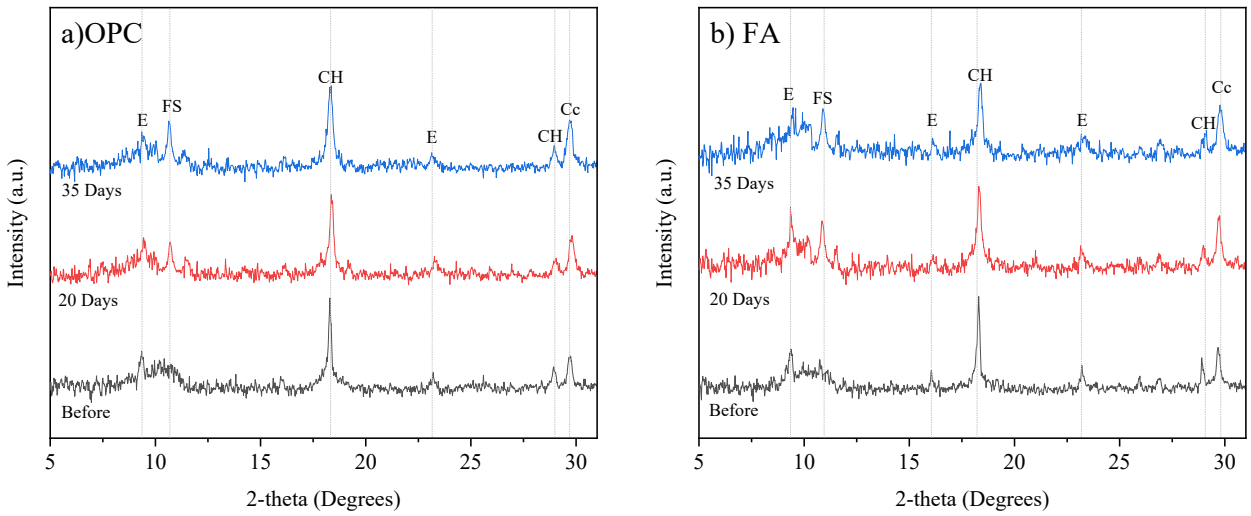

Figure 4.52.XRD scans for surface layer of pastes before and after chloride exposure a) OPC and b) FA (E: Ettringite, FS: Friedel's salt, CH: Portlandite, and Cc: Calcium carbonate (calcite))

The XRD was performed on surface (0-5 mm) and inner layers (5-15 mm) of pastes as shown in Figure 4.53. In both pastes the peak associated with Friedel's salt is stronger in the surface layers than the inner layers, meaning the quantity of chemically bound chloride in the surface layer is higher.

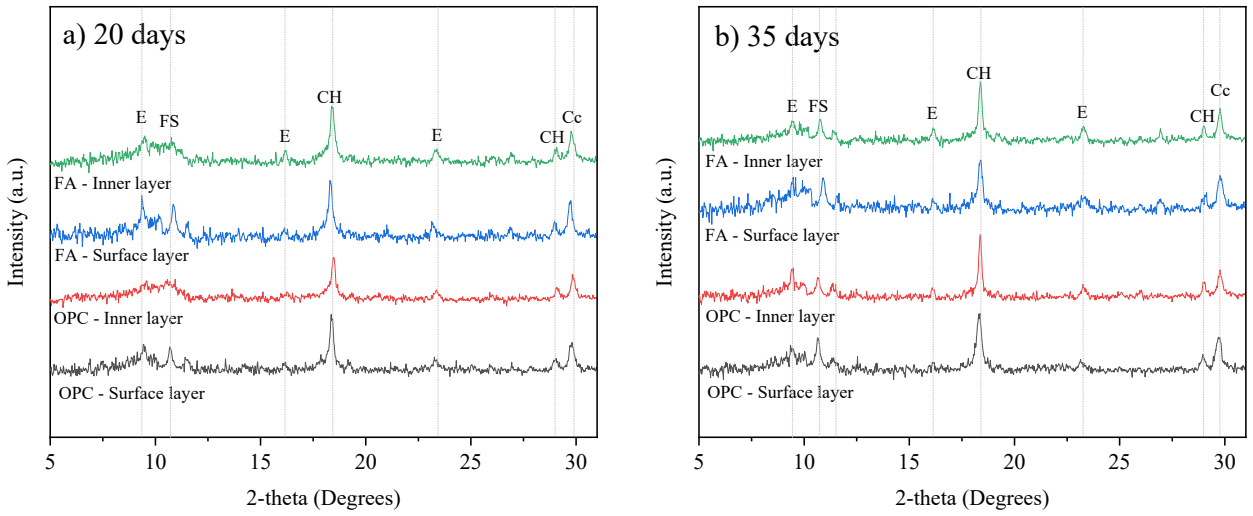

Figure 4.53. XRD scans for OPC and FA pastes after chloride exposure a) 20 days and b) 35 days (E: Ettringite, FS: Friedel's salt, CH: Portlandite, and Cc: Calcium carbonate (calcite))

4.4.4. pH After Exposure to NaCl Solution

After exposure to 2 M NaCl solution, the pH of pastes was monitored for up to 35 days at defined intervals (10 days, 20 days, 35 days). Figure 4.54 shows the pH change up to 35 days for pastes fully immersed in the salt solution. The results reveal that pH dropped when pastes were exposed to NaCl solution, and the surface layer experienced a lower pH level compared to inner layers. The average pH level in OPC paste, as shown in Figure 4.54a, before immersing in NaCl solution was 12.99. The pH of the surface layer (depth 1: 0-5 mm) dropped to 12.70 after 10 days, 12.56 after 20 days, and 12.48 after 35 days immersion in NaCl solution. Due to a low chloride diffusion rate, 10^{-13} to 10^{-10} m^2/s [194], the chloride penetration depth increases slowly and consequently chloride concentrations in the layers near the surface of the samples are higher than at deeper depths. When chloride ions penetrate into pastes, as explained before, Friedel's salt forms at the expense of portlandite ($Ca(OH)_2$) consumption (consumption of hydroxide ions), reducing the alkalinity of the system and lowering the pH. The same trend was observed for FA pastes.

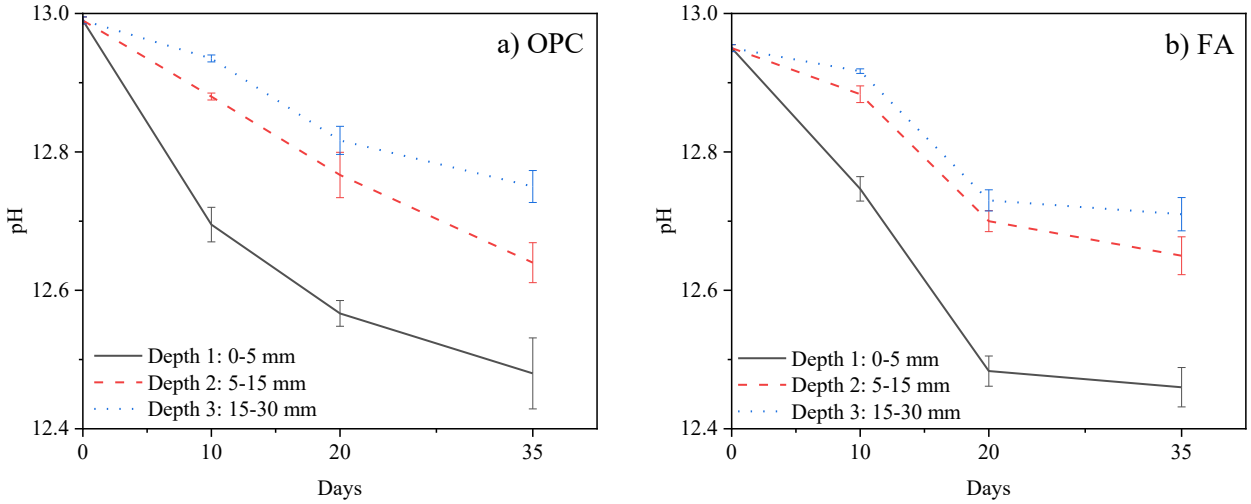

Figure 4.54. pH change in a) OPC and b) fly ash containing pastes exposed to 2 M NaCl solution up to 35 days

The results showed that the pH of pastes exposed to NaCl solution slightly decreased. The pH decrease is not drastic because the cement paste contains a significant amount of calcium hydroxide and other alkaline components that buffer the pH. The longer the samples were exposed to the salt solution the more the pH dropped. For instance, the average pH level in OPC paste before chloride exposure at all depths was 12.99. After 10 days of exposure the pH in OPC paste dropped to 12.70 in the surface layer and after 20 days and 35 days the average measured pH were 12.56 and 12.48, respectively. In the inner layers, pH was 12.93 after 10 days chloride exposure and dropped to 12.81 and 12.75 after 20 and 35 days, respectively. After immersion of the sample in NaCl solution the chloride ions start penetrating into the sample through capillary suction and diffusion. As discussed in the previous section, 4.4.3, the chloride diffusion rate impacts how far chloride ions can penetrate in the allowed time.

4.4.5. Compositional Change After Carbonation

Figure 4.55 shows the DTG curves after a week of carbonation in the surface and inner layers in OPC and FA pastes. It should be reminded that paste samples were first immersed in 2 M

NaCl solution for 35 days and then went through accelerated carbonation test. The main observation was that the dip associated with Friedel's salt is different compared to DTG curves after only chloride exposure. The results show a shallower dip for Friedel's salt after carbonation which represents less bound chloride and chloride desorption after a week of carbonation. The weight loss percentage associated to Friedel's salt in TGA results after 35 days chloride exposure was 0.417%, compared to only 0.121% after 35 days chloride exposure and then a week carbonation. Using Eq (4.1), the calculated Friedel's salt mass was 2.85 wt.% after 35 days chloride exposure which reduced to 0.63 wt.% after 35 days chloride exposure and a week of carbonation. In other words, after a week, due to carbonation, Friedel's salt quantity is reduced, and chloride desorption is observed. The surface layer was exposed to carbonation more than the inner layer because carbonation is a slow process and cannot diffuse to deep depths. Pade et al. [257] reported an average carbonation depth of 9.6 mm after 70 years of natural carbonation for concrete structures in Nordic countries and they claimed that the carbonation process for concrete structures with a high strength class (> 35 MPa (5100 psi)) is a notably slow process during their service life (70 years).

Friedel's salt and AFm phases in concrete exposed to chloride ions are unstable when carbonation takes place [258]. This phenomenon combined with decalcification of the C-S-H phase releases physical chloride bonds, increasing the chloride concentration in pore solution in carbonated regions of the concrete. Geng et al. [167] also reported the same results that carbonation releases the bound chloride in the form of Friedel's salt from chloride-exposed concrete by dissolution of Friedel's salt and decomposition of C-S-H.

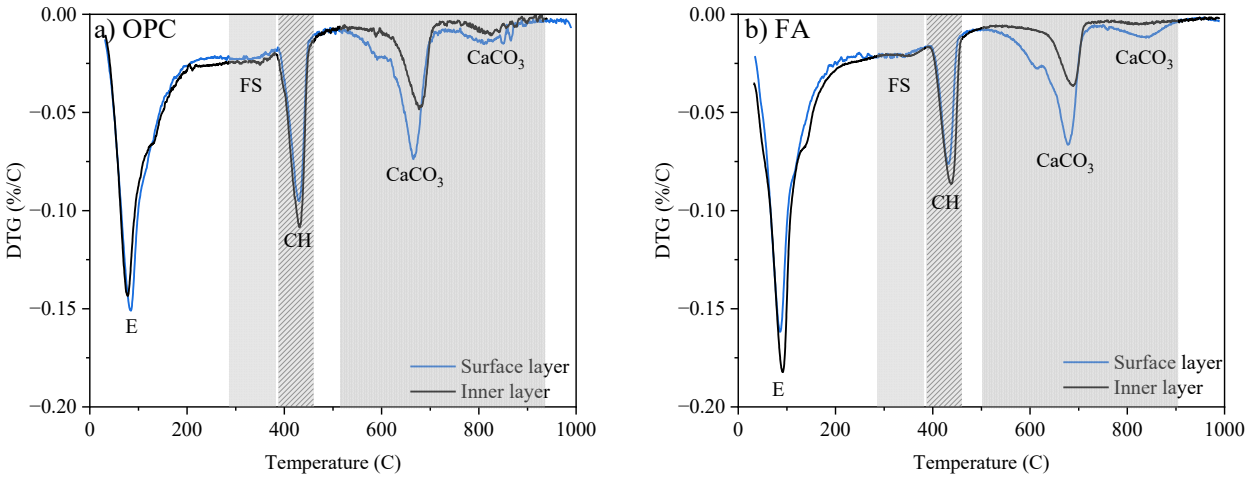

Figure 4.55. DTG curves after exposure to salt solution and 1 week of carbonation a) OPC and b) FA (E:Ettringite, FS: Friedel's salt, CH: Portlandite, and CaCO3: Calcium carbonate (calcite))

Figure 4.56 displays DTG curves for samples before and after two weeks of carbonation. In the temperature range of 250 to 400 ºC, there is no sign of the Friedel's salt dip. The results reveal that carbonation almost completely caused Friedel's salt dissolution. The DTG plots clearly highlight the deeper dips of $CaCO_3$ after carbonation compared to non-carbonated samples. Figure 4.56 shows that the dip corresponding to calcium carbonate took place in the temperature range of around 640 ºC to 710 ºC in non-carbonated paste and around 570 ºC to 710 ºC in carbonated samples. The results show that the weight loss of $CaCO_3$ in OPC paste before exposure was 1.91% and increased to 4.35% after one week of carbonation and 5.00% after two weeks of exposure to CO_2. The same trend was observed for FA paste in which the weight loss of $CaCO_3$ was 1.49% before carbonation and 4.33% and 4.63% after one- and two-weeks of carbonation, respectively.

Figure 4.56 shows DTG curves for pastes after two weeks carbonation. A higher calcium carbonate content is seen in the surface layer compared to the inner layer in both pastes. For instance, in OPC paste the weight loss corresponding to $CaCO_3$ content was 4.35% in the surface and 2.27% in the inner layer. Higher weight loss of $CaCO_3$ confirmed the occurrence of higher

carbonation in the surface layer. In the presence of humidity, when specimens are exposed to carbon dioxide, CO_2 dissolves in water forming carbonic acid. Carbonic acid reacts with portlandite to form calcium carbonate ($CaCO_3$) and water [171, 259].

An interesting observation is the difference between portlandite (CH) in the surface and inner layers of pastes. The portlandite content is lower on the surface than the inner layer, because portlandite was consumed by CO_2, as part of carbonation process to form calcium carbonate. The weight loss associated with portlandite was 3.26% in the inner layer which reduced to 2.76% on the surface.

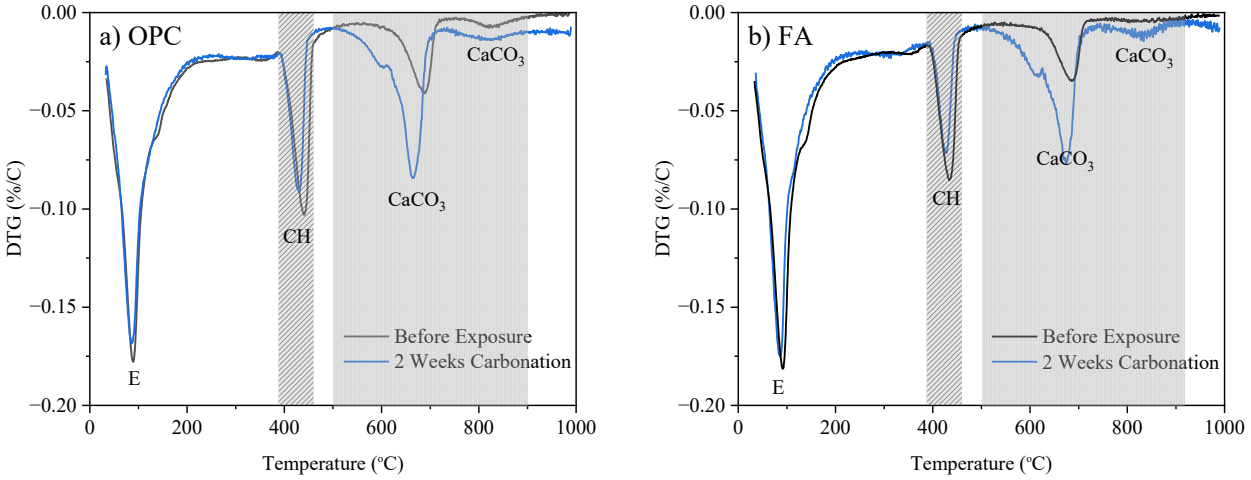

Figure 4.56. DTG curves after 2 weeks carbonation a) OPC and b) FA (E:Ettringite, FS: Friedel's salt, CH: Portlandite, and CaCO3: Calcium carbonate (calcite))

Figure 4.57 shows XRD traces for pastes before and after carbonation. In both pastes, the intensity of calcium carbonate (Cc) is higher after carbonation (the peak around 30 degrees). On the other hand, the portlandite (CH) peak around 18 degrees is weaker as the carbonation time increased. The higher intensity of calcium carbonate indicates carbonation occurred in the samples. Carbonation increases the solubility of Friedel's salt. Carbonation of ettringite and aluminum bearing phases also can occur [260]. Carbon dioxide also can react with C-S-H gel to form silica

gel and calcium carbonate. The stability of ettringite is also pH dependent [233] and a reduction in ettringite (a slightly shallower dip in DTG plot) can be associated to ettringite carbonation.

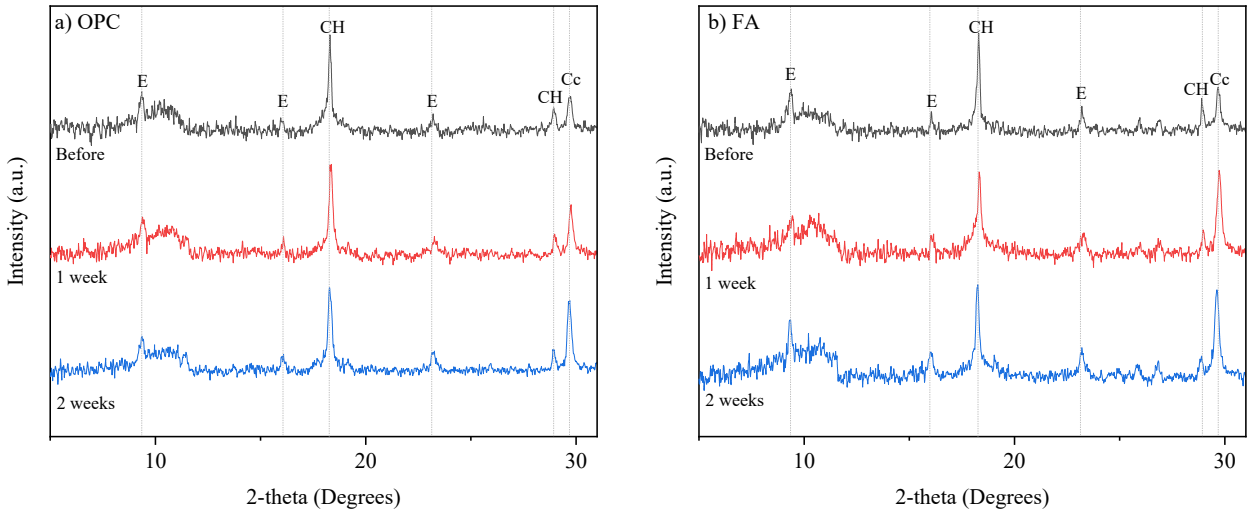

Figure 4.57. XRD scans before and after carbonation a) OPC pastes and b) FA pastes (E: Ettringite, CH: Portlandite, and Cc: Calcium carbonate (calcite))

Figure 4.58 displays XRD results for pastes after 2 of carbonation. The XRD scans are shown at different depths from surface to inner layers. Figure 4.58a clearly shows that the calcium carbonate peaks, around 30 degrees, were higher at the surface than at inner depths, meaning that the carbonation was more significant on the surface of OPC pastes. The same trend was observed in FA pastes. Another important observation from the XRD traces is related to Friedel's salt. The XRD result for both pastes after chloride exposure, Figure 4.52 and Figure 4.53, Friedel's salt peak were observed around 12 degrees. However, after carbonation, Figure 4.58, the is no sing of this peak. This observation confirms the dissolution of Friedel's salt after carbonation. The XRD results are in well agreement with TGA results (DTG curves). In both OPC and FA pastes, Figure 4.58, stronger calcite (Cc) peaks were observed in surface layers and weaker portlandite peaks. These

observations show the consumption of portlandite in the carbonation process to produce carbonic acid and then calcium carbonate. The TGA and XRD results align well.

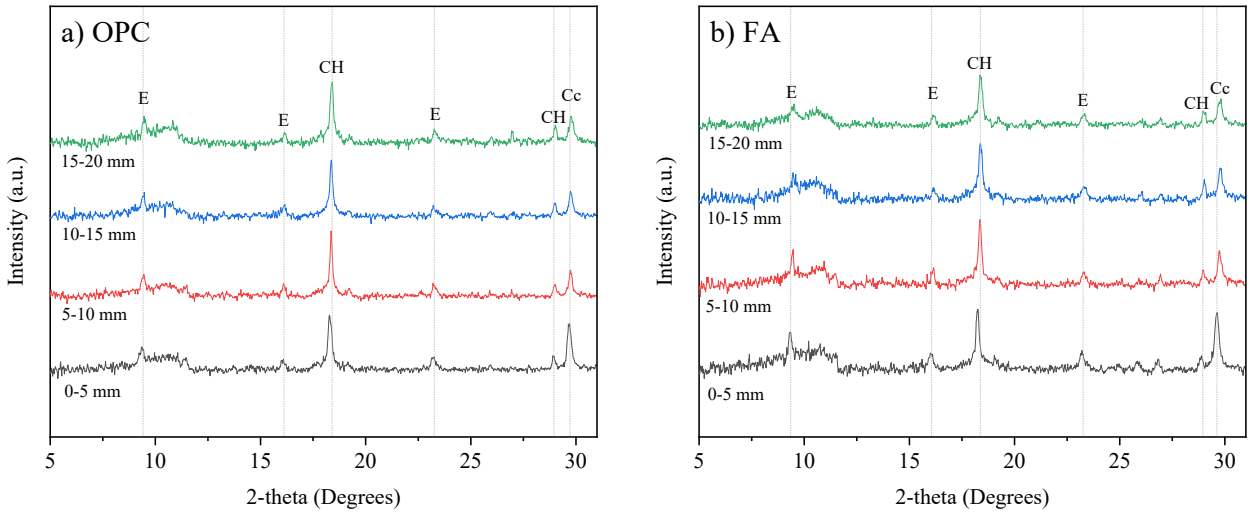

Figure 4.58. XRD scans at different depths after 2 weeks of carbonation a) OPC and b) FA (E: Ettringite, CH: Portlandite, and Cc: Calcium carbonate (calcite))

4.4.6. pH Change After Carbonation

The pH was measured at four different depths from the surface (0-5 mm, 5-10 mm, 10-15 mm, and 15-20 mm) after 1 week, 2 weeks, and 4 weeks of carbonation. Figure 4.59 shows the average pH after carbonation in the cement pastes. The results show that fly ash containing pastes experienced a lower pH during carbonation compared to OPC pastes. The primary reason as discussed earlier is associated with a lower portlandite content in FA pastes. Portlandite is the cement hydrate phase that start decomposition when cement pH is dropped below 12.6 [171] and buffers the effect of acid. Thus, because less portlandite is available in FA pastes, the pH drop is more significant and carbonation front more rapidly pushes inwards. Previous studies reported a weaker carbonation resistance [261-263], higher carbonation depths, and higher carbonation rate [264-266] when fly ash was incorporated into the paste mixture.

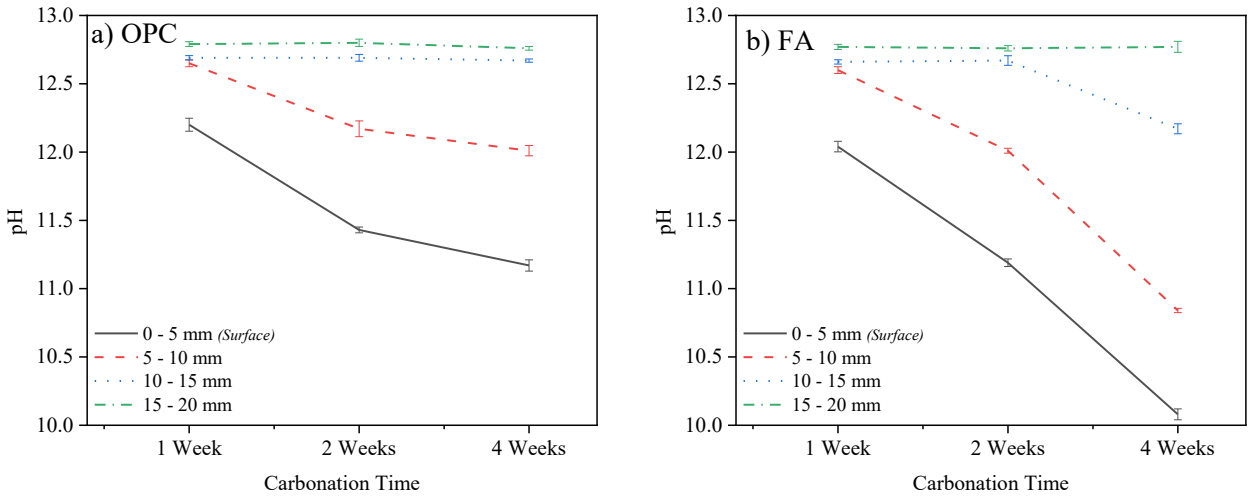

Figure 4.59. pH change in paste after carbonation a) OPC and b) FA

The results also indicate that the inner layer (last depth: 15-20 mm) had almost the same pH range before and after carbonation as the CO_2 diffusion rate is quite slow and cannot reach this depth in a short time. Figure 4.59a reveals that in OPC pastes the pH in inner layers, 10-15 mm and 15-20 mm, was above 12.5 and remained the same after carbonation. The results show that the surface layer is more drastically influenced by carbonation. At the surface, the pH before starting carbonation, at the end of chloride exposure, was 12.48 (Figure 4.54a). The pH dropped to 12.20 after a week of carbonation. Further exposure to carbonation reduced the pH level to 11.44 and 11.17 after two- and four-weeks, respectively. The same pH reduction trend was observed for FA pastes as shown in Figure 4.59b. The FA paste before carbonation had a pH of 12.42 (Figure 4.54b) and the pH dropped to 12.04 after a week, 11.19 after 2 weeks and 10.08 after 4 weeks of carbonation.

The primary reason for pH reduction in cement pastes after carbonation is related to the reaction between CO_2 in the chamber and portlandite ($Ca(OH)_2$) as one of the dominant phases of OPC cement paste. Thermodynamic simulation using CemGEMS [267] shows that in a cement

paste with w/c ratio of 0.4, portlandite forms approximately 17% of paste volume and is the second primary phase after C-S-H. When 15% fly ash is incorporated in the cement paste the portlandite forms 11.8% of the volume, still the second main solid phase after C-S-H. In addition, in the presence of carbon dioxide and humidity in cement paste two main reaction occurs. The reaction of carbon dioxide and humidity forms carbonic acid and then the reaction of a portion of this acid with available portlandite in cement paste forms calcium carbonate. A portion of calcium carbonate produced in carbonation process can react with remaining carbonic acid and leach out Ca^{2+}, lowering the buffering capacity of cement paste and making cement paste susceptible to pH changes.

Monitoring the hydroxide ion concentration is vital to understand and estimate the extent of corrosion in existing structures. As reported by many researchers including Alonso et al. [268] chloride-induced corrosion of embedded steel reinforcement is more likely to initiate at aqueous $[Cl^-]/[OH^-]$ ratios more than 0.6. The concentration of hydroxide ions can be quantified based on the measured pH as described by [269]. pH calculates as the negative logarithm of the hydroxide ions concentration (OH^-), a higher pH means higher OH^- concentration. Eq. (4.2) shows the normalized hydroxide ion concentration.

$$[OH^-]_{paste} = (e^{-(14-pH)}) \times (\frac{V \times 17}{m}) \times 100 \quad (4.2)$$

OH^-: Normalized hydroxide ion concentration in the paste sample (wt.%)

pH: Measured pH of powdered paste suspension

V: Volume of suspension (Liter)

m: Mass of powdered paste sample (g)

In Eq. (4.2) 17 is the molar mass of hydroxide ions (17 g/mol). The hydroxide ion concentration reduction for carbonated samples is calculated by comparing the hydroxide ion concentration before and after carbonation. Figure 4.60 shows the hydroxide ion (OH^-) concentrations before and after carbonation at different depths of OPC and FA pastes. The lower concentration of OH^- is equal to a lower pH in a layer. The results show that the OH^- concentration reduces after carbonation. The longer carbonation durations led to lower hydroxide ion concentrations. For instance, the initial hydroxide ion concentration was 2.17 wt.% before carbonation which reduced to 0.45 % and 0.13% in the surface layer of OPC pastes after two- and four-weeks of carbonation, respectively. The same trend was observed for FA pastes where the initial hydroxide ion concentration dropped from 2.08% to 0.35% after two weeks of carbonation and 0.11% after four weeks of carbonation.

A lower OH^- concentration due to carbonation, as shown in Figure 4.60, combined with increasing Cl^- concentration due to exposure to seawater or deicing salts leads to chloride-induced corrosion initiation. A higher Cl^-/ OH^- in the pore solution, increases the risk of chloride induced corrosion in two ways. First, it is well established chloride ions concentration is not the only factor that influence chloride-induced corrosion risk and depassivation of reinforcements, but the OH^- concentration play a key role in passive film protective and chloride-induced corrosion rate [270]. A higher Cl^-/ OH^- ratio accelerates the deterioration of passive film that protects reinforcement. Secondly, the Cl^-/ OH^- ratio impact the chloride binding as chloride ions and alkalis are competing to adsorption on cement hydrates such as C-S-H and make chloride binding [131].

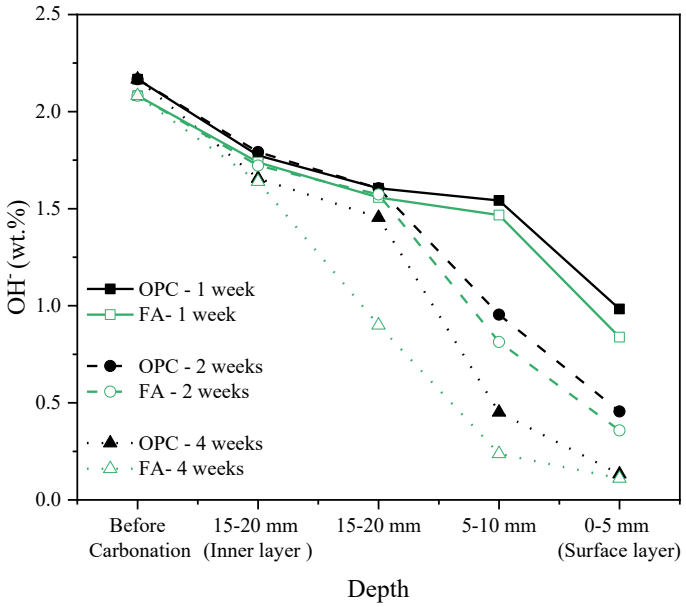

Figure 4.60. Hydroxide ion concentrations before and after carbonation, at different depths

Figure 4.60 also reveals that in general the FA pastes had lower hydroxide ion concentrations compared to OPC pastes. The lower content of portlandite in fly ash containing pastes is the primary reason, which is well-investigated in previous investigation [271], and thermodynamic modeling of cement hydration using CemGEMS also confirmed the rationale. The pH does not considerably reduce as long as the portlandite is not fully consumed by carbonation. After the portlandite is fully carbonated, C-S-H decalcification occurs and pH drops.

4.4.7. Chloride Desorption and pH Change

The percentage of weight loss obtained for TGA tests are used to calculate the mass of Friedel's salt, portlandite, and calcium carbonate as described by Scrivener et al [255]. Eqs. (4.3) to (4.5) show the formula for mass calculation of Friedel's salt, portlandite, and calcite.

$$\text{Friedel's salt mass (wt.\%)} = \frac{(\text{molar mass Friedel}'\text{salt})}{6 \times \text{molar mass water}} \times (\text{weight loss \% from TGA}) \qquad (4.3)$$

$$\text{Portlandite mass (wt.\%)} = \frac{(molar\ mass\ Ca(OH)2)}{molar\ mass\ water} \times (\text{weight loss \% from TGA})) \quad (4.4)$$

$$\text{Calcite mass (wt.\%)} = \frac{(molar\ mass\ CaCO3)}{molar\ mass\ CO2} \times (\text{weight loss \% from TGA}) \quad (4.5)$$

(Friedel's salt molar mass: 561.3 g/mol, Water molar mass18.02 g/mol, Calcium hydroxide molar mass: 74 g/mol, Calcium carbonate molar mass:100 g/mol, Carbon dioxide molar mass: 44 g/mol)

The weight loss measured from TGA tests was measured and used to calculate the mass of Friedel's salt, portlandite, and calcite shown in Table 4.10 and Table 4.11. The weight loss of the primary layer of water obtained from TGA for Friedel's salt, portlandite, and calcite was determined from TGA curves by subtracting results for the non-exposed paste from the pastes which were exposed to salt (or salt and carbonation) in the temperature range in which Friedel's salt, portlandite, and calcite were observed. The weight loss percentage in TGA curves was measured using the tangential baseline method as described in [272] using TA instruments Trios software.

Table 4.10 and Table 4.11 show the measured mass of Friedel's salt in the surface layer (0-5 mm) and the temperature range that the dips occurred in OPC and FA pastes. The results reveal that Friedel's salt content significantly reduced after carbonation. The Friedel's salt mass reduction in OPC and FA pastes after one week of carbonation compared to its content before carbonation was approximately 78.0% and 86.7%, respectively. After two weeks of carbonation, Friedel's salt mass reduction was 95.4% in OPC paste and 97.6% in FA pastes.

Table 4.10. Friedel's salt, portlandite, and calcite contents in the surface layer of OPC paste

		Before exposure	20 days chloride exposure	35 days chloride exposure	1 week carbonation	2 weeks carbonation
Friedel's salt	Temperature (ºC)	-	250-382	250-385	265-387	269-388
	Weight loss (%)	0	0.417	0.549	0.121	0.03
	Mass (wt.%)	0	2.16	2.85	0.63	0.13
Portlandite	Temperature (ºC)	408-454	400- 445	401-444	404-442	407- 441
	Weight loss (%)	3.552	3.236	3.060	2.764	2.052
	Mass (wt.%)	14.60	13.30	12.58	11.36	8.44
Calcite	Temperature (ºC)	640-704	620- 692	646-691	576-688	575-693
	Weight loss (%)	1.909	2.181	2.128	4.35	6.00
	Mass (wt.%)	4.34	4.96	4.84	9.89	13.64

Table 4.11. Friedel's salt, portlandite, and calcite contents in the surface layer of FA paste

		Before exposure	20 days chloride exposure	35 days chloride exposure	1 week carbonation	2 weeks carbonation
Friedel's salt	Temperature (ºC)	-	250-383	250- 389	262-393	262-389
	Weight loss (%)	0	0.588	0.819	0.109	0.02
	Mass (wt.%)	0	3.05	4.25	0.57	0.10
Portlandite	Temperature (ºC)	408-449	403-441	408-446	411-445	411- 436
	Weight loss (%)	2.791	2.499	2.274	1.993	1.06
	Mass (wt.%)	11.48	10.27	9.35	8.19	4.36
Calcite	Temperature (ºC)	649- 703	616-692	641-694	582-698	587-693
	Weight loss (%)	1.489	2.203	1.737	4.33	5.69
	Mass (wt.%)	3.38	5.01	3.95	9.85	12.93

The results in Table 4.10 for OPC pastes show the portlandite content is reduced by exposure to chlorides. The percentage of portlandite content reduction was around 8.9% and 13.9% after 20 days and 35 days of exposure to the chloride solution. After carbonation, the

portlandite consumption rate increased. For instance, after two weeks, more than one-third of the portlandite was consumed by carbon dioxide to form calcite. Compared to the non-carbonated sample the portlandite content in OPC pastes dropped 22.2% and 42.2% after one and two weeks of carbonation, respectively. On the other hand, the calcium carbonate content in OPC pastes after carbonation is drastically increased. For instance, after a week of carbonation the calcite content increased 128% and after two weeks of carbonation it increased 214.3%. The same trend was observed for FA pastes, Table 4.11. The percentage of reduction in portlandite quantity in FA pastes after 1 week of carbonation was 28.6% and after two weeks was 62.0%. The percentage of increase in calcite content in the FA paste were 190.9% after a week and 282.1% after 2 weeks of carbonation. The results show more extensive carbonation in fly ash containing samples. The results agree well with previous findings in which the carbonation rate and depth were higher when fly ash incorporated in cement pastes [262, 266].

Another interesting observation in both pastes was the Friedel's salt quantity change. No Friedel's salt was detected in pastes before starting exposure of samples to chloride ions by the TGA results. The XRD scans also confirm this obsevation. Upon exposure to chloride ions the Friedel's salt content significantly increased, increasing the chloride binding quantity as Friedel's salt is chemically bound chloride with aluminium bearing phases in cement paste. However, after a week of carbonation the Friedel's salt content drastically dropped by around 78.0% in OPC paste and 86.7% in FA paste. A decrease in Friedel's salt with carbonation means that chloride desorption occurred because the quantity of chemically bound chloride reduced. As the free chloride ions are responsible for deteriorating the passive film on rebar in concrete structures (depassivation), lower Friedel's salt content increases the free chloride coneenteration. After two weeks almost all Friedel's salt decomposed and the reduction in its quantity was 95.4% (from 2.85 wt.% before

carbonation to 0.13 wt.% after two weeks of carbonation) in OPC paste and 97.6% (from 4.25 wt.% before carbonation to 0.10 wt.% after two weeks of carbonation) in FA paste.

Figure 4.61 shows the impact of pH change in different exposure conditions on the Friedel's salt mass, which represents the bound chloride formation or desorption, and calcium carbonate mass ($CaCO_3$). which represents carbonation deterioration in cement paste. Before exposure of the samples to salt or carbon dioxide the alkalinity is high, the pH is around 13, the Friedel's salt content is zero, and calcite quantity comes from the cement production process and is less than 5%.

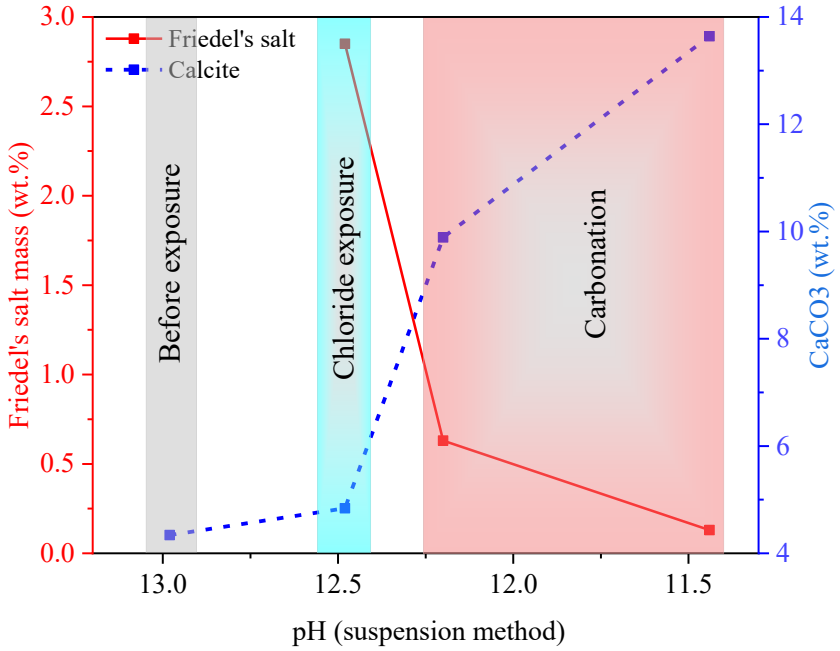

Figure 4.61.Effect of pH change in Friedel's salt and calcite mass in OPC paste after 35 days chloride exposure and two weeks carbonation

Upon exposure to NaCl solution, Friedel's salt formed, and the pH slightly reduced. During two weeks of carbonation, the pH of the cement paste dropped and the calcite mass increased, clearly showing the significant carbonation of the sample. The interesting observation is that as calcite content increased, Friedel's salt content drastically reduced due to the pH reduction. The

pH of powder was tested using a suspension method. One of the drawbacks of this method is that unhydrated cement can increase the pH of the suspension due to its reaction to water. In other words, the real pH in concrete when carbonation is in progress is less than the measured pH using the suspension method. There is no common or even standardized method for measuring pH in concrete and cement paste and while the ex-situ (suspension) method has been reported to have acceptable conformity with in-situ and expression methods, further investigation is needed, especially for carbonated and existing concrete structures contaminated with diverse chemical agents.

The observations in this study showed that a considerable portion of bound chloride (Friedel's salt) was released after carbonation (more than 95%) and chloride desorption took place. The results are in agreement with previous investigations in which dissolution of Friedel's salt after accelerated carbonation was reported [140, 147, 256]. Guo et al. [256] reported that the major reason for Friedel's salt dissolution with a continuous carbonation is that the hydrate phases containing aluminum change into straetlingite. Geng et al. [256] also found that the solubility of Friedel's salt increases when the pH drops due to carbonation, which is the key player in Friedel's salt disappearance in composition. Eq. (4.6) and (4.7) show Friedel's salt decomposition when the pH drops and its conversion to insoluble aluminum hydroxide.

$$3CaO.\ Al_2O_3.CaCl_2.10H_2O \rightarrow 4\ Ca^{2+} + 2Cl^{-} + 4OH^{-} + 2Al(OH)_3 \quad (4.6)$$

$$Al(OH)_3 + OH^{-} \rightarrow Al(OH)_4 \quad (4.7)$$

While the dissolution of chemically bound chloride was monitored and measured, in this study the physical binding of chloride ions with cement phases was not measured. A cement paste exposed to natural and accelerated carbonation partially retains physical binding ability , but if the

carbonation is severe and the pH drops to around 9, severe decalcification of C-S-H phases occurs and the physical chloride binding capacity reaches to zero [256]. Gue et al. [256] found there is a relationship between the free chloride concentration and the loss in physical binding capacity of the C-S-H phase in cement paste. At low free chloride concentrations, like 0.05 mol/L, almost all physical binding is lost due to carbonation but at higher chloride concentrations like 0.67 mol/L and 1 mol/L, the loss in physical binding capacity of C-S-H is 61.9% and 52.7%, respectively.

Therefore, carbonation not only causes the release of bound chloride and dissolution of phases that have the ability to form physical and chemical chloride binding [167] but also hinders the chloride binding. It is worth mentioning that in service life models for concrete structures exposed to chloride ions, distinguishing bound chloride from total chloride is vital due to the retardation impact of bound chloride on the corrosion process. Thus, if the impact of carbonation in lowering bound chloride quantities is neglected, the estimated service life is overestimated [167].

A limited amount of carbonation can be beneficial for the surface layer of pastes and concretes because the calcium carbonate formed during carbonation fills the pores due to the higher volume compared to portlandite [259] and lower permeability [171]. But further carbonation reduces the alkalinity of the pore solution and impacts the cement paste microstructure by dissolution of cement hydrates. In addition, if embedded reinforcement is in place, a lower alkalinity and pH reduction initiate depassivation of the rebar. Calcite formed in the carbonation process has around 11% more volume than the original portlandite [251], which can initiate cracks and deterioration in concrete.

4.4.8. Summary of Main Findings (Objective 4)

In this study, the combined effects of chloride contamination and carbonation on the pH and composition of cement paste containing (OPC) and fly ash were investigated. Samples were exposed to a 2 molar NaCl solution for 35 days, during which their pH and composition were monitored using XRD and TGA tests. Subsequently, the chloride-contaminated samples underwent accelerated carbonation to quantify the release of bound chloride (chloride desorption) and to measure the pH and the quantity of main phases, including portlandite, Friedel's salt, and calcite. Here are the main findings:

1- The pH of the paste sample exposed to a high concentration of chloride solution slightly changed from around 13 to 12.5.
2- After carbonation, the pH was significantly reduced to around 11 for OPC paste and 10 for FA paste. The lower pH level in fly ash-containing pastes is associated with their lower portlandite content.
3- Due to carbonation, roughly all of Friedel's salt content (which represents bound chloride in cement paste) was dissolved, and chloride desorption was clearly observed. The chloride desorption after 2 weeks of carbonation in both pastes was more than 95%.
4- Monitoring pH can provide valuable insights regarding chloride desorption in cement paste. While it cannot directly provide the quantity of released bound chloride, a reduction in pH (from 13 to less than 11) can be an alarming sign to initiate more accurate monitoring for an existing structure.
5- Fly ash incorporation led to weaker carbonation resistance compared to OPC pastes. The percentage increase in calcite mass in the FA paste content was 190.9% after a week and

282.1% after 2 weeks of carbonation. This significant increase in calcite could initiate cracks and deterioration in carbonated concrete.

Chapter 5 : Conclusion and Recommendations for Future Works

5.1. Research Contribution and Main Outcomes

This novel research contained four independent yet interconnected objectives that delved into the chloride binding and desorption capacity and mechanisms of cement paste. Pastes made with Type I/II cement and three SCMs (fly ash, slag, and silica fume) were exposed to the three most used de-icing salt solutions (NaCl, $CaCl_2$, $MgCl_2$). The release of bound chloride, chloride desorption, was monitored and quantified under low pH environments and carbonation.

Given that chloride-induced corrosion in concrete structures is a leading cause of deterioration, resulting in significant economic costs and sustainability issues, the findings of this thesis contribute valuable insights to the current body of knowledge on chloride-induced corrosion. This research was among the first studies to methodically investigate the chloride desorption mechanism in blended cement containing supplementary cementitious materials (SCMs), exposed to de-icing brine solutions in low pH environments caused by acid attack and carbonation. In the following sections, the main outcomes for each objective are listed.

5.1.1. Importance of Controlling Parameters in Chloride Binding Evaluation

In the first objective, due to lack of standard procedure for chloride binding measurements lights were shed on factors that impact the chloride binding measurements. The vital factors including sample form, sample saturation level, the solution type (composition), and the mass ratio of sample to solution discussed and their impact on chloride binding measurements were explained. Meticulously considering factors impacting chloride binding test results will enhance the consistency and comparability of results across different laboratories and studies, leading to more accurate results.

1. The degree of saturation of the sample significantly affects chloride binding results. Vacuum-saturated samples showed a notably higher chloride binding capacity compared to those that were 50% saturated or dried. This variation is due to differences in water-filled pores, transport channels, and the accessibility of chlorides to binding sites. The rivalry between chloride and hydroxyl ions for binding sites was another factor that led to a decrease in chloride binding in samples that were less saturated.
2. The samples' shape was found to affect the chloride binding measurements and capacity. Powdered samples, with their larger surface area, exhibited higher chloride binding compared to crushed or disk-shaped specimens. Solid samples, which more closely resemble field conditions, had lower surface area and thus reduced chloride binding potential.
3. A higher solid-to-exposure solution mass ratio led to increased chloride binding. This is attributed to more moles of chlorides per unit mass of concrete, improved mobility of chloride ions within pores, and a decrease in the ionic strength within the paste.
4. The addition of ions like calcium, potassium, and sodium to the chloride solution significantly influences chloride binding. Solutions with these ions showed less chloride binding compared to pure NaCl solutions, attributed to changes in pH and ionic strength, as well as increased ion competition affecting chloride's ability to bond with cement hydration products.

5.1.2. Effects of Cation type of Brine Solution on Chloride Desorption

In the second and third objectives, first the chloride desorption mechanism for OPC cement pastes and then for pastes containing diverse types and replacement levels of SCMs were investigated and discussed. One of the primary goals of the current thesis was highlighting the

importance of chloride desorption as an underrated phenomenon in service life modeling of concrete structures. One of the primary influencers that can impact concrete deterioration due to chloride induced corrosion is the type and the concentration of brine solution. The cation type of the brine solution, e.g. Na^{+}, Ca^{2+}, or Mg^{2+}, impacts chloride desorption in the following ways:

1. The type of cation significantly influences the amount of bound chloride with a decreasing effectiveness observed in the order of $MgCl_2$ (highest binding) > $CaCl_2$ > NaCl (lowest binding).
2. The Langmuir isotherm more accurately describes the chloride binding behavior in ground OPC paste.
3. The pH of different brine solutions are different. In this study, the distilled water had a pH of 5.86. The pH levels measured for the 2-molar solutions were as follows: 6.8 for NaCl, 9.4 for $CaCl_2$, and 8.7 for $MgCl_2$. One of the reasons that different cation types of salt solutions have different chloride binding capacity and chloride desorption is the inherit differences in the salt solutions.
4. Experimental tests reveal that the formation of Friedel's salt, a form of chemical chloride binding, is affected by both the type and concentration of the salt solution.

5.1.3. Effects of Supplementary Cementitious Materials on Chloride Desorption

The application of supplementary cementitious materials is widespread in the concrete industry due to numerous reasons such as reducing the carbon footprint of concrete and increasing the long-term mechanical and durability properties of the concrete. The findings indicated an interesting interaction between the released bound chlorides, the type of salt, pH level, and the level of SCMs replacement. Here are the main effects of supplementary cementitious materials on chloride desorption:

1. The incorporation of SCMs represents a compromise between achieving higher chloride binding and significantly reducing portlandite ($Ca(OH)_2$) contents in cement pastes. Portlandite provides the necessary high alkaline environment, and its absence make cement paste more susceptible to pH change due to acid addition (acid attack). Increasing SCMs replacement levels decreased the paste sample's ability to buffer pH under acidic conditions. This suggests that slag-blended paste is less effective in resisting acid attacks compared to OPC.
2. In terms of promoting Friedel's salt formation, slag inclusion was the most effective compared to other SCMs and OPC paste, while silica fume was the least.
3. The SG25 (25% Slag) and SG50 (50% Slag) results indicated that, regardless of the cation type, higher slag inclusion increased chloride binding and reduced the percentage of released bound chlorides.
4. The addition of fly ash to the mix increased the chloride binding capacity of the blended system. Notably, when the paste samples were exposed to $CaCl_2$ and $MgCl_2$ solutions, the inclusion of FA resulted in a more substantial formation of Friedel's salt, indicating enhanced chloride binding.
5. The degree of chloride desorption under an acid attack largely depends on the acid volume to paste mass (A/P) ratio. At low A/P ratios, the paste can buffer the pH drop, which slows down or halts the chloride desorption process. When desorption stops, the system may restart chloride binding if free chlorides reach the paste's unaffected layers. However, exposure to high volumes of acid can cause significant deterioration and release a large number of bound chlorides.

6. There is a notable relationship between the binding capacity and the pH of the salt solutions. While NaCl tends to result in lower binding and can increase the concentration of free chlorides in fly ash-blended concrete, it does not significantly lower the pH compared to $MgCl_2$. Therefore, in acidic environments, the damage extent is expected to be lesser in concrete exposed to NaCl solutions.
7. Introducing acid to chloride-exposed samples led to the release of a considerable amount of bound chlorides. In OPC samples, more than 80% of bound chlorides were released when A/P ratio were 4% and 8%. In contrast, pastes containing fly ash showed a lower release of bound chloride in $MgCl_2$ and $CaCl_2$ solutions. This indicates higher durability and a reduced risk of corrosion in fly ash-containing pastes.

5.1.4. Synergic Effects of Exposure to NaCl Salt Solution and Carbonation on pH and Composition of Blended Cement Pastes Containing Fly Ash

Finally, in the last objective, the synergic effects of chloride contamination and carbonation, as the two most leading deterioration types for concrete structures, on the pH and composition of cement paste containing OPC cement and fly ash were studied. Carbonation is one of the primary causes of deterioration in concrete, impacting the service life of concrete structures. The combined impacts of chloride contamination and carbonation can drastically change the composition of cement hydrates and pH level. pH is one of the most influential properties in the cement paste which not only affects chloride binding and chloride desorption, but also impacts cement microstructure. Here are the key findings:

1. OPC paste outperformed pastes containing fly ash in terms of carbonation resistance. While observations in objective 3 confirmed the effectiveness of fly ash in improving chloride

binding capacity and resistance to chloride desorption, the incorporation of fly ash causes a more significant pH reduction after carbonation.

2. The percentage of chloride desorption, which represents the quantity of released bound chloride after carbonation, exceeded 95% in both pastes after 2 weeks of carbonation.
3. The portlandite content in pastes containing fly ash was lower than in OPC paste, which significantly impacts the buffer capacity of the paste when carbonation occurs, resulting in lower pH levels after carbonation in FA pastes.
4. A lower pH level in fly ash-containing pastes was observed which is associated with their lower portlandite content. After carbonation, the pH was significantly reduced to around 11 for OPC paste and 10 for FA paste.
5. There is a non-linear relationship between pH reduction and chloride desorption for pastes exposed to carbonation. A higher carbonation duration increases the quantity of chloride desorption.

5.2. Study Limitations

While the experimental design, hypothesis, objectives, and methods were meticulously chosen to maximize the applicability of the outcomes and minimize the limitations of this study, like all investigations, this thesis is not without its limitations. The investigation also uncovered several limitations that, if taken into account, can improve future research in similar and related fields.

1- Portland cement Type I/II, the most commonly used cement in construction, was utilized in this study. However, emerging cement types in the U.S. and Europe, such as commercially available Type IL and LC3, are gaining popularity due to decarbonization policies. The proposed chloride desorption mechanism might not apply to these cements

because of their different compositions. The study also focused on three types of SCMs, which are the most widely used supplementary cementitious materials in the construction industry. The results are specific to these SCM types and may not extend to bio-based SCMs or SCMs with significant compositional differences from those used in this study.

2- In this investigation, pure salt solutions (de-icers) were utilized. However, various state and private agencies employ combined salt solutions, such as NaCl and $MgCl_2$. Additionally, this study did not account for experimental factors like wetting-drying cycles, freeze-thaw cycles, loads, and cracks.

3- The lack of standardized methods for certain experimental procedures, such as pH measurements and the form of samples during chloride exposure, could potentially affect the results. Addressing some of these factors was one of the objectives of this study (the first objective). Therefore, caution should be exercised when interpreting the results in relation to design parameters.

4- The natural carbonation process takes decades to occur. In this study, accelerated carbonation was conducted on samples, which may overestimate the results compared to natural carbonation. It is important to distinguish the impacts of accelerated carbonation from those of natural carbonation.

5.3. Recommendations for Future Work

1- Revising Testing Procedure for Chloride Desorption: While most investigations use a type of acid to simulate the pH reduction, adopting a new approach could reduce the complexity of the investigation. An alternative approach could be instead of adding acid, samples are removed from salt solution, crystallized salts are cleaned off the surface, and then the samples are immersed in a solution with a controlled pH (e.g. 12, 10, 9), preferably using

DI water a diluted NaOH solution. The pH of DI water is around 6 to 7, thus using NaOH solution would help to reach the pH level that design for a specific experiment like chloride desorption measurement. It is worth mentioning that maintaining a consistent pH level throughout the experiment is nearly impossible due to the buffering capacity of the paste sample.

2- Standardize pH Measurement in Existing Concrete Carbonated Structures: After years of laboratory and practical applications in infrastructure and construction, there is no standard, practical, and accurate method for pH measurements in cement paste and concrete. In addition, most investigations are focused on pH measurement in non-chloride contaminated and non-carbonated concrete. In a metaphorical way, one can say the pH for concrete is like temperature for a human body. As temperature is one of the first parameters in a patient's body to be checked, pH for a concrete structure plays the same role and a single measurement can provide lots of insight. It is recommended that further and comprehensive investigation be carried out into existing concrete infrastructures to find a practical, cheap (or at least comparable in price to current methods), and accurate method for routine and frequent pH monitoring.

3- Using Field Samples: Laboratory samples differ from field samples not just in terms of casting and pouring but also when considering aspects such as concrete maturity, curing practices, and microstructural development more broadly. For future research, obtaining cores (drilled samples) from existing structures represents the most straightforward method to ensure the authenticity of concrete samples. Although obtaining field samples can be challenging due to restrictive policies in many city street departments, incorporating such samples could significantly enhance the accuracy of research findings.

4- Incorporating Cracks and Loads on Test Setups: One of the primary disadvantages of laboratory testing for chloride-induced corrosion, particularly for studying chloride binding and desorption, is the complexity and difficulty of simulating the impacts of loading and cracks. For example, concrete pavements are subjected to deicers, freeze-thaw cycles, loads from vehicles, carbonation, and more. Various types of cracks with different depths can develop in concrete pavements for multiple reasons. These cracks facilitate the penetration of chloride-bearing salts and accelerate the deterioration of the concrete. Therefore, including cracks and loads as parameters in the study of chloride binding and desorption mechanisms would yield more accurate and realistic outcomes.

5- Considering Mixed Salt Solutions: Future studies should use mixed de-icing salts (like blends of NaCl and $MgCl_2$) rather than pure salt solutions typically used in laboratories. One of the limitations of this study was using pure salt solutions, whereas in real-world scenarios, state and local departments often employ a blend of NaCl, $MgCl_2$, and various other chemical solutions during winter to reduce the risk of freezing.

6- Considering the Impact of Weathering: Examine how environmental conditions like wet-dry and freeze-thaw cycles affect chloride desorption in samples, to better simulate real-world conditions of concrete structures.

7- Studying Chloride Desorption Capacity for Type IL (Portland Limestone Cement): Due to the environmental policies most cement plants shifted from Type I/II to Type IL. While at least the 85% of clinker in Type IL is the same as Type I/II, due to differences in limestone composition and replacement levels from one producer to another producer, a detailed study of chloride desorption capacity for Type IL cements is worthy of investigation.

References

1. Adesina, A., *Recent advances in the concrete industry to reduce its carbon dioxide emissions.* Environmental Challenges, 2020. **1**: p. 100004.
2. Gates, B., *How to avoid a climate disaster: the solutions we have and the breakthroughs we need*. 2021: Vintage.
3. Böhni, H., *Corrosion in reinforced concrete structures*. 2005: Elsevier.
4. Dousti, A., et al., *Binding of externally supplied chlorides in micro silica concrete under field exposure conditions.* Cement and Concrete Composites, 2011. **33**(10): p. 1071-1079.
5. Mangat, P. and B. Molloy, *Chloride binding in concrete containing PFA, gbs or silica fume under sea water exposure.* Magazine of concrete research, 1995. **47**(171): p. 129-141.
6. Zaucha, J. and M. Matczak. *Role of maritime ports and shipping in the creation of the economic value of the sea areas*. in *SHS Web of Conferences*. 2018. EDP Sciences.
7. Sparacino, H., et al., *Review of reduced salt, snow, and ice management practices for commercial businesses.* Transportation Research Record, 2022. **2676**(3): p. 507-520.
8. Jain, J., et al., *Effects of deicing salt solutions on physical properties of pavement concretes.* Transportation research record, 2012. **2290**(1): p. 69-75.
9. Envirotechservices. *MeltDown Apex*. Available from: https://envirotechservices.com/meltdown-apex/#:~:text=MeltDown%20Apex%20delivers%20a%2012,ice%20buildup%20on%20road%20surfaces.
10. Silva, N., *Chloride induced corrosion of reinforcement steel in concrete: threshold values and ion distributions at the concrete-steel interface*. 2013: Chalmers Tekniska Hogskola (Sweden).
11. Shakouri, M. and D. Trejo, *Estimating the critical chloride threshold of reinforcing steel in concrete using a hierarchical Bayesian model.* Sustainable and Resilient Infrastructure, 2019. **4**(4): p. 152-172.
12. Angst, U., et al., *Critical chloride content in reinforced concrete—A review.* Cement and concrete research, 2009. **39**(12): p. 1122-1138.
13. Chalhoub, C., R. François, and M. Carcasses, *Critical chloride threshold values as a function of cement type and steel surface condition.* Cement and Concrete Research, 2020. **134**: p. 106086.
14. Poursaee, A. and B. Ross, *The Role of Cracks in Chloride-Induced Corrosion of Carbon Steel in Concrete.* Corrosion and Materials Degradation, 2022. **3**(2): p. 258-269.
15. Andrade, C., *Propagation of reinforcement corrosion: principles, testing and modelling.* Materials and Structures, 2019. **52**(1): p. 2.
16. Behnood, A., K. Van Tittelboom, and N. De Belie, *Methods for measuring pH in concrete: A review.* Construction and Building Materials, 2016. **105**: p. 176-188.
17. Carnot, A., et al., *Corrosion mechanisms of steel concrete moulds in the presence of a demoulding agent.* Journal of applied electrochemistry, 2002. **32**: p. 865-869.
18. Dousti, A., J.J. Beaudoin, and M. Shekarchi, *Chloride binding in hydrated MK, SF and natural zeolite-lime mixtures.* Construction and Building Materials, 2017. **154**: p. 1035-1047.
19. Yuan, Q., et al., *Chloride binding of cement-based materials subjected to external chloride environment–a review.* Construction and building materials, 2009. **23**(1): p. 1-13.

20. Vollpracht, A., et al., *The pore solution of blended cements: a review.* Materials and Structures, 2016. **49**: p. 3341-3367.
21. Rasheeduzzafar, *INFLUENCE OF CEMENT COMPOSITION ON CONCRETE DURABILITY.* ACI MATERIALS JOURNAL, 1992. **89**(6): p. 574-586.
22. Mundra, S., et al., *Chloride-induced corrosion of steel rebars in simulated pore solutions of alkali-activated concretes.* Cement and Concrete Research, 2017. **100**: p. 385-397 DOI: https://doi.org/10.1016/j.cemconres.2017.08.006.
23. Angst, U., et al., *Critical chloride content in reinforced concrete — A review.* Cement and Concrete Research, 2009. **39**(12): p. 1122-1138 DOI: https://doi.org/10.1016/j.cemconres.2009.08.006.
24. Sui, S., et al., *Quantification methods for chloride binding in Portland cement and limestone systems.* Cement and Concrete Research, 2019. **125**: p. 105864 DOI: https://doi.org/10.1016/j.cemconres.2019.105864.
25. Florea, M.V.A. and H.J.H. Brouwers, *Chloride binding related to hydration products: Part I: Ordinary Portland Cement.* Cement and Concrete Research, 2012. **42**(2): p. 282-290 DOI: https://doi.org/10.1016/j.cemconres.2011.09.016.
26. Machner, A., P. Hemstad, and K. De Weerdt, *Towards the understanding of the pH dependency of the chloride binding of Portland cement pastes.* Nordic Concrete Research, 2018. **58**(1): p. 143-162.
27. *Infrastructure Report Card 2021- Overview of Bridges*. 2021; Available from: https://infrastructurereportcard.org/.
28. Technology, F.H.A.R.a., *Corrosion resistant alloys for reinforced concrete, Chapter 1*, in *FHWA-HRT-07-039*. 2007.
29. Construction, B.C.f.C., *Guide to the maintenance,repair and monitoring of reinforced concrete structures.* 2001. **DME Report No. 4.Watford,** .
30. Alexander, M. and H. Beushausen, *Durability, service life prediction, and modelling for reinforced concrete structures–review and critique.* Cement and Concrete Research, 2019. **122**: p. 17-29.
31. Angst, U.M., *Challenges and opportunities in corrosion of steel in concrete.* Materials and Structures, 2018. **51**: p. 1-20.
32. Ye, H., et al., *Chloride-induced steel corrosion in concrete under service loads*. 2020: Springer.
33. Presuel-Moreno, F., *Corrosion Resistant Alloys for Reinforced Concrete*. 2009: Turner-Fairbank Highway Research Center.
34. Shi, X., et al., *Durability of steel reinforced concrete in chloride environments: An overview.* Construction and Building Materials, 2012. **30**: p. 125-138.
35. Kassem, E., A. Muftah, and J. Pinto, *Pavement Winter Operations in Cold Regions*. 2023.
36. Hansson, C., A. Poursaee, and S. Jaffer, *Corrosion of reinforcing bars in concrete.* The Masterbuilder, 2012. **15**(3): p. 106-124.
37. Angst, U.M. and B. Elsener, *The size effect in corrosion greatly influences the predicted life span of concrete infrastructures.* Science advances, 2017. **3**(8): p. e1700751.
38. Ahmad, S., *Reinforcement corrosion in concrete structures, its monitoring and service life prediction—a review.* Cement and concrete composites, 2003. **25**(4-5): p. 459-471.
39. Hansson, C., A. Poursaee, and A. Laurent, *Macrocell and microcell corrosion of steel in ordinary Portland cement and high performance concretes.* Cement and concrete research, 2006. **36**(11): p. 2098-2102.

40. Qian, S., J. Zhang, and D. Qu, *Theoretical and experimental study of microcell and macrocell corrosion in patch repairs of concrete structures.* Cement and Concrete Composites, 2006. **28**(8): p. 685-695.
41. Montemor, M., A. Simoes, and M. Ferreira, *Chloride-induced corrosion on reinforcing steel: from the fundamentals to the monitoring techniques.* Cement and concrete composites, 2003. **25**(4-5): p. 491-502.
42. Broomfield, J.P., *Corrosion of steel in concrete: understanding, investigation and repair*. 2023: Crc Press.
43. Hay, R. and C.P. Ostertag, *Acidification at rebar-concrete interface induced by accelerated corrosion test in aggressive chloride environment.* Cement and Concrete Composites, 2020. **110**: p. 103573.
44. Hovde, P.J. and K. Moser, *Performance based methods for service life prediction.* State of the art reports, CIB Report: Publication, 2004. **294**.
45. Maage, M., et al., *Service life prediction of existing concrete structures exposed to marine environment.* Materials Journal, 1996. **93**(6): p. 602-608.
46. Martın-Pérez, B., et al., *A study of the effect of chloride binding on service life predictions.* Cement and concrete research, 2000. **30**(8): p. 1215-1223.
47. Samson, E. and J. Marchand, *Numerical solution of the extended Nernst-Planck model.* Journal of Colloid and Interface Science, 1999. **215**(1): p. 1-8 DOI: DOI 10.1006/jcis.1999.6145.
48. Samson, E., et al., *Modelling ion diffusion mechanisms in porous media.* International Journal for Numerical Methods in Engineering, 1999. **46**(12): p. 2043-2060.
49. Marchand, J. and E. Samson, *Predicting the service-life of concrete structures – Limitations of simplified models.* Cement and Concrete Composites, 2009. **31**(8): p. 515-521 DOI: http://dx.doi.org/10.1016/j.cemconcomp.2009.01.007.
50. Glass, G. and N. Buenfeld, *The influence of chloride binding on the chloride induced corrosion risk in reinforced concrete.* Corrosion Science, 2000. **42**(2): p. 329-344.
51. Qiao, C., et al., *Prediction of chloride ingress in saturated concrete using formation factor and chloride binding isotherm.* Advances in Civil Engineering Materials, 2018. **7**(1): p. 206-220.
52. Weiss, W.J., et al., *Prediction of chloride ingress in saturated concrete using formation factor and chloride binding isotherm.* Advances in Civil Engineering Materials, 2018. **7**(1): p. 206-220.
53. Wang, Y., et al., *Understanding the chloride binding and diffusion behaviors of marine concrete based on Portland limestone cement-alumina enriched pozzolans.* Construction and Building Materials, 2019. **198**: p. 207-217.
54. Shafikhani, M. and S. Chidiac, *Quantification of concrete chloride diffusion coefficient–A critical review.* Cement and Concrete Composites, 2019. **99**: p. 225-250.
55. Al-Gadhib, A.H., *Numerical simulation of chloride diffusion in RC structures and the implications of chloride binding capacities and concrete mix.* International Journal of Civil & Environmental Engineering, 2010. **10**(5): p. 19-28.
56. Geng, J., et al., *The stability of bound chlorides in cement paste with sulfate attack.* Cement and Concrete Research, 2015. **68**: p. 211-222.
57. Suryavanshi, A., J. Scantlebury, and S. Lyon, *Mechanism of Friedel's salt formation in cements rich in tri-calcium aluminate.* Cement and concrete research, 1996. **26**(5): p. 717-727.

58. Florea, M. and H. Brouwers, *Chloride binding related to hydration products: Part I: Ordinary Portland Cement.* Cement and Concrete Research, 2012. **42**(2): p. 282-290.
59. Rasheeduzzafar, S. Ehtesham Hussain, and S.S. Al-Saadoun, *Effect of cement composition on chloride binding and corrosion of reinforcing steel in concrete.* Cement and Concrete Research, 1991. **21**(5): p. 777-794 DOI: https://doi.org/10.1016/0008-8846(91)90173-F.
60. Rasheeduzzafar, *Influence of Cement Composition on Concrete Durability.* Materials, 1992. **89**: p. 574-586.
61. Huang, X., et al., *The effect of supplementary cementitious materials on the permeability of chloride in steam cured high-ferrite Portland cement concrete.* Construction and Building Materials, 2019. **197**: p. 99-106 DOI: https://doi.org/10.1016/j.conbuildmat.2018.11.107.
62. Thomas, M., et al., *The effect of supplementary cementitious materials on chloride binding in hardened cement paste.* Cement and Concrete Research, 2012. **42**(1): p. 1-7.
63. Then, N.W., *Chloride Binding of Portland Limestone Cement containing Supplementary Cementitious Materials*. Oregon State University.
64. Yuan, Q., et al., *Chloride binding isotherm from migration and diffusion tests.* Journal of Wuhan University of Technology-Mater. Sci. Ed., 2013. **28**(3): p. 548-556 DOI: 10.1007/s11595-013-0729-y.
65. Chen, X., et al., *Effects of curing regimes on the chloride binding capacity of cementitious materials.* Construction and Building Materials, 2022. **342**: p. 127929.
66. Teymouri, M., M. Shakouri, and N.P. Vaddey, *pH-dependent chloride desorption isotherms of Portland cement paste.* Construction and Building Materials, 2021. **312**: p. 125415.
67. Ukpata, J.O., P.A.M. Basheer, and L. Black, *Slag hydration and chloride binding in slag cements exposed to a combined chloride-sulphate solution.* Construction and Building Materials, 2019. **195**: p. 238-248 DOI: https://doi.org/10.1016/j.conbuildmat.2018.11.055.
68. Cao, Y., et al., *Thermodynamic modelling and experimental investigation on chloride binding in cement exposed to chloride and chloride-sulfate solution.* Construction and Building Materials, 2020. **246**: p. 118398.
69. Zibara, H., *Binding of external chlorides by cement pastes*. 2001, National Library of Canada.
70. Roberts, M.H., *Effect of calcium chloride on the durability of pre-tensioned wire in prestressed concrete.* Magazine of Concrete Research, 1962. **14**(42): p. 143-154 DOI: 10.1680/macr.1962.14.42.143.
71. Qiao, C., et al., *Chloride binding of cement pastes with fly ash exposed to CaCl2 solutions at 5 and 23° C.* Cement and Concrete Composites, 2019. **97**: p. 43-53.
72. Mohammed, T.U. and H. Hamada, *Relationship between free chloride and total chloride contents in concrete.* Cement and Concrete Research, 2003. **33**(9): p. 1487-1490 DOI: https://doi.org/10.1016/S0008-8846(03)00065-6.
73. Xu, J., et al., *Influence of surfactants on chloride binding in cement paste.* Construction and Building Materials, 2016. **125**: p. 369-374 DOI: https://doi.org/10.1016/j.conbuildmat.2016.08.075.
74. Feng, W., et al., *Influence of polycarboxylate superplasticizer on chloride binding in cement paste.* Construction and Building Materials, 2018. **158**: p. 847-854 DOI: https://doi.org/10.1016/j.conbuildmat.2017.10.086.

75. Jiang, L., et al., *Effect of Ca2+ and Na+ on the curing performance of chloride ions in cement under carbonization.* Case Studies in Construction Materials, 2020. **13**: p. e00430 DOI: https://doi.org/10.1016/j.cscm.2020.e00430.
76. Chen, Y., et al., *Impact of phosphate corrosion inhibitors on chloride binding and release in cement pastes.* Construction and Building Materials, 2020. **236**: p. 117469 DOI: https://doi.org/10.1016/j.conbuildmat.2019.117469.
77. Qiao, C., et al., *Chloride binding of cement pastes with fly ash exposed to CaCl2 solutions at 5 and 23 °C.* Cement and Concrete Composites, 2019. **97**: p. 43-53 DOI: https://doi.org/10.1016/j.cemconcomp.2018.12.011.
78. Delagrave, A., et al., *Chloride binding capacity of various hydrated cement paste systems.* Advanced cement based materials, 1997. **6**(1): p. 28-35.
79. Ipavec, A., et al., *Chloride binding into hydrated blended cements: The influence of limestone and alkalinity.* Cement and Concrete Research, 2013. **48**: p. 74-85 DOI: https://doi.org/10.1016/j.cemconres.2013.02.010.
80. Wang, Y.Y., et al., *Understanding the chloride binding and diffusion behaviors of marine concrete based on Portland limestone cement-alumina enriched pozzolans.* CONSTRUCTION AND BUILDING MATERIALS, 2019. **198**: p. 207-217 DOI: 10.1016/j.conbuildmat.2018.11.270.
81. Rostami, R., A.J. Klemm, and F.C.R. Almeida, *The Effect of SCMs in Blended Cements on Sorption Characteristics of Superabsorbent Polymers.* Materials, 2021. **14**(7) DOI: 10.3390/ma14071609.
82. De Weerdt, K., et al., *Impact of the associated cation on chloride binding of Portland cement paste.* Cement and Concrete Research, 2015. **68**: p. 196-202.
83. Hemstad, P., A. Machner, and K. De Weerdt, *The effect of artificial leaching with HCl on chloride binding in ordinary Portland cement paste.* Cement and Concrete Research, 2020. **130**: p. 105976.
84. Giergiczny, Z., *Fly ash and slag.* Cement and Concrete Research, 2019. **124**: p. 105826.
85. Ramírez-Ortíz, A.E., F. Castellanos, and P.F.d.J. Cano-Barrita, *Ultrasonic Detection of Chloride Ions and Chloride Binding in Portland Cement Pastes.* International Journal of Concrete Structures and Materials, 2018. **12**(1): p. 20 DOI: 10.1186/s40069-018-0254-7.
86. Institute for Energy Economics and Financial Analysis. *U.S. Coal Outlook 2020: Market Trends Pushing Industry Ever Closer to a Reckoning*. 2020 March 2020; 17]. Available from: https://ieefa.org/wp-content/uploads/2020/03/US-Coal-Outlook-2020_March-2020.pdf.
87. Slag Cement Association. *The 'State' of Slag Cement*. 2022; Available from: https://www.slagcement.org/resources/news/articleid/204.aspx.
88. Slag Cement Association. *An Industry Average Environmental Product Declaration for Slag Cement*. 2021; Available from: https://www.slagcement.org/Portals/11/xBlog/uploads/2021/8/19/SCAEPDFinal_30072021_withupdatedlogos.pdf.
89. Portland Cement Association. *Environmental Product Declaration*. 2016; Available from: https://www.cement.org/docs/default-source/sustainabilty2/pca-portland-cement-epd-062716.pdf.
90. Manmohan, D. and P. Mehta, *Influence of pozzolanic, slag, and chemical admixtures on pore size distribution and permeability of hardened cement pastes.* Cement, Concrete and Aggregates, 1981. **3**(1): p. 63-67.

91. Sengul, O. and M.A. Tasdemir, *Compressive strength and rapid chloride permeability of concretes with ground fly ash and slag.* Journal of materials in civil engineering, 2009. **21**(9): p. 494-501.
92. Häkkinen, T., *The influence of slag content on the microstructure, permeability and mechanical properties of concrete Part 1 Microstructural studies and basic mechanical properties.* Cement and Concrete Research, 1993. **23**(2): p. 407-421.
93. Komljenović, M., et al., *External sulfate attack on alkali-activated slag.* Construction and Building Materials, 2013. **49**: p. 31-39.
94. Gollop, R. and H. Taylor, *Microstructural and microanalytical studies of sulfate attack. IV. Reactions of a slag cement paste with sodium and magnesium sulfate solutions.* Cement and Concrete Research, 1996. **26**(7): p. 1013-1028.
95. Lumley, J., *The ASR expansion of concrete prisms made from cements partially replaced by ground granulated blastfurnace slag.* Construction and Building Materials, 1993. **7**(2): p. 95-99.
96. He, P., et al., *A ternary optimization of alkali-activated cement mortars incorporating glass powder, slag and calcium aluminate cement.* Construction and Building Materials, 2020. **240**: p. 117983.
97. Ukpata, J.O., P. Basheer, and L. Black, *Slag hydration and chloride binding in slag cements exposed to a combined chloride-sulphate solution.* Construction and Building Materials, 2019. **195**: p. 238-248.
98. Adesanya, E., et al., *Ladle slag cement–Characterization of hydration and conversion.* Construction and Building Materials, 2018. **193**: p. 128-134.
99. Luo, R., et al., *Study of chloride binding and diffusion in GGBS concrete.* Cement and Concrete Research, 2003. **33**(1): p. 1-7.
100. Hope, B.B., J.A. Page, and J.S. Poland, *The determination of the chloride content of concrete.* Cement and Concrete Research, 1985. **15**(5): p. 863-870.
101. Dhir, R., M. El-Mohr, and T. Dyer, *Chloride binding in GGBS concrete.* Cement and Concrete Research, 1996. **26**(12): p. 1767-1773.
102. Cheng, A., et al., *Influence of GGBS on durability and corrosion behavior of reinforced concrete.* Materials Chemistry and Physics, 2005. **93**(2-3): p. 404-411.
103. Yeau, K.Y. and E.K. Kim, *An experimental study on corrosion resistance of concrete with ground granulate blast-furnace slag.* Cement and Concrete Research, 2005. **35**(7): p. 1391-1399.
104. Backus, J. and D. McPolin, *Effect of cyclic carbonation on chloride ingression in GGBS concrete.* Journal of Materials in Civil Engineering, 2016. **28**(7): p. 04016037.
105. Chakraborty, U.B., S. Bajaj, and S. Dhanote, *Experimental Investigation to Study the Properties of Concrete Incorporated with GGBS and GBS*, in *Advances in Sustainable Construction Materials and Geotechnical Engineering*. 2020, Springer. p. 261-270.
106. Khan, M., O. Kayali, and U. Troitzsch, *Chloride binding capacity of hydrotalcite and the competition with carbonates in ground granulated blast furnace slag concrete.* Materials and Structures, 2016. **49**(11): p. 4609-4619.
107. Lothenbach, B., K. Scrivener, and R.D. Hooton, *Supplementary cementitious materials.* Cement and Concrete Research, 2011. **41**(12): p. 1244-1256 DOI: https://doi.org/10.1016/j.cemconres.2010.12.001.
108. Lv, Z., et al., *Chloride binding of AFm in the presence of Na+, Ca2+ and Ba2+.* Construction and Building Materials, 2023. **364**: p. 129804.

109. Chang, H., et al., *A novel method for assessing CSH chloride adsorption in cement pastes.* Construction and Building Materials, 2019. **225**: p. 324-331.
110. ACI 234R-06, *Guide for the use of silica fume in concrete*. 2012, American Concrete Institute: Farmington Hills, MI
111. Arya, C., N. Buenfeld, and J. Newman, *Factors influencing chloride-binding in concrete.* Cement and Concrete research, 1990. **20**(2): p. 291-300.
112. Florea, M. and H. Brouwers, *Modelling of chloride binding related to hydration products in slag-blended cements.* Construction and Building Materials, 2014. **64**: p. 421-430.
113. Beaudoin, J.J., V.S. Ramachandran, and R.F. Feldman, *Interaction of chloride and C-S-H.* Cement and Concrete Research, 1990. **20**(6): p. 875-883.
114. Thomas, M.D.A., et al., *The effect of supplementary cementitious materials on chloride binding in hardened cement paste.* Cement and Concrete Research, 2012. **42**(1): p. 1-7 DOI: https://doi.org/10.1016/j.cemconres.2011.01.001.
115. Xu, J., et al., *Releases of bound chlorides from chloride-admixed plain and blended cement pastes subjected to sulfate attacks.* Construction and Building Materials, 2013. **45**: p. 53-59 DOI: https://doi.org/10.1016/j.conbuildmat.2013.03.068.
116. Campos, H., et al., *Low-cement high-strength concrete with partial replacement of Portland cement with stone powder and silica fume designed by particle packing optimization.* Journal of cleaner production, 2020. **261**: p. 121228.
117. Soliman, N. and A. Tagnit-Hamou, *Partial substitution of silica fume with fine glass powder in UHPC: Filling the micro gap.* Construction and Building Materials, 2017. **139**: p. 374-383.
118. Lin, Y., et al., *Effect of silica fumes on fluidity of UHPC: Experiments, influence mechanism and evaluation methods.* Construction and Building Materials, 2019. **210**: p. 451-460.
119. Kadri, E.-H. and R. Duval, *Hydration heat kinetics of concrete with silica fume.* Construction and Building Materials, 2009. **23**(11): p. 3388-3392.
120. Wang, X., et al., *The effects of silica fume on C3A hydration.* Construction and Building Materials, 2020. **250**: p. 118766.
121. Zelić, J., et al., *The role of silica fume in the kinetics and mechanisms during the early stage of cement hydration.* Cement and Concrete Research, 2000. **30**(10): p. 1655-1662.
122. Byfors, K., *Influence of silica fume and flyash on chloride diffusion and pH values in cement paste.* Cement and Concrete research, 1987. **17**(1): p. 115-130.
123. Shekarchi, M., A. Rafiee, and H. Layssi, *Long-term chloride diffusion in silica fume concrete in harsh marine climates.* Cement and Concrete Composites, 2009. **31**(10): p. 769-775.
124. Zhu, Q., et al., *Effect of chloride salt type on chloride binding behavior of concrete.* Construction and Building Materials, 2012. **37**: p. 512-517.
125. Szklarek, S., A. Górecka, and A. Wojtal-Frankiewicz, *The effects of road salt on freshwater ecosystems and solutions for mitigating chloride pollution-A review.* Science of The Total Environment, 2022. **805**: p. 150289.
126. De Weerdt, K., *Chloride binding in concrete: recent investigations and recognised knowledge gaps: RILEM Robert L'Hermite Medal Paper 2021.* Materials and Structures, 2021. **54**(6): p. 214.
127. Babaahmadi, A., et al. *Chloride binding in blended binder systems: Importance of the structures of CSH gel*. in *15th International Congress on the Chemistry of Cement*. 2019.

128. De Weerdt, K., D. Orsáková, and M.R. Geiker, *The impact of sulphate and magnesium on chloride binding in Portland cement paste.* Cement and Concrete Research, 2014. **65**: p. 30-40.
129. Avet, F. and K. Scrivener, *Influence of pH on the chloride binding capacity of Limestone Calcined Clay Cements (LC3).* Cement and Concrete Research, 2020. **131**: p. 106031.
130. Shi, C., et al., *Effects of chloride ion binding on microstructure of cement pastes.* Journal of Materials in Civil Engineering, 2016. **29**(1): p. 1-7.
131. Tritthart, J., *Chloride binding in cement II. The influence of the hydroxide concentration in the pore solution of hardened cement paste on chloride binding.* Cement and Concrete Research, 1989. **19**(5): p. 683-691.
132. Mohammed, T. and H. Hamada, *Relationship between free chloride and total chloride contents in concrete.* Cement and concrete research, 2003. **33**(9): p. 1487-1490.
133. Chen, Z., et al., *The relationship between the free and the bound chloride in high performance concrete.* Applied Mechanics and Materials, 2012. **117**: p. 1387-1390.
134. Ye, H., et al., *Prediction of chloride binding isotherms for blended cements.* Comput. Concr, 2016. **17**(5): p. 655-672.
135. Yuan, Q., et al., *Chloride binding isotherm from migration and diffusion tests.* Journal of Wuhan University of Technology-Mater. Sci. Ed., 2013. **28**: p. 548-556.
136. Jain, A., et al., *Influence of pH on chloride binding isotherms for cement paste and its components.* Cement and Concrete Research, 2021. **143**: p. 106378.
137. Vollpracht, A., et al., *The pore solution of blended cements: a review.* Materials and Structures, 2016. **49**(8): p. 3341-3367.
138. Luping, T. and L.-O. Nilsson, *Chloride binding capacity and binding isotherms of OPC pastes and mortars.* Cement and concrete research, 1993. **23**(2): p. 247-253.
139. Castellote, M., C. Andrade, and C. Alonso, *Chloride-binding isotherms in concrete submitted to non-steady-state migration experiments.* Cement and Concrete Research, 1999. **29**(11): p. 1799-1806.
140. Chang, H., *Chloride binding capacity of pastes influenced by carbonation under three conditions.* Cement and Concrete Composites, 2017. **84**: p. 1-9 DOI: https://doi.org/10.1016/j.cemconcomp.2017.08.011.
141. Csizmadia, J., G. Balázs, and F.D. Tamás, *Chloride ion binding capacity of aluminoferrites.* Cement and Concrete Research, 2001. **31**(4): p. 577-588.
142. De Weerdt, K., D. Orsáková, and M. Geiker, *The impact of sulphate and magnesium on chloride binding in Portland cement paste.* Cement and Concrete Research, 2014. **65**: p. 30-40.
143. Gbozee, M., et al., *The influence of aluminum from metakaolin on chemical binding of chloride ions in hydrated cement pastes.* Applied Clay Science, 2018. **158**: p. 186-194.
144. Geng, J., et al., *Chloride binding in cement paste with calcined Mg-Al-CO3 LDH (CLDH) under different conditions.* Construction and Building Materials, 2021. **273**: p. 121678.
145. Kayali, O., M. Khan, and M.S. Ahmed, *The role of hydrotalcite in chloride binding and corrosion protection in concretes with ground granulated blast furnace slag.* Cement and Concrete Composites, 2012. **34**(8): p. 936-945.
146. Long, W.-J., et al., *Investigation on chloride binding capacity and stability of Friedel's salt in graphene oxide reinforced cement paste.* Cement and Concrete Composites, 2022: p. 104603.

147. Saillio, M., V. Baroghel-Bouny, and F. Barberon, *Chloride binding in sound and carbonated cementitious materials with various types of binder.* Construction and Building Materials, 2014. **68**: p. 82-91 DOI: https://doi.org/10.1016/j.conbuildmat.2014.05.049.
148. Shakouri, M., C.L. Exstrom, and G.D. Piccini, *Chloride binding and desorption properties of the concrete containing corn stover ash.* Journal of Sustainable Cement-Based Materials, 2022. **11**(1): p. 62-82.
149. Shakouri, M., et al., *Development of empirical models for chloride binding in cementitious systems containing admixed chlorides.* Construction and Building Materials, 2018. **189**: p. 157-169.
150. Song, H., et al., *Development of chloride binding capacity in cement pastes and influence of the pH of hydration products.* Canadian Journal of Civil Engineering, 2008. **35**(12): p. 1427-1434.
151. Suryavanshi, A., J. Scantlebury, and S. Lyon, *The binding of chloride ions by sulphate resistant Portland cement.* Cement and Concrete Research, 1995. **25**(3): p. 581-592.
152. Wang, Y., et al., *Chloride binding behaviors of metakaolin-lime hydrated blends: Influence of gypsum and atmospheric carbonation.* Construction and Building Materials, 2019. **201**: p. 380-390.
153. Teymouri, M. and M. Shakouri, *Chloride desorption mechanisms of cement pastes containing fly ash.* Construction and Building Materials, 2023. **370**: p. 130667.
154. Zhang, Y., M. Zhang, and G. Ye, *Influence of moisture condition on chloride diffusion in partially saturated ordinary Portland cement mortar.* Materials and Structures, 2018. **51**: p. 1-18.
155. Xi, Y. and Z.P. Bažant, *Modeling chloride penetration in saturated concrete.* Journal of Materials in Civil Engineering, 1999. **11**(1): p. 58-65.
156. Baroghel-Bouny, V., et al., *AgNO 3 spray tests: advantages, weaknesses, and various applications to quantify chloride ingress into concrete. Part 1: Non-steady-state diffusion tests and exposure to natural conditions.* Materials and structures, 2007. **40**: p. 759-781.
157. de Vera, G., et al., *A test method for measuring chloride diffusion coefficients through partially saturated concrete. Part II: The instantaneous plane source diffusion case with chloride binding consideration.* Cement and concrete research, 2007. **37**(5): p. 714-724.
158. Chindaprasirt, P. and W. Chalee, *Effect of sodium hydroxide concentration on chloride penetration and steel corrosion of fly ash-based geopolymer concrete under marine site.* Construction and building materials, 2014. **63**: p. 303-310.
159. Yang, Z., et al., *The influence of sodium sulfate and magnesium sulfate on the stability of bound chlorides in cement paste.* Construction and Building Materials, 2019. **228**: p. 116775.
160. Cao, Y., L. Guo, and B. Chen, *Influence of sulfate on the chloride diffusion mechanism in mortar.* Construction and Building Materials, 2019. **197**: p. 398-405.
161. Bothe Jr, J.V. and P.W. Brown, *PhreeqC modeling of Friedel's salt equilibria at 23±1° C.* Cement and Concrete Research, 2004. **34**(6): p. 1057-1063.
162. Cai, W., et al., *Chloride binding behavior of synthesized reaction products in alkali-activated slag.* Composites Part B: Engineering, 2022. **238**: p. 109919.
163. Zheng, Y., et al., *Influence of carbonation on the bound chloride concentration in different cementitious systems.* Construction and Building Materials, 2021. **302**: p. 124171.

164. Brown, P.W. and S. Badger, *The distributions of bound sulfates and chlorides in concrete subjected to mixed NaCl, MgSO4, Na2SO4 attack.* Cement and Concrete Research, 2000. **30**(10): p. 1535-1542 DOI: https://doi.org/10.1016/S0008-8846(00)00386-0.
165. Tang, L., L.-O. Nilsson, and P.M. Basheer, *Resistance of concrete to chloride ingress: Testing and modelling*. 2011: CRC Press.
166. Long, W.-J., et al., *Investigation on chloride binding capacity and stability of Friedel's salt in graphene oxide reinforced cement paste.* Cement and Concrete Composites, 2022. **132**: p. 104603 DOI: https://doi.org/10.1016/j.cemconcomp.2022.104603.
167. Geng, J., et al., *Effect of carbonation on release of bound chlorides in chloride-contaminated concrete.* Magazine of Concrete Research, 2016. **68**(7): p. 353-363.
168. Sun, M., et al., *Influence of carbonation on chloride binding of mortars made with simulated marine sand.* Construction and Building Materials, 2021. **303**: p. 124455.
169. Shen, X.-h., et al., *Numerical study of carbonation and its effect on chloride binding in concrete.* Cement and Concrete Composites, 2019. **104**: p. 103402.
170. Bouikni, A., R. Swamy, and A. Bali, *Durability properties of concrete containing 50% and 65% slag.* Construction and Building Materials, 2009. **23**(8): p. 2836-2845.
171. Allahverdi, A. and F. Škvára, *Acidic corrosion of hydrated cement based materials.* Ceram. Silikáty, 2000. **44**(4): p. 152-160.
172. Pavlík, V., *Corrosion of hardened cement paste by acetic and nitric acids part II: formation and chemical composition of the corrosion products layer.* Cement and Concrete research, 1994. **24**(8): p. 1495-1508.
173. Pavlik, V., *Corrosion of hardened cement paste by acetic and nitric acids Part III: Influence of water/cement ratio.* Cement and Concrete Research, 1996. **26**(3): p. 475-490.
174. Pavlik, V. and S. Unčík, *The rate of corrosion of hardened cement pastes and mortars with additive of silica fume in acids.* Cement and Concrete Research, 1997. **27**(11): p. 1731-1745.
175. Gutberlet, T., H. Hilbig, and R. Beddoe, *Acid attack on hydrated cement—Effect of mineral acids on the degradation process.* Cement and Concrete Research, 2015. **74**: p. 35-43.
176. Machner, A., P. Hemstad, and K. De Weerdt, *Towards the understanding of the pH dependency of the chloride binding of Portland cement pastes.* 2018.
177. Zhang, C.-l., et al., *Numerical investigation of external sulfate attack and its effect on chloride binding and diffusion in concrete.* Construction and Building Materials, 2021. **285**: p. 122806.
178. Nijland, T. and J. Larbi, *Microscopic examination of deteriorated concrete*, in *Non-destructive evaluation of reinforced concrete structures*. 2010, Elsevier. p. 137-179.
179. Thomas, M., *The durability of concrete for marine construction: Materials and properties*, in *Marine Concrete Structures*. 2016, Elsevier. p. 151-170.
180. Srinivasan, R., et al. *Embedded micro-sensor for monitoring pH in concrete structures*. in *Smart Structures and Materials 2000: Smart Systems for Bridges, Structures, and Highways*. 2000. SPIE.
181. Jiang, W.-q., et al., *Binding capacity and diffusivity of concrete subjected to freeze-thaw and chloride attack: A numerical study.* Ocean Engineering, 2019. **186**: p. 106093.
182. Mangat, P. and O.O. Ojedokun, *Free and bound chloride relationships affecting reinforcement cover in alkali activated concrete.* Cement and Concrete Composites, 2020. **112**: p. 103692.

183. Hirao, H., et al., *Chloride binding of cement estimated by binding isotherms of hydrates.* Journal of Advanced Concrete Technology, 2005. **3**(1): p. 77-84.
184. ASTM C150, *Standard Specification for Portland Cement*. 2020, ASTM International: Philadelphia, PA.
185. AASHTO M 85, *Standard Specification for Portland Cement*. 2020, American Association of State Highway and Transportation Officials
186. ASTM C305, *Standard practice for mechanical mixing of hydraulic cement pastes and mortars of plastic consistency*. 2020, ASTM International: Philadelphia, PA.
187. ASTMC1876, *Standard test method for bulk electrical resistivity or bulk conductivity of concrete.* ASTM International, 2019.
188. ASTM D3282 *Standard Practice for Classification of Soils and Soil-Aggregate Mixtures for Highway Construction Purposes*. 2015, ASTM International: Philadelphia, PA.
189. ASTM, *C150/C150M − 12; Standard Specification for Portland Cement*. 2012, American Society for Testing and Materials United States. p. 1-9.
190. ASTM C305, *Standard Practice for Mechanical Mixing of Hydraulic Cement Pastes and Mortars of Plastic Consistency.* ASTM International, 2014.
191. Gražulis, S., A. Merkys, and A. Vaitkus, *Crystallography open database (COD).* Handbook of Materials Modeling: Methods: Theory and Modeling, 2020: p. 1863-1881.
192. Gražulis, S., et al., *Crystallography Open Database–an open-access collection of crystal structures.* Journal of applied crystallography, 2009. **42**(4): p. 726-729.
193. Loh, P.-Y., et al., *Effect of filtering method on the pH measurement of cement mortar in ex-situ leaching.* Heliyon, 2024: p. e25859 DOI: https://doi.org/10.1016/j.heliyon.2024.e25859.
194. Li, L., J. Nam, and W.H. Hartt, *Ex situ leaching measurement of concrete alkalinity.* Cement and concrete research, 2005. **35**(2): p. 277-283.
195. Shakouri, M. and M. Teymouri, *Investigating the effects of testing protocol factors on chloride binding capacity in cementitious materials.* Construction and Building Materials, 2023. **409**: p. 134067.
196. Nielsen, E.P. and M.R. Geiker, *Chloride diffusion in partially saturated cementitious material.* Cement and Concrete Research, 2003. **33**(1): p. 133-138.
197. Guimarães, A.T.d.C., et al., *Determination of chloride diffusivity through partially saturated Portland cement concrete by a simplified procedure.* Construction and Building Materials, 2011. **25**(2): p. 785-790.
198. Wu, Y.-Y., F.J. Presuel-Moreno, and R. Simmons, *Chloride Diffusivity through Partially Saturated, Binary-Blended Concrete.* ACI Materials Journal, 2018. **115**(5): p. 695-705.
199. Elakneswaran, Y., *Multi-ionic transport in cementitious materials with ion-cement hydrates interactions*. 2009, Hokkaido University, Solid Waste, Resources and Geoenviromental Engineering ….
200. Yang, M., C. Neubauer, and H. Jennings, *Interparticle potential and sedimentation behavior of cement suspensions: Review and results from paste.* Advanced Cement Based Materials, 1997. **5**(1): p. 1-7.
201. Nguyen, P.T. and O. Amiri, *Study of electrical double layer effect on chloride transport in unsaturated concrete.* Construction and Building Materials, 2014. **50**: p. 492-498.
202. Helmholtz, H.v., *Ueber einige Gesetze der Vertheilung elektrischer Ströme in körperlichen Leitern, mit Anwendung auf die thierisch ‐ elektrischen Versuche (Schluss.).* Annalen der Physik, 1853. **165**(7): p. 353-377.

203. Yang, Y., et al., *Multiscale modeling of ion diffusion in cement paste: electrical double layer effects.* Cement and Concrete Composites, 2019. **96**: p. 55-65.
204. Grahame, D.C., *The electrical double layer and the theory of electrocapillarity.* Chemical reviews, 1947. **41**(3): p. 441-501.
205. Zhu, Y., et al., *Solidification of chloride ions in alkali-activated slag.* Construction and Building Materials, 2022. **320**: p. 126219.
206. Parkhurst, D.L., *User's guide to PHREEQC: A computer program for speciation, reaction-path, advective-transport, and inverse geochemical calculations*. 1995: US Department of the Interior, US Geological Survey.
207. Plummer, L.N., *A computer program incorporating Pitzer's equations for calculation of geochemical reactions in brines*. Vol. 88. 1988: Department of the Interior, US Geological Survey.
208. Yuan, Q., et al., *Chloride binding of cement-based materials subjected to external chloride environment – A review.* Construction and Building Materials, 2009. **23**(1): p. 1-13 DOI: https://doi.org/10.1016/j.conbuildmat.2008.02.004.
209. Qiao, C., et al., *Damage in cement pastes exposed to MgCl2 solutions.* Materials and Structures, 2018. **51**(3): p. 74 DOI: 10.1617/s11527-018-1191-2.
210. De Weerdt, K., B. Lothenbach, and M.R. Geiker, *Comparing chloride ingress from seawater and NaCl solution in Portland cement mortar.* Cement and Concrete Research, 2019. **115**: p. 80-89 DOI: https://doi.org/10.1016/j.cemconres.2018.09.014.
211. Hansson, C., T. Frølund, and J. Markussen, *The effect of chloride cation type on the corposion of steel in concrete by chloride salts.* Cement and Concrete Research, 1985. **15**(1): p. 65-73.
212. Scrivener, K., R. Snellings, and B. Lothenbach, *A practical guide to microstructural analysis of cementitious materials*. 2016: Taylor & Francis.
213. Shi, C., et al., *Effects of Chloride Ion Binding on Microstructure of Cement Pastes.* Journal of Materials in Civil Engineering, 2017. **29**(1): p. 04016183 DOI: 10.1061/(ASCE)MT.1943-5533.0001707.
214. Bernard, E., et al., *Effect of magnesium on calcium silicate hydrate (C-S-H).* Cement and Concrete Research, 2017. **97**: p. 61-72 DOI: https://doi.org/10.1016/j.cemconres.2017.03.012.
215. Arya, C., N.R. Buenfeld, and J.B. Newman, *Factors influencing chloride-binding in concrete.* Cement and Concrete Research, 1990. **20**(2): p. 291-300 DOI: https://doi.org/10.1016/0008-8846(90)90083-A.
216. Allahverdi, A. and F. Škvára, *Acidic corrosion of hydrated cement based materials.* Ceramics− Silikáty, 2000. **44**(4): p. 152-160.
217. Lolivier, J. *Determination of chloride in hardened concrete*. in *International symposium on admixtures in mortars and concrete, RILEM-ABEM, report*. 1967.
218. Ahmed, A.A. and D. Trejo, *Assessing standard tests for admixtured chlorides in calcium aluminate and calcium sulfoaluminate cement systems.* ACI Materials Journal, 2020. **117**(1): p. 71-84.
219. Berman, H.A., *Determination of chloride in hardened portland cement paste, mortar, and concrete.* Journal of Materials, 1972. **7**(3): p. 330-335.
220. Trejo, D., N.P. Vaddey, and M. Shakouri, *Factors influencing chloride test results of cementitious systems.* ACI Materials Journal, 2019. **16**(1): p. 135-145.

221. Ahmed, A.A. and D. Trejo, *Assessing standard tests for admixtured chlorides in calcium aluminate and calcium sulfoaluminate cement systems.* ACI Materials Journal. **117**(1): p. 71-84 DOI: 10.14359/51720290.
222. Trejo, D. and A.A. Ahmed, *Adopting auto-titration to assess chlorides in concrete.* ACI Materials Journal, 2019. **116**(3): p. 43-52.
223. Allahverdi, A. and F. Škvára, *Acidic corrosion of hydrated cement based materials. Part 1. Mechanism of the phenomenon.* Ceramics - Silikaty, 2000. **44**: p. 114-120.
224. Gabrisova, A., J. Havlica, and S. Sahu, *Stability of calcium sulphoaluminate hydrates in water solutions with various pH values.* Cement and Concrete Research, 1991. **21**(6): p. 1023-1027.
225. Amer, A.A., et al., *Synthesis and characterization of some calcium aluminate phases from nano-size starting materials.* Boletín de la Sociedad Española de Cerámica y Vidrio, 2020 DOI: https://doi.org/10.1016/j.bsecv.2020.07.006.
226. Teymouri, M. and M. Shakouri, *Effect of pH on Desorption of Bound Chlorides in Cement Pastes Containing Granulated Blast-Furnace Slag.* Journal of Materials in Civil Engineering, 2023. **35**(12): p. 04023476.
227. Suraneni, P., *Recent developments in reactivity testing of supplementary cementitious materials.* RILEM Technical Letters, 2021. **6**: p. 131-139.
228. Lothenbach, B., K. Scrivener, and R. Hooton, *Supplementary cementitious materials.* Cement and concrete research, 2011. **41**(12): p. 1244-1256.
229. Chindaprasirt, P., C. Jaturapitakkul, and T. Sinsiri, *Effect of fly ash fineness on microstructure of blended cement paste.* Construction and Building Materials, 2007. **21**(7): p. 1534-1541.
230. Kocak, Y. and S. Nas, *The effect of using fly ash on the strength and hydration characteristics of blended cements.* Construction and Building Materials, 2014. **73**: p. 25-32.
231. Skibsted, J. and R. Snellings, *Reactivity of supplementary cementitious materials (SCMs) in cement blends.* Cement and Concrete Research, 2019. **124**: p. 105799.
232. Leklou, N., V.-H. Nguyen, and P. Mounanga, *The effect of the partial cement substitution with fly ash on Delayed Ettringite Formation in heat-cured mortars.* KSCE Journal of Civil Engineering, 2017. **21**(4): p. 1359-1366 DOI: 10.1007/s12205-016-0778-9.
233. Suryavanshi, A. and R.N. Swamy, *Stability of Friedel's salt in carbonated concrete structural elements.* cement and Concrete Research, 1996. **26**(5): p. 729-741.
234. Muthu, M., N. Ukrainczyk, and E. Koenders, *Effect of graphene oxide dosage on the deterioration properties of cement pastes exposed to an intense nitric acid environment.* Construction and Building Materials, 2021. **269**: p. 121272 DOI: https://doi.org/10.1016/j.conbuildmat.2020.121272.
235. Desarnaud, J., D. Bonn, and N. Shahidzadeh, *The pressure induced by salt crystallization in confinement.* Scientific reports, 2016. **6**(1): p. 1-8.
236. Bharadwaj, K., O.B. Isgor, and W.J. Weiss, *A Dataset Containing Statistical Compositions and Reactivities of Commercial and Novel Supplementary Cementitious Materials; Dataset Version 1.0*. 2022: Oregon State University DOI: http://localhost/files/2z10wz01n.
237. Atkins, M., F. Glasser, and A. Kindness, *Phase Relations and Solubility Modelling in the Cao-SiO2-Al2O3-MgO-SO3-H2O System: For Application To Blended Cementss.* MRS Online Proceedings Library (OPL), 1990. **212**.

238. Kolani, B., et al., *Hydration of slag-blended cements.* Cement and concrete composites, 2012. **34**(9): p. 1009-1018.
239. Zhao, J., et al., *Thermodynamic, mechanical, and electronic properties of ettringite and AFm phases from first-principles calculations.* Construction and Building Materials, 2022. **350**: p. 128777.
240. Song, Z., et al., *Influence of cation type on diffusion behavior of chloride ions in concrete.* Construction and Building Materials, 2015. **99**: p. 150-158.
241. Hansson, C.M., T. Frølund, and J.B. Markussen, *The effect of chloride cation type on the corposion of steel in concrete by chloride salts.* Cement and Concrete Research, 1985. **15**(1): p. 65-73 DOI: https://doi.org/10.1016/0008-8846(85)90009-2.
242. Anderson, J.L., F. Rauh, and A. Morales, *Particle diffusion as a function of concentration and ionic strength.* The Journal of Physical Chemistry, 1978. **82**(5): p. 608-616.
243. Brown, T.L., et al., *Chemistry: the central science*. 2002: Pearson Educación.
244. Bellmann, F. and J. Stark, *Activation of blast furnace slag by a new method.* Cement and Concrete Research, 2009. **39**(8): p. 644-650.
245. TAMAS, P. *Acceleration and retardation of Portland cement hydration by additives*. in *Symposium on Structure of Portland Cement Paste and Concrete*. 1966.
246. Xie, N., Y. Dang, and X. Shi, *New insights into how MgCl2 deteriorates Portland cement concrete.* Cement and Concrete Research, 2019. **120**: p. 244-255.
247. Fenter, F.F., F. Caloz, and M.J. Rossi, *Kinetics of nitric acid uptake by salt.* The Journal of Physical Chemistry, 1994. **98**(39): p. 9801-9810.
248. Perrin, D.D., *Dissociation contants of inorganic acids and bases in aqueous solution.* Pure and Applied Chemistry, 1969. **20**(2): p. 133-236.
249. Scrivener, K., R. Snellings, and B. Lothenbach, *A practical guide to microstructural analysis of cementitious materials*. Vol. 540. 2016: Crc Press Boca Raton, FL, USA: .
250. Zhu, Z., et al., *Effect of silica fume and fly ash on the stability of bound chlorides in cement mortar during electrochemical chloride extraction.* Construction and Building Materials, 2020. **256**: p. 119481.
251. Guo, Y., et al., *Physically and chemically bound chlorides in hydrated cement pastes: A comparison study of the effects of silica fume and metakaolin.* Journal of Materials Science, 2019. **54**: p. 2152-2169.
252. Arvaniti, E.C., et al., *Determination of particle size, surface area, and shape of supplementary cementitious materials by different techniques.* Materials and Structures, 2015. **48**(11): p. 3687-3701.
253. Song, H.-W., et al., *Estimation of the permeability of silica fume cement concrete.* Construction and Building Materials, 2010. **24**(3): p. 315-321.
254. Oner, A., S. Akyuz, and R. Yildiz, *An experimental study on strength development of concrete containing fly ash and optimum usage of fly ash in concrete.* Cement and Concrete Research, 2005. **35**(6): p. 1165-1171.
255. Scrivener, K., R. Snellings, and B. Lothenbach, *A practical guide to microstructural analysis of cementitious materials*. 2018: Crc Press.
256. Guo, B., et al., *Effect of natural carbonation on chloride binding behaviours in OPC paste investigated by a thermodynamic model.* Journal of Building Engineering, 2022. **49**: p. 104021 DOI: https://doi.org/10.1016/j.jobe.2022.104021.
257. Pade, C. and M. Guimaraes, *The CO2 uptake of concrete in a 100 year perspective.* Cement and concrete research, 2007. **37**(9): p. 1348-1356.

258. Wan, X.-m., et al., *Chloride content and pH value in the pore solution of concrete under carbonation.* Journal of Zhejiang University SCIENCE A, 2013. **14**(1): p. 71-78.
259. Šavija, B. and M. Luković, *Carbonation of cement paste: Understanding, challenges, and opportunities.* Construction and Building Materials, 2016. **117**: p. 285-301 DOI: https://doi.org/10.1016/j.conbuildmat.2016.04.138.
260. Yin, S.-h., et al., *Effect of carbonic acid water on the degradation of Portland cement paste: Corrosion process and kinetics.* Construction and Building Materials, 2015. **91**: p. 39-46 DOI: https://doi.org/10.1016/j.conbuildmat.2015.05.046.
261. Ashraf, W., *Carbonation of cement-based materials: Challenges and opportunities.* Construction and Building Materials, 2016. **120**: p. 558-570.
262. Khunthongkeaw, J., S. Tangtermsirikul, and T. Leelawat, *A study on carbonation depth prediction for fly ash concrete.* Construction and Building Materials, 2006. **20**(9): p. 744-753 DOI: https://doi.org/10.1016/j.conbuildmat.2005.01.052.
263. Xu, Z., et al., *Effects of temperature, humidity and CO2 concentration on carbonation of cement-based materials: A review.* Construction and Building Materials, 2022. **346**: p. 128399.
264. Hussain, S., D. Bhunia, and S.B. Singh, *Comparative study of accelerated carbonation of plain cement and fly-ash concrete.* Journal of Building Engineering, 2017. **10**: p. 26-31 DOI: https://doi.org/10.1016/j.jobe.2017.02.001.
265. Van den Heede, P., M. De Schepper, and N. De Belie, *Accelerated and natural carbonation of concrete with high volumes of fly ash: chemical, mineralogical and microstructural effects.* Royal Society open science, 2019. **6**(1): p. 181665.
266. Jiang, L., B. Lin, and Y. Cai, *A model for predicting carbonation of high-volume fly ash concrete.* Cement and concrete research, 2000. **30**(5): p. 699-702.
267. Kulik, D.A., et al., *CemGEMS–an easy-to-use web application for thermodynamic modelling of cementitious materials.* RILEM Technical Letters, 2021. **6**: p. 36-52.
268. Alonso, C., et al., *Chloride threshold values to depassivate reinforcing bars embedded in a standardized OPC mortar.* Cement and Concrete research, 2000. **30**(7): p. 1047-1055.
269. Bahman-Zadeh, F., A.A. Ramezanianpour, and A. Zolfagharnasab, *Effect of carbonation on chloride binding capacity of limestone calcined clay cement (LC3) and binary pastes.* Journal of Building Engineering, 2022. **52**: p. 104447.
270. Hussain, S.E. and S. Al-Saadoun, *Effect of cement composition on chloride binding and corrosion of reinforcing steel in concrete.* Cement and Concrete Research, 1991. **21**(5): p. 777-794.
271. Xu, G. and X. Shi, *Characteristics and applications of fly ash as a sustainable construction material: A state-of-the-art review.* Resources, Conservation and Recycling, 2018. **136**: p. 95-109.
272. Wang, Y., et al., *A rapid furnace-based gravimetry test for assessing reactivity of supplementary cementitious materials.* Materials and structures, 2022. **55**(7): p. 193.